

Review Article

Excited-state quantum phase transitions

Pavel Cejnar¹, Pavel Stránský¹,
Michal Macek², Michal Kloc^{1,3}

¹ Institute of Particle and Nuclear Physics, Faculty of Mathematics and Physics,
Charles University, V Holešovičkách 2, 180 00 Prague, Czechia

² Institute of Scientific Instruments, The Czech Academy of Sciences,
Královopolská 147, 612 64 Brno, Czechia

³ Department of Physics, University of Basel, Klingelbergstrasse 82, 4056 Basel,
Switzerland

E-mail: cejnar@ipnp.troja.mff.cuni.cz

Abstract. We review the effects of excited-state quantum phase transitions (ESQPTs) in interacting many-body systems with finite numbers of collective degrees of freedom. We classify typical ESQPT signatures in the spectra of excited states with respect to the underlying classical dynamics and outline a variety of quantum systems in which they occur. We describe some thermodynamic and dynamical consequences of ESQPTs, like those in microcanonical thermodynamics, quantum quench dynamics, driven dynamics and dissipative dynamics. At last we hint at some generalizations of the ESQPT concept in spatial and time crystals and in scattering systems.

Keywords: Singularities in quantized energy spectra, Dynamic phases of quantum systems, Semiclassical quantum mechanics.

1. Introduction

The excited-state quantum phase transition (ESQPT) is an extension of the notion of quantum phase transition (QPT) in an isolated (i.e., having no external thermal bath) quantum system to the excited domain. While a standard QPT [1–4] affects the ground state of the system and generates its singular evolution with a control parameter λ (an external field intensity or an internal coupling strength), the ESQPT affects the excited states (possibly a subset of them) and produces their singular variations with λ and the energy E . The ESQPT shows up as a non-analyticity of the level density and the level flow at the critical borderline $E = E_c(\lambda)$ in the plane $\lambda \times E$, and implies some anomalies in the structure of the Hamiltonian eigenvectors. The point $\lambda = \lambda_c$, where the curve $E_c(\lambda)$ eventually reaches the ground-state energy $E_{\text{gs}}(\lambda)$, becomes a QPT critical point, yielding non-analytic evolution of $E_{\text{gs}}(\lambda)$. In this sense, the ESQPTs extend the quantum phase diagrams from the line of λ to the plane $\lambda \times E$, similarly as thermal phase transitions (TPTs) extend these diagrams to temperatures $T > 0$ for systems that thermalize in contact with a bath. In analogy to QPTs and TPTs, the ESQPTs become nonanalytic only in the limit of infinite size of the system, $N \rightarrow \infty$. However, since finite-size precursors of the true singularity are often meaningful already for moderate size parameter N , it makes sense to study these effects in finite systems.

The notion of ESQPT has many predecessors (see below), but it was for the first time *explicitly* considered by Cejnar, Macek, Heinze, Jolie and Dobeš in Refs. [5, 6], closely following the results of Refs. [7, 8]. The idea was subsequently established on a firmer theoretical ground by Caprio, Cejnar and Iachello in Ref. [9], which gave several examples of ESQPTs in quantum many-body models with a single effective degree of freedom (DOF), $f = 1$. The ESQPT effects in systems with two DOFs, $f = 2$, were first mentioned by Cejnar and Stránský in Ref. [10] and then systematically investigated by the same authors together with Macek and Leviatan in the series of papers [11–13].

Most of the known ESQPTs are associated with stationary points of the underlying classical Hamiltonian at energies above the global minimum. Properties of the corresponding spectral singularity can be deduced from the type of the stationary point. The classification of the most common ESQPTs due to non-degenerate stationary points of the classical Hamiltonian (i.e., points having only non-zero eigenvalues of the Hessian matrix) for any f was given by Stránský and Cejnar in Ref. [14]. For such locally quadratic stationary points, the singularities appear in the $(f-1)$ st energy derivative of the smoothed (quasiclassical) level density $\bar{\rho}(E)$, which in an infinitesimal vicinity of the critical energy $E_c(\lambda)$ obeys the formula

$$\frac{\partial^{f-1}}{\partial E^{f-1}} \bar{\rho}(\lambda, E) \propto h(E) \pm \begin{cases} \theta[E - E_c(\lambda)] & \text{for even index,} \\ \ln|E - E_c(\lambda)| & \text{for odd index,} \end{cases} \quad (1)$$

where $h(E)$ is an unspecified smooth function and $\theta(x)$ denotes the step function ($\theta = 0$ for $x < 0$ and $\theta = 1$ for $x \geq 0$). The index of the non-degenerate stationary point (the number of negative eigenvalues of the Hessian matrix) is the number of independent directions in the phase space for which the stationary point represents a local maximum. This number, as we will see below, also determines the valid sign in Eq. (1). Qualitatively the same types of singularities appear in the $(f-1)$ st energy derivative of the smoothed flow $\bar{j}(\lambda, E)$ of individual energy levels with running parameter λ . On the other hand, the degenerate (flatter than quadratic) stationary points cause singularities in lower derivatives of the level density and flow. Some additional types of ESQPTs in bounded many-body systems were described in Ref. [13].

Today there exists extensive literature studying various effects of ESQPTs in numerous models, which is the reason for this review. These models in general describe many-body systems that exhibit some kind of collective dynamics with a moderate number of effective DOFs. They include quantum optical systems, qubits with long-range interactions, interacting boson systems describing collective motions of molecules, atomic nuclei and cold atoms, as well as interacting Fermi and Bose-Fermi systems. Effects connected with ESQPTs are reported in driven dynamics, thermodynamics and dissipation. Analogies of the ESQPT phenomenon exist in related areas of quantum physics. Particularly the following authors and groups made essential contribution to the ESQPT field: Brandes, Bastidas and Kopylov *et al.*, Iachello *et al.*, Pérez-Bernal and Pérez-Fernández *et al.*, Bastarrachea-Magnani and Hirsch *et al.*, and Relaño, Puebla and Dukelsky *et al.* The relevant references will be given below.

Before proceeding to these issues, we have to briefly mention the closely related (though usually more specialized) concepts preceding the notion of ESQPT. In systems with $f = 1$, the impact of *phase-space separatrix* on quantum spectra was studied in the early 1990s by Cary and Rusu [15, 16]. Continuation of such analyses in the many-body context [17–21] roughly coincides with the dawn of the ESQPT physics. We stress that diverging oscillation periods connected with crossing of a phase-space separatrix were experimentally measured in spinor Bose-Einstein condensates of ^{23}Na atoms [22].

Even an earlier predecessor of the ESQPT-focused research was the study of *monodromy* in integrable $f = 2$ systems, introduced by Duistermaat, Cushman and Vũ Ngoc in 1980s [23–25]. Monodromy represents a topological singularity in the system’s phase space, which disables a global introduction of action-angle variables. On the quantum level it exhibits as a defect in two-dimensional lattices of conserved quantum numbers associated with individual energy eigenstates, which was incorporated into the ESQPT phenomenology already in the first papers [5, 7, 8]. Note that these effects were verified in experimental spectra of some molecules, including H₂O [26, 27], which up to now remain the clearest spectroscopic examples of ESQPT singularities [52].

A very close antecedent of the ESQPT is the microcanonical thermodynamic singularity caused by a stationary point of classical dynamics, investigated already in 2000s by Franzosi and Pettini [29] and Kastner *et al.* [30–32]. We will see that these *microcanonical phase transitions* in a low- f systems are equivalent to ESQPTs. However, the cited works aimed more at the identification of an underlying mechanism of standard TPTs in systems with $\aleph \sim f \rightarrow \infty$ through some bulk properties of the microcanonical singularities.

The number of effective DOFs of the given system, as emphasized in connection with all the above-mentioned results, represents an essential characteristics of the ESQPT. Indeed, the low- f condition seems necessary to observe strong ESQPT signatures in not-too-high derivatives of the level density and flow. That is why ESQPTs are most commonly identified (at least under this name) in collective many-body systems, for which the size parameter \aleph can grow independently of the effective number of DOFs associated solely with some *collective modes* of motions.

However, various forms of criticality in excited states of isolated quantum systems were found in many-body systems with local interactions, for which non-collective DOFs play an important role and $\aleph \rightarrow \infty$ in general implies $f \rightarrow \infty$. One example is the so-called *metastable* QPT introduced by Carr *et al.* [33, 34] in a model describing Bose-Einstein condensation of locally interacting bosons on a ring. Similarly, the *eigenstate phase transition*, described by Huse *et al.* in the context of interacting spin and Majorana/Dirac fermion lattices [35, 36], characterizes the onset of many-body localization (breakdown of eigenstate thermalization) in individual excited states with varying Hamiltonian parameters. Another type of ESQPT-like criticalities in two-dimensional periodic lattice systems with local interactions is related to the old concept of the *van Hove singularity* [37]. The energy spectrum of a particle moving through such a lattice is determined via the dispersion relation in the quasimomentum space. Its extremes and saddles produce singularities in the single-particle density of states, which are observed in electronic and vibrational spectra of two-dimensional crystals like graphene [38–40].

The ESQPTs, as we understand them in this review, represent a merge of the above-mentioned specific incarnations. We propose three defining properties of the ESQPT: (i) It represents a non-analyticity of the discrete energy spectrum (Hamiltonian eigenstates) of an isolated bound quantum system in the $\aleph \rightarrow \infty$ limit. (ii) It typically (though not necessarily) extends the ground-state QPT in the same system. (iii) It originates in a singularity of the underlying classical dynamics.

Recent work on ESQPTs can be sorted to the following categories: recognition of ESQPTs in various specific models and identification of their signatures in quantum spectra and classical dynamics [13, 41–80], analysis of thermodynamic consequences of ESQPTs [81–87], search for dynamic effects caused by ESQPTs [88–105], and extension of the ESQPT concept out of its home territory [38, 106–110]. This division of literature

also roughly determines the structure of our review: Section 2 offers an opening example of a quantum system with several types of ESQPTs. Section 3 outlines a variety of models to which the notion of ESQPT has already been applied. Section 4 analyzes the model-independent typology of ESQPTs and describes their manifestation in energy spectra and eigenstates. Section 5 summarizes known thermodynamic consequences of ESQPTs. Section 6 describes various signatures of ESQPTs in driven dynamics. Section 7 reports on generalizations of ESQPTs to spatially extended, kicked and scattering systems. Section 8 brings conclusions.

Note that we take all quantities as dimensionless, i.e., expressed in suitable units carrying the respective dimension. This facilitates the theoretical analysis, but requires adjustment of all formulas to proper physical scales in particular implementations.

2. Opening example: Dicke superradiance models

As an invitation to the ESQPT field we outline in this section spectral signatures of ESQPTs in the Dicke model and its various extensions. The model we consider represents a slight modification [50] of the original Dicke Hamiltonian [111], known for its superradiant TPT and QPT. These transitions are nowadays available to experimental investigation by means of advanced quantum simulators [114–117]. The ESQPTs, whose structure is richer in the extended version of the model, may be detected by similar techniques in future. Studies of various aspects of ESQPTs in the Dicke and related models can be found, e.g, in Refs. [49–51, 53, 54, 56, 58, 61–63, 65, 67, 69, 73, 74, 77, 79] (identification of ESQPTs and their various signatures), [81, 83] (thermodynamic properties) and [90, 99, 101, 105] (dynamic consequences).

2.1. The model and its thermal and quantum phase transitions

At first we describe the model and its standard phase transitions. The model was proposed in the 1950s to illustrate the effect of dynamic superradiance, i.e., collectivity-enhanced coherent irradiation of atoms in a cavity [111]. It can be cast as a schematic description of the interaction of one-mode electromagnetic field with a dense ensemble of N two-level atoms. Photons with energy ω are created and annihilated by operators \hat{b}^\dagger and \hat{b} . The ensemble of atoms is described by operators

$$\hat{J}_0 = \frac{1}{2} \sum_{i=1}^N \hat{\sigma}_0^{(i)}, \quad \hat{J}_+ = \frac{1}{2} \sum_{i=1}^N \hat{\sigma}_+^{(i)}, \quad \hat{J}_- = \frac{1}{2} \sum_{i=1}^N \hat{\sigma}_-^{(i)}, \quad (2)$$

where $\hat{\sigma}_0^{(i)} = \hat{\sigma}_z^{(i)}$ and $\hat{\sigma}_\pm^{(i)} = \hat{\sigma}_x^{(i)} \pm i\hat{\sigma}_y^{(i)}$ are Pauli matrices in the two-dimensional space of the i th atom with level energies $\pm\omega_0/2$. The total Hilbert space of the system is the direct product $\mathcal{H} = \mathcal{H}_A \otimes \mathcal{H}_B$, where \mathcal{H}_A is a 2^N -dimensional Hilbert space of the atomic subsystem, spanned by all combinations of $\hat{\sigma}_z^{(i)}$ eigenstates of individual atoms, and \mathcal{H}_B is an infinite-dimensional Hilbert space of the boson field, spanned by basis vectors describing states with 0, 1, 2... field quanta.

The model represents an elementary example of a *coupled system*. A general discussion of such systems, including proper definition of their size parameters, will be outlined in Sec. 4.3. In the following, we assume that elementary excitation energies ω and ω_0 of both subsystems are of the same order of magnitude. Arbitrary redistribution of a given energy E between the field and atoms then implies roughly the same overall numbers of excitation quanta—photons, excited atoms, or the sum

of both. In this situation the number of atoms N is a good measure of the system's total size, so we set $N = N$. Asymmetric regimes with $\omega \ll \omega_0$ or $\omega \gg \omega_0$ need to be treated differently, see Sec. 2.3.

The Hamiltonian of the extended Dicke model reads

$$\hat{H}(\lambda, \delta) = \underbrace{\omega \hat{b}^\dagger \hat{b} + \omega_0 \hat{J}_0}_{\hat{H}_0} + \underbrace{\lambda \frac{1}{\sqrt{N}} (\hat{b}^\dagger \hat{J}_- + \hat{b} \hat{J}_+ + \delta \hat{b}^\dagger \hat{J}_+ + \delta \hat{b} \hat{J}_-)}_{\hat{H}'(\delta)}, \quad (3)$$

where λ and δ are two control parameters [50]. The first parameter, $\lambda \in [0, \infty)$, represents the overall field-atom coupling strength. The second parameter, $\delta \in [0, 1]$, weights so-called counter-rotating terms in the interaction Hamiltonian $\hat{H}'(\delta)$ [112]. The latter parameter extends the original Dicke model which has $\delta = 1$ [111]. The $\delta = 0$ limit represents an integrable, so-called Tavis-Cummings version of the model [113]. The variation of δ between these limiting values realizes the crossover between completely regular Tavis-Cummings (TC) and more chaotic Dicke (D) regimes. We note that our present “extended Dicke model” differs from various other extensions used under similar names, see, e.g., Refs. [77, 118].

In the weak-coupling regime, for λ small, the excited states of the non-interacting $\lambda = 0$ system shows the dynamic superradiance, i.e., a non-exponential (flash-like) decay of the atomic ensemble from its fully excited to fully de-excited state. This is a consequence of uniformity of the atom-field interaction [111]. However, the model exhibits also another type of superradiance—the one encoded in its equilibrium properties at low temperatures for large values of the coupling strength λ [119, 120]. In particular, for λ above a critical value $\lambda_c(\delta) = \sqrt{\omega \omega_0}/(1 + \delta)$ there exists a certain critical temperature $T_c(\lambda, \delta)$ such that the equilibrium phase below T_c (so-called *superradiant phase*) generates macroscopic excitation of both atomic and field subsystems while the phase above T_c (*normal phase*) resembles the non-interacting regime. The transition has a critical character and is classified as a second-order TPT.

Soon after the first phase-transitional analysis of the Dicke model [119, 120] it was pointed out that the inclusion of the physical term proportional to squared electromagnetic vector potential into the Hamiltonian of the type (3) destroys its critical properties [121]. However, as turned out later (see, e.g., Ref. [122]), an effective Hamiltonian of the form (3) is approximately valid in the setup of confined quantum optical systems, which is relevant in many present-day laboratory realizations. In these situations, the above-described critical properties are realistic. In particular, the parameter value $\lambda_c(\delta)$ defined in the previous paragraph represents the quantum critical point where the critical temperature $T_c(\lambda, \delta)$ is zero and the system therefore exhibits a QPT from the normal to superradiant phase in its *ground state*. This continuous (second-order) phase transition and its quantum signatures were for the first time studied theoretically by Emery and Brandes [123, 124]. The transition was recently verified experimentally by Baumann *et. al.* [114, 115] using the Bose gas confined in an optical cavity.

The Hamiltonian (3) obviously conserves the quantity $\hat{\mathbf{J}}^2 = \hat{J}_x^2 + \hat{J}_y^2 + \hat{J}_z^2$ whose spin-like quantum number j can be set to any integer or half-integer value from $j_{\min} = 0$ or $\frac{1}{2}$ (for N even or odd, respectively) to $j_{\max} = \frac{1}{2}N$. The physical meaning of j will be discussed in Sec. 3.1, for now we just note that its most usual choice is $j = j_{\max}$, which selects a subspace $\mathcal{H}_{j_{\max}} \subset \mathcal{H}_A$ which is fully symmetric with respect to all permutations of atoms. This subspace is invariant under the action

of the evolution operator and enables one to constitute a representation in terms of coordinate and momentum operators $\hat{\phi}$ and $\hat{\zeta}$ in the following way:

$$\begin{pmatrix} \hat{J}_x \\ \hat{J}_y \\ \hat{J}_z \end{pmatrix} = \sqrt{j(j+1)} \begin{pmatrix} \sqrt{1 - \hat{\zeta}^2} \cos \hat{\phi} \\ \sqrt{1 - \hat{\zeta}^2} \sin \hat{\phi} \\ \hat{\zeta} \end{pmatrix} \quad \text{with } [\hat{\phi}, \hat{\zeta}] = \frac{i}{\sqrt{j(j+1)}}. \quad (4)$$

The number $[j(j+1)]^{-1/2}$, which for $j = j_{\max}$ and $N \gg 1$ roughly equals to $2/N$, plays the role of an effective Planck constant of the model. The system therefore becomes classical in the $N \rightarrow \infty$ limit with $[\hat{\phi}, \hat{\zeta}] \rightarrow 0$. In this limit, the coordinate and momentum are ordinary numbers $\phi \in [0, 2\pi]$ and $\zeta \in [-1, +1]$, and the sphere (so-called Bloch sphere) of radius $\sqrt{j(j+1)} \approx j$ with spherical angles $\theta \equiv \arccos \zeta$ and ϕ represents the classical phase space of the atomic subsystem.

The classical limit of the field subsystem can be constructed via the coordinate-momentum representation of the boson operators

$$\begin{pmatrix} \hat{b}^\dagger \\ \hat{b} \end{pmatrix} = \sqrt{\frac{\varkappa}{2}} \begin{pmatrix} \hat{q} - i\hat{p} \\ \hat{q} + i\hat{p} \end{pmatrix} \quad \text{with } [\hat{q}, \hat{p}] = \frac{i}{\varkappa}, \quad (5)$$

where \varkappa is an adjustable parameter quantifying classicality of the field subsystem. The choice $\varkappa = \sqrt{j(j+1)}$ yields the same value of the effective Planck constant as above (this symmetric choice is justified for balanced systems with comparable energies ω and ω_0). So the number of DOFs of our atom-field system is $f = 2$, the corresponding phase space \mathcal{P} being identified with the Cartesian product $\mathcal{P}_A \times \mathcal{P}_B$, where the finite phase space \mathcal{P}_A of the atomic ensemble with a fixed j is the Bloch sphere (ϕ, ζ) and the infinite phase space \mathcal{P}_B of the field is the plane of variables (q, p) .

We observe that a general Hamiltonian (3) changes the overall number of field and atomic excitations only by numbers 0 or 2, so it has an additional integral of motion represented by a parity operator $\hat{\Pi} = (-1)^{\hat{M}}$, where $\hat{M} = \hat{N}_b + \hat{N}_*$ is a sum of the number of field bosons $\hat{N}_b = \hat{b}^\dagger \hat{b}$ and the number of excited atoms expressed for any fixed value of j as $\hat{N}_* = \hat{J}_z + j$. This discrete symmetry is spontaneously broken in the superradiant QPT. Indeed, it turns out that while in the normal phase the ground state has positive parity, in the superradiant phase in the limit $N \rightarrow \infty$ the lowest energy states with positive and negative parity become degenerate and allow for parity-violating ground-state solutions.

It is easy to check that for $\delta = 0$ the quantity \hat{M} itself becomes an integral of motion, making the TC version of the model fully integrable. As shown in Refs. [73, 74], this conservation law enables one to construct, for any fixed value M of \hat{M} , a canonical transformation from the four-dimensional ($f = 2$) phase space defined by two independent pairs of conjugate variables (ϕ, ζ) and (q, p) , describing separately the atoms and the field, to a two-dimensional ($f = 1$) phase space with a single pair of coupled atom-field variables.

2.2. Singularities in excited-state spectra

Besides the above-outlined TPT and QPT, the extended Dicke model exhibits also several types of ESQPTs. The key quantity allowing us to detect these effects is the density of energy eigenstates, or shortly the *level density*. This is defined as

$$\rho(E) = \sum_i \delta(E - E_i), \quad (6)$$

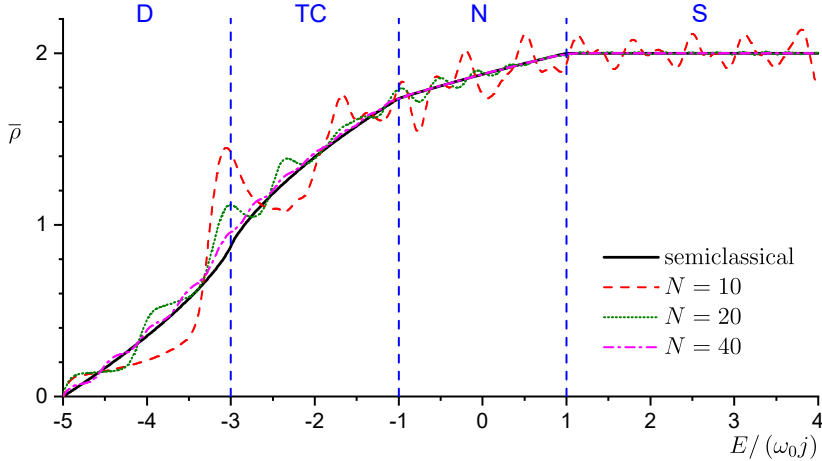


Figure 1. The energy dependence of the smoothed level density $\bar{\rho}(E)$ of the extended Dicke Hamiltonian (3) with $\omega = \omega_0 = 1$, $\lambda = 2.78$, $\delta = 0.132$ in the $j = \frac{1}{2}N$ subspace. Various curves represent dependencies for several finite values of N obtained by numerical smoothing according to formula (7) with $\sigma = 0.1$. The full curve is calculated by the semiclassical $N \rightarrow \infty$ formula (26). Vertical lines indicate ESQPT critical energies and acronyms D, TC and N mark quantum phases between these energies (see below).

where E_i represent discrete eigenvalues of a general Hamiltonian of any bound quantum system (for the moment we skip their dependence on control parameters). The level density as a chain of δ functions is usually smoothed by folding with a convenient normalized distribution function $\bar{\delta}(E)$, typically the Gaussian with zero mean and variance σ^2 such that the width σ is larger than an average distance between neighboring levels. In this way we obtain a smoothed level density

$$\bar{\rho}(E) = \int dE' \bar{\delta}(E - E') \rho(E') = \sum_i \bar{\delta}(E - E_i). \quad (7)$$

Figure 1 depicts the smoothed level density of the extended Dicke Hamiltonian (3) in the subspace with $j = j_{\max}$ for parameters specified in the caption and for several values of N . We observe that with increasing N the level density converges to an asymptotic dependence shown by the full curve. It will be explained in Sec. 4.1 that this $N \rightarrow \infty$ curve can be obtained independently of smoothing parameter σ by means of semiclassical techniques involving the phase-space integration. This asymptotic curve has three points of non-analyticity at energies indicated by the vertical dashed lines. At the second and third line, the curve $\bar{\rho}(E)$ shows a break, so the slope $\frac{\partial}{\partial E} \bar{\rho}(E)$ jumps. At the first line, $\bar{\rho}(E)$ has a vertical tangent, so $\frac{\partial}{\partial E} \bar{\rho}(E)$ locally diverges. In view of Eq. (1) we can say that these singularities represent typical signatures of ESQPTs in systems with $f = 2$.

Level densities $\rho(E)$ and $\bar{\rho}(E)$ depend on the control parameters of the system. The behavior of the slope $\frac{\partial}{\partial E} \bar{\rho}(E)$ in the plane $\lambda \times E$ is presented (for other model parameters fixed at the values indicated) in Fig. 2. We see that the singularities from Fig. 1, namely the jumps and divergences of the level-density first derivative, exist within the whole $\lambda \times E$ plane and in some cases join to the QPT nonanalyticity affecting the ground state. The curves where the level-density derivative is singular

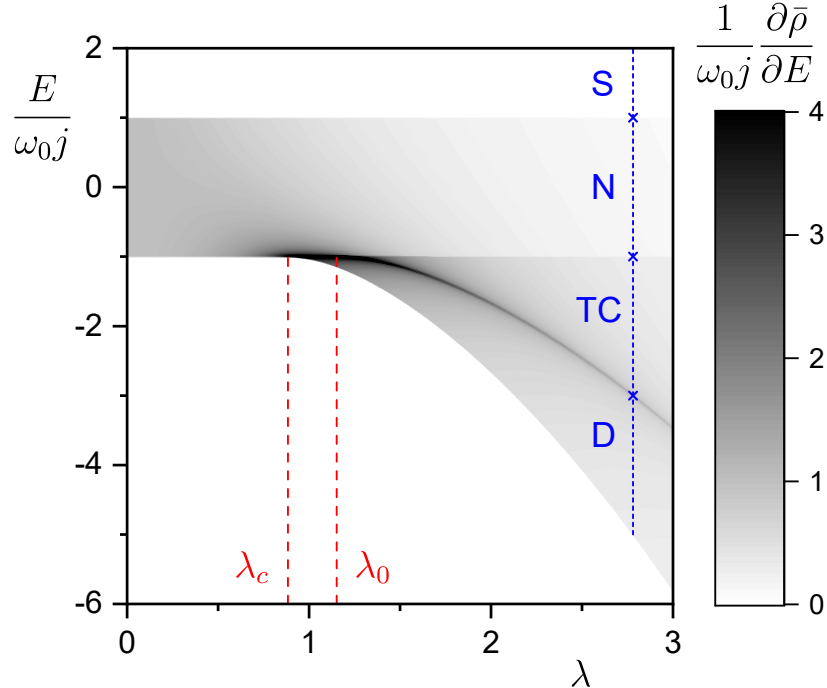


Figure 2. The first energy derivative of the smoothed level density (encoded in the shades of gray) for Hamiltonian (3) with $\omega = \omega_0 = 1$, $\delta = 0.132$ and $j = \frac{1}{2}N$ as a function of the coupling parameter λ and energy E . The ground-state QPT is the sudden drop of the lowest energy at $\lambda = \lambda_c$, while the ESQPTs show as jumps or divergences of the level density derivative (λ_0 is a branch point of two such singularities). The vertical line with crosses at the corresponding ESQPT critical energies marks the value $\lambda = 2.78$ used in Figs. 1 and 3. Adapted from Ref. [125].

define *critical borderlines* of the ESQPTs in our model. These curves separate domains in the spectrum of excited energy eigenstates that will be later identified with different *quantum phases* of the model (here distinguished by acronyms D, TC, N and S explained below). For the critical borderlines in Fig. 2 there exist simple analytic expressions derived, e.g., in Ref. [73].

To see the ESQPT spectral singularities from another perspective, we present in Fig. 3 a so-called *Peres lattice* of the quantity $\hat{A} \propto \frac{\partial}{\partial \lambda} \hat{H}(\lambda, \delta) = \hat{H}'(\delta)$ at the value of λ corresponding to the vertical line in Fig. 2 and the other parameters being the same as in this figure. Observable $\hat{H}'(\delta)$ in the extended Dicke model, see Eq. (3), describes the collective atom-field interaction Hamiltonian.

In general, the Peres lattice displays expectation values $\langle \hat{A} \rangle_i = \langle \psi_i | \hat{A} | \psi_i \rangle$ of any observable \hat{A} in the eigenstates $|\psi_i\rangle$ of the Hamiltonian of a bound quantum system as a mesh in the plane $E_i \times \langle \hat{A} \rangle_i$. This kind of representation of discrete spectra was used to distinguish regular and chaotic subsets of eigenstates, or to identify other relevant dynamic properties by which the spectrum can be sorted. Peres lattices also visualize effects of ESQPTs. Indeed, in Fig. 3 we can notice that the ESQPT critical energies of the extended Dicke model (cf. Fig. 2) split the lattice into domains showing

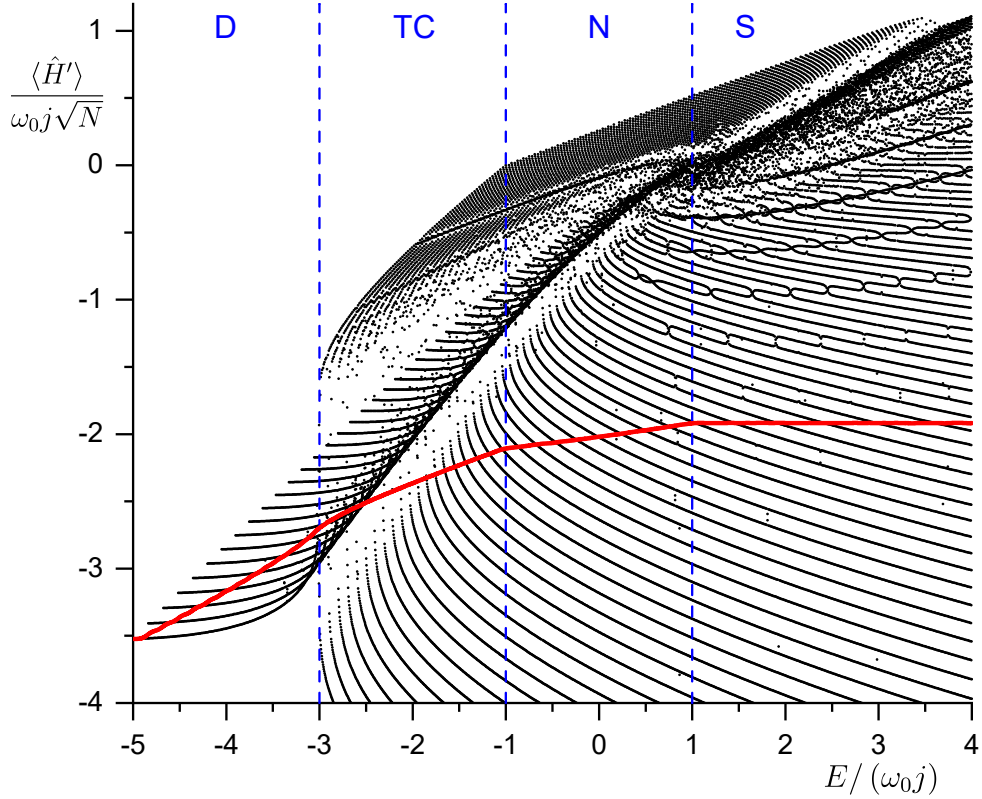


Figure 3. Peres lattice for observable $\propto \hat{H}'(\delta)$ of the model (3) with $\lambda = 2.78$ (see the vertical line in Fig. 2), $\delta = 0.132$, $\omega = \omega_0 = 1$ and $N = 2j = 120$. The red curve shows the smoothed energy dependence (8). Vertical lines mark the ESQPT critical energies (the same as in Fig. 1). Adapted from Ref. [125].

partially different arrangements of points. At each critical borderline, there is a certain qualitative feature of the lattice that changes abruptly, while between the borderlines the qualitative features of the lattice remain the same. It is clear that the specific types of such changes must be strongly model-dependent, but we anticipate that ESQPTs in a general system imply some qualitative changes of patterns observed in Peres lattices of any generic observable. In the present model we use the following abbreviated names of the quantum phases: Acronyms D and TC stand for Dicke and Tavis-Cummings types of superradiant phase (the corresponding Peres lattices are closer to the $\delta = 1$ and 0 limits, respectively), N denotes the normal (i.e., non-superradiant) phase, and S marks the “saturated” phase (with constant level density, see Figs. 1 and 2). More information can be found in Ref. [73].

Given a general observable \hat{A} , we define its *energy density* in the discrete spectrum: $A(E) = \sum_i \langle \hat{A} \rangle_i \delta(E - E_i)$. The corresponding smoothed density

$$\bar{A}(E) = \sum_i \langle \hat{A} \rangle_i \bar{\delta}(E - E_i). \quad (8)$$

can be also used for detection of ESQPTs. The quantity in Eq. (8), obtained by a local smoothening of points in the Peres lattice $E_i \times \langle \hat{A} \rangle_i$, exhibits singularities at the

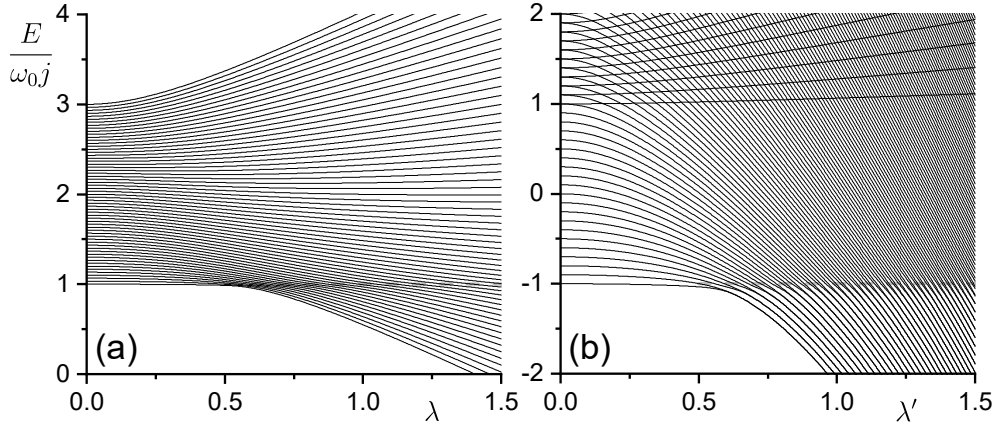


Figure 4. The $f = 1$ ESQPT structures (marked by gray dashed lines) in the Tavis-Cummings (a) and Rabi (b) regimes of the Dicke model. Panel (a) depicts the spectrum of $M = 2j = N$ states of the $\delta = 0$ Hamiltonian with $\omega = 2, \omega_0 = 1$ for $N = 60$. Panel (b) shows the spectrum of the $N = 1 = 2j$ system with $\omega = 1, \omega_0 = R\omega = 20$ and $\delta = 1$.

ESQPT critical borderlines. In Sec. 4.2 we will see that the type of singularity in $\bar{A}(E)$ likely coincides with the type of singularity in $\bar{\rho}(E)$. For the extended Dicke model this is illustrated in Fig. 3, where the smoothed energy density of the observable $\propto \hat{H}'(\delta)$ is shown by the thick red curve. We see breaks of the curve at the ESQPT energies between various quantum phases. Let us point out that moderate-size calculations do not allow us to unambiguously detect the assumingly diverging slope of the smoothed energy density of $\hat{H}'(\delta)$ at the interface between the D and TC phases (cf. Fig. 2).

2.3. Tavis-Cummings and Rabi regimes

We have seen that the extended Dicke model shows ESQPTs in the first derivative of the level density, as expected for the number of DOFs $f = 2$. However, the model also presents special regimes in which exact or approximate integrals of motions enable us to apply to specific subsets of states effective descriptions with $f = 1$. Some of these subsets show abrupt changes of the lowest energy state, in a full analogy to the ground-state QPT, while the spectra of states with higher energies exhibit ESQPT singularities. Due to the reduced DOF number, these ESQPTs affect the zeroth instead of first derivative of the level density and produce sharper signatures in Peres lattices.

An immediate example of such a regime is the *Tavis-Cummings version* of the extended Dicke Hamiltonian (3) with $\delta = 0$. As explained above, the model in this case conserves the summed number of atomic and field excitations \hat{M} and for each fixed value M a canonical transformation maps the system to a reduced $f = 1$ phase space [73, 74]. The λ -dependent spectra of states in a given M -subspace can be analyzed independently from other M -subspaces. The dimension of these subspaces is $M + 1$ for $M \leq 2j$ and $2j + 1$ for $M > 2j$. The value $M = 2j$ is critical not only because it is the highest M number that permits states with $N_b = 0$, but also because the corresponding spectrum exhibits both QPT and ESQPT effects in the limit $N, j \rightarrow \infty$ [49, 73, 74, 90]. A finite- N sample of the $M = 2j$ spectrum is shown in panel

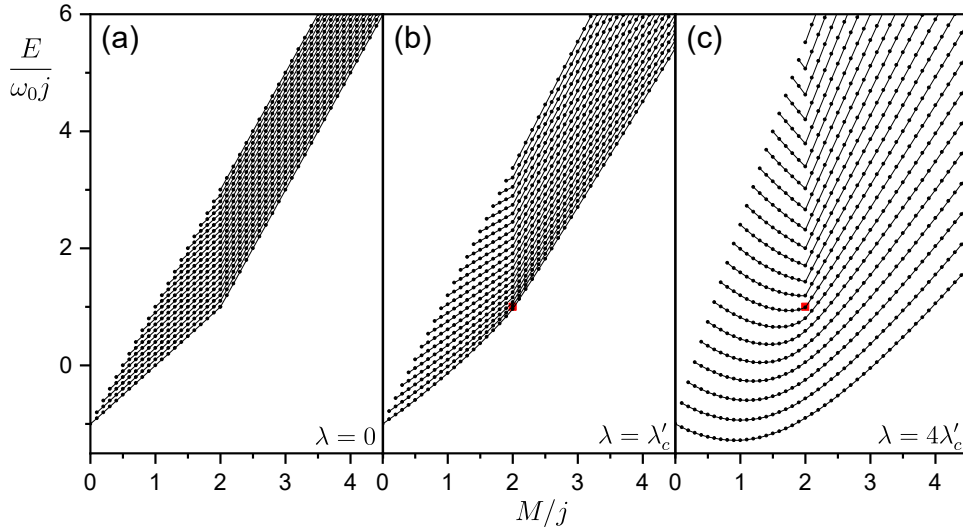


Figure 5. Peres lattices of the Tavis-Cummings Hamiltonian in the plane M vs. E for three values of λ indicated in panels (a)–(c). The critical interaction strength is $\lambda'_c = 0.5$, see Fig. 4(a). The other parameters are as follows: $\omega = 2$, $\omega_0 = 1$ and $N = 2j = 20$. The QPT and ESQPT points of the $M = 2j$ spectrum are marked by the red rectangle. In panel (c) this rectangle represents a point defect of the lattice indicating quantum monodromy.

(a) of Fig. 4. We observe a precursor of a second-order QPT at a critical value of λ equal to $\frac{1}{2}|\omega - \omega_0|$ [different from the critical coupling $\lambda_c(\delta = 0)$ associated with the global ground state of the whole model] and a subsequent bunching of states indicating divergent density of states at the ESQPT above the critical point. This is the most familiar form of ESQPT present in numerous $f = 1$ models, which initiated the study of ESQPTs in the past [5–9] and represents the case most discussed in the literature up to now (cf. Sec. 3).

Peres lattices of the TC Hamiltonian with $\omega = 2\omega_0$ for various values of parameter λ are presented in Fig. 5. The energy is on the vertical axis, while the horizontal axis shows values of M ; so both axes now correspond to conserved quantities, in contrast to Fig. 3. The vertical chain of points at $M/j = 2$ represents the energy spectrum of the critical M -subspace. Figure 5 in its three panels depicts lattices at (a) $\lambda = 0$ (non-interacting case), (b) $\lambda = \lambda'_c$ (the QPT critical value for $M = 2j$), and at $\lambda = 4\lambda'_c$ (the case with ESQPT). The red rectangle in panel (b) corresponds to the critical-point ground state of the $M = 2j$ subset of states [cf. Fig. 4(a)] and that in panel (c) marks the critical ESQPT energy $E'_c = \omega_0 j$.

In panel (a) of Fig. 5 we see that all lines connecting points with the same principal quantum number $i = 0, 1, \dots$ enumerating energy levels E_{Mi} exhibit a break at $M = 2j$. This is so because above this value the increase of M is possible only by adding photons whose energy ω differs from energy ω_0 of the atomic excitation quantum (the break angle depends on these energies). The form of the lattice remains qualitatively the same for $\lambda \leq \lambda'_c$ (panel b), but for $\lambda > \lambda'_c$ (panel c) the lattice gets split into the upper part with the V-shaped break of the constant- i lines, and the lower part with a U-shaped bent of these lines. The central point (the red rectangle) separating these

structures at the ESQPT energy E'_c of the $M = 2j$ spectrum represents a point defect of the whole lattice. It can be demonstrated that elementary cells of the lattice are getting distorted on a path around the defect so that after completing a full circle the final cell differs from the initial one. This is a manifestation of quantum monodromy—a specific anomaly in quantized spectra of some integrable systems associated with the existence of a singular bundle of classical trajectories in the phase space [23–25]. Classical and quantum monodromy in the context of the TC model was studied in Refs. [74, 126]. We note that the connection of ESQPTS to monodromy was described in a number of other integrable models with $f = 2$, particularly in the molecular vibron models [48, 52] and in the nuclear interacting boson model along the transition between $U(5)$ and $SO(6)$ dynamical symmetries [5–8], see Sec. 3.2.

Another possibility to reduce the number of DOFs in the Dicke model is connected with the *Rabi regime*, achieved under the condition of adiabatic separation of atomic and field variables [65, 69]. In particular, we assume that the atom to photon energy ratio $R = \omega_0/\omega$ is very large, $R \gg 1$. This violates the above-mentioned assumption of comparable energy costs for excitations of both subsystems. As the expected number of photons $\langle \hat{N}_b \rangle_i$ in a typical eigenstate $|\psi_i\rangle$ at energies $E_i \sim N\omega_0$ fairly exceeds the expected number of atomic excitations $\langle \hat{N}_* \rangle_i$, the field and atomic subsystems need to be characterized by different size parameters. It turns out (cf. Sec. 4.3) that convenient size parameters are N for the atomic subsystem and NR for the field subsystem. Using the coordinate-momentum representation of the field operators from Eq. (5) with $\kappa = NR$, we rewrite the Hamiltonian (3) in the form

$$\frac{\hat{H}}{NR} = -\frac{\omega}{2NR} + \frac{\omega}{2}(\hat{q}^2 + \hat{p}^2) + \underbrace{\left(\sqrt{2}\lambda'(1+\delta)\hat{q}, \sqrt{2}\lambda'(1-\delta)\hat{p}, \frac{\omega}{N}\right)}_{\hat{\mathbf{B}}} \cdot \hat{\mathbf{J}} \quad (9)$$

with $\hat{\mathbf{J}} \equiv (\hat{J}_x, \hat{J}_y, \hat{J}_z)$ and $\lambda' = \lambda/NR^{1/2}$.

For very large values of R the field subsystem is close to the classical limit, so the field operators (\hat{q}, \hat{p}) can be replaced by the corresponding classical variables (q, p) . The operators $\hat{\mathbf{B}}$ in Eq. (9) turn into ordinary numbers \mathbf{B} and the Hamiltonian becomes a (q, p) dependent operator acting solely in the atomic Hilbert space \mathcal{H}_A . Defining $\hat{J}_{z'} = \mathbf{B} \cdot \hat{\mathbf{J}} / |\mathbf{B}|$ as the quasispin operator projected to a new z' axis pointing along the $\mathbf{B}/|\mathbf{B}|$ direction, the diagonalization of the Hamiltonian (9) becomes trivial. The eigenenergies $E_{m'}(q, p)$ are enumerated by the projection quantum number $m' = -j, \dots, +j$ of the operator $\hat{J}_{z'}$ and depend on the field variables. They can be interpreted as effective classical Hamiltonians $H_{m'}(q, p)$ controlling slow dynamics of the field subsystem for individual fixed quasispin projections m' . Semiclassical quantization of the field states for each of these effective Hamiltonians yields a discrete energy spectrum enumerated by $i = 1, 2, \dots$. The full spectrum resulting from this procedure is labeled by a pair of quantum numbers m' and i , and consists of bands of densely spaced field excitations distinguished by i built on sparsely spaced atomic excitations characterized by m' . In this approximation, the energies $E_{m'i}$ of levels in different m' bands can cross each other without repulsion, which is a consequence of the approximate integral of motion $\hat{J}_{z'}$.

As follows from Eq. (9), some of the effective classical-limit Hamiltonian $H_{m'}(q, p)$ that determine the states within the same m' band undergo a phase transitional change. In particular, for $m' < 0$, at a certain critical value of λ' , for $m' = -\frac{1}{2}N$ equal to $\omega/N(1+\delta)$, the $(q, p) = 0$ global minimum of $H_{m'}(q, p)$ switches into a local maximum. Hence the bandhead state ($i = 1$) shows a transition interpreted as a

QPT, and an accompanying ESQPT structure corresponding to the DOF number $f = 1$ is observed in the spectrum of excited states ($i > 1$). For $\delta < 1$, the system even exhibits ESQPTs of several types, in analogy to the richer ESQPT structure of the extended Dicke model. As the size parameter that determines the sharpness of these critical effects is associated with R rather than N , well developed phase-transitional structures can be studied even in a system with $N = 1$ [63, 127]. An example of such a spectrum is shown in panel (b) of Fig. 4.

The above treatment of the Rabi regime is a specific application of the Born-Oppenheimer approximation based on an adiabatic separation of slow and fast modes of motions. Numerous other examples exist within the models overviewed in Sec. 3. A general discussion of ESQPT effects in such imbalanced systems will continue in Sec. 4.3

3. Zoo of collective many-body models

Proceeding from the atom-field system discussed above, we overview in this section a variety of other many-body systems whose quantal spectra were proven to show similar ESQPT singularities. A common property of these systems is a moderate number f of collective DOFs, which implies that the limit of infinite number of constituents can be associated with the classical limit of the collective dynamics.

3.1. Quasispin systems

We start with a class of models describing a collection of N interacting two-state systems (qubits). Individual qubits, represented for instance by spin- $\frac{1}{2}$ particles or two-level atoms, are connected with identical two-dimensional Hilbert spaces $\mathcal{H}^{(i)} = \mathbb{C}^2$ enumerated by $i = 1, 2, \dots, N$. So the Hilbert space of the N -qubit system is $\mathcal{H} = \bigotimes_{i=1}^N \mathcal{H}^{(i)}$ with overall dimension $d = 2^N$. Observables related to each qubit can be written in terms of Pauli matrices $\hat{\sigma}_\alpha^{(i)}$, with $\alpha = (0, +, -)$ or (x, y, z) , and the unit operator $\hat{I}^{(i)}$ acting in the respective space. As operators $\frac{1}{2}\hat{\sigma}_\alpha^{(i)}$ have commutation relations of spin, we unify the present kind of models under the term “quasispin”. In this sense, the atoms in the Dicke model form a quasispin subsystem. In the same way as described in Sec. 2.1, each qubit can be attributed by an elementary Bloch sphere with radius $\frac{\sqrt{3}}{2}$ and can therefore be associated with a single DOFs. The full N -qubit system has $f = N$ quantum DOFs which do not become classical as $N \rightarrow \infty$.

Each qubit is supposed to have the same self-Hamiltonian such as $\hat{H}_0^{(i)} = \frac{1}{2}\omega\hat{\sigma}_z^{(i)}$, where ω is the difference between energy levels. Hence the non-interacting part of an N -qubit Hamiltonian reads $\hat{H}_0 = \sum_{i=1}^N \hat{H}_0^{(i)} = \omega\hat{J}_z$, cf. Eq. (2). The interaction between qubits is usually assumed to be of the two-body type, so the coupling between i th and i' th qubits is written in terms of expressions like $[\hat{\sigma}_\alpha^{(i)}\hat{\sigma}_{\alpha'}^{(i')} + \text{H.c.}]$. For example, the celebrated *Ising model* associates the qubits with spins, assuming the Hamiltonian

$$\hat{H} = B\hat{J}_z - A \sum_{\langle ii' \rangle} \hat{\sigma}_x^{(i)}\hat{\sigma}_x^{(i')}, \quad (10)$$

where coefficient B measures one-body interactions of individual spins with a magnetic field in direction z , and A quantifies the strength of mutual two-body interactions between spins. The spins are located in vertices of a spatial grid of dimension D and their interactions involve only the spin pairs with the smallest distance in the grid (closest neighbors); this is expressed by the symbol $\langle ii' \rangle$ in the sum.

The model (10) has the well known phase structure. For $D \geq 2$ grids, at a certain critical temperature T_c , it shows a TPT between the ferromagnetic ($T < T_c$) and paramagnetic ($T > T_c$) thermal phases. Quantitative description of this transition requires the use of the renormalization group theory [128]. For arbitrary D , at some critical value of the ratio $\eta = B/A$ (for $D \geq 2$ coinciding with the place where $T_c = 0$), the model also shows a QPT between the ferromagnetic ($\eta < \eta_c$) and paramagnetic ($\eta > \eta_c$) ground-state phases [3]. However, the equality $f = N$ disables observations of ESQPTs as the condition $N \rightarrow \infty$ implies $f \rightarrow \infty$ and does not lead to the classical limit. The ESQPTs appear in quasispin systems only if a kind of collectivity reduces the number of effective DOFs to a moderate value not increasing with N .

The commonly discussed example of this collective behavior is the case of infinite-range interactions, i.e., interactions connecting with the same strength any pair of spins in the ensemble. Such modification of Hamiltonian (10) leads to

$$\hat{H} = B\hat{J}_z - \frac{A}{N} \sum_{i < i'} \hat{\sigma}_x^{(i)} \hat{\sigma}_x^{(i')} = B\hat{J}_z - \frac{A}{N} \hat{J}_x^2 + \frac{A}{4}, \quad (11)$$

where we used the collective quasispin operators from Eq. (2). The interaction strength is attenuated with increasing N to prevent complete dominance of the interaction term in the total energy for $N \rightarrow \infty$. Hamiltonian (11) is a special case of what is called the *Lipkin-Meshkov-Glick model*, or simply the Lipkin model [130]. It replaces the multiple SU(2) algebras of quasispin operators $\frac{1}{2}\hat{\sigma}_\alpha^{(i)}$ associated with individual qubits by a single SU(2) algebra of the collective quasispin operators \hat{J}_α . Hence a unique collective Bloch sphere can be attributed to the whole system, reducing the number of DOFs to $f = 1$.

Hamiltonian (11) and all its variations written in terms of collective operators \hat{J}_α ,

$$\hat{H} = \omega \hat{J}_z + \sum_{\alpha, \alpha'} \frac{\chi_{\alpha \alpha'}}{2N} \left(\hat{J}_\alpha \hat{J}_{\alpha'} + \hat{J}_{\alpha'}^\dagger \hat{J}_\alpha^\dagger \right) + \dots, \quad (12)$$

where ω and $\chi_{\alpha \alpha'}$ (and so on) are coefficients at linear, quadratic (and eventually higher) terms, conserve the total squared quasispin $\hat{\mathbf{J}}^2$. Subspaces of the full Hilbert space \mathcal{H} with a fixed value of j are dynamically invariant, i.e., if the initial state is in this subspace, the evolved state never goes out. To investigate the dynamics of the model, one can therefore choose any of these subspaces.

Properties of subspaces with different j were discussed for instance in Ref. [129]. As already mentioned in Sec. 2.1, the values of j are integers (for N even) or half-integers (for N odd) between 0 and $\frac{1}{2}N$. For each j , the total quasispin projection takes $2j+1$ values from $-j$ to $+j$. The match with the exponential overall dimension $d = 2^N$ of the full space \mathcal{H} is achieved because the subspaces of states with a given j appear in multiple replicas $\mathcal{H}_j^{(s)}$ enumerated by number s , so we can write: $\mathcal{H} = \bigoplus_{j=j_{\min}}^{j_{\max}} \bigoplus_{s=1}^{\nu_j} \mathcal{H}_j^{(s)}$. The multiplicity ν_j of the space with given j is a very large number for $0 \ll j \ll \frac{1}{2}N$. The subspaces differ in the symmetry with respect to exchange of qubits. Each value j is associated with a particular form of the Young tableaux and various replicas $\mathcal{H}_j^{(s)}$ correspond to various permutations of qubits within this tableaux (note that due to the symmetry of operators \hat{J}_α under the qubit exchange, the above-mentioned dynamical invariance concerns each of the replica subspaces separately). For a given j , the number $N - 2j$ counts qubits that appear in exchange antisymmetric states, mutually compensating their contributions

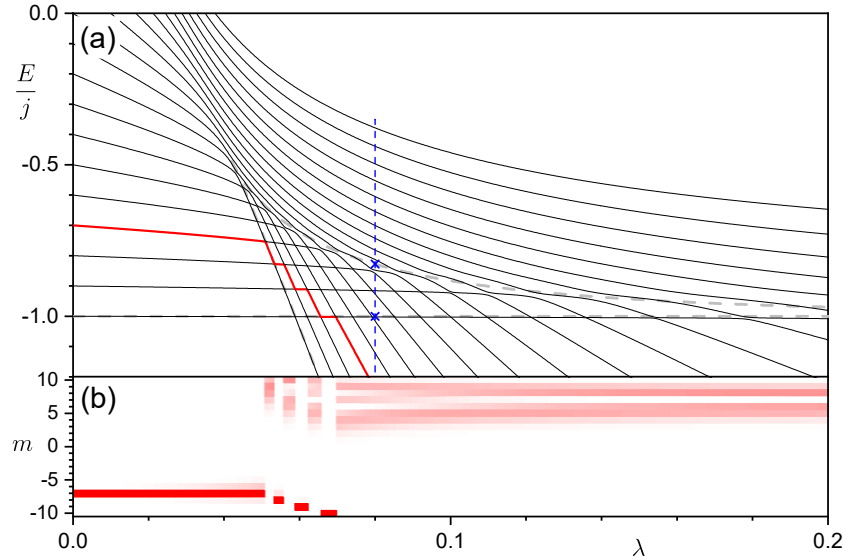


Figure 6. The ESQPT structures in the spectrum of the Lipkin Hamiltonian (13) with $\chi = 4$ with running parameter λ for $N = 2j = 20$. Panel (a): Energy levels (full curves) are shown together with energies of stationary points of the classical-limit Hamiltonian (gray dashed lines). The straight dashed lines correspond to two minima of the Hamiltonian. The lower one represents the ground-state and their crossing at $\lambda_c = \frac{1}{17}$ indicates the first-order QPT. The higher of the two minima on both sides of the QPT generates an ESQPT that shows up as a sharp step in the $N \rightarrow \infty$ level density. The bent dashed line, which corresponds to the Hamiltonian saddle point between both minima, is connected with another ESQPT, giving rise to a local increase (divergence for $N \rightarrow \infty$) of the level density. Panel (b): The evolving structure of the 4th eigenstate [the thicker curve in panel (a)] is shown by the squared overlap $|\langle j, m | \psi_4(\lambda) \rangle|^2$ of the instantaneous eigenstate with basis states $|j, m\rangle$, $m = -j, \dots, +j$ (darker shades mean larger overlaps). We note sharp changes of the overlaps at each avoided level crossing inside the area enclosed by the dashed lines in panel (a). The dashed vertical line (with crosses at ESQPTs) marks λ used in Fig. 11.

to the total quasispin projection m , while the number $2j$ represents unpaired active **quibits** which contribute to the value of m . The subspace $\mathcal{H}_{j_{\max}}$ with the maximal number $2j = N$ is totally symmetric under the exchange of any pair of qubits and therefore unique in \mathcal{H} . This subspace represents the usual choice for any dynamical study.

Models based on the SU(2) algebra, which all belong to the family of Lipkin-like models, are probably the most frequently used playgrounds in various ESQPT-related studies. Besides an elegant mathematical formulation, relatively undemanding numerical solubility (moderate-dimensional Hilbert space $\mathcal{H}_{j_{\max}}$) and large versatility of such models, the main advantage of this choice is the lowest possible number of collective DOFs, $f = 1$, for which the ESQPT signatures are most pronounced. They can be detected even for moderate values of the naturally defined size parameter N . In some examples below we will employ the Lipkin Hamiltonian with two control

parameters λ and χ , namely

$$\hat{H} = \hat{J}_z - \frac{\lambda}{N} \left[\hat{J}_x + \chi \left(\hat{J}_z + \frac{N}{2} \right) \right]^2, \quad (13)$$

which interpolates between the first-order ground-state QPT and the accompanying ESQPT for $\chi=0$ [cf. Eq. (11)], and the first-order QPT and the associated ESQPTs for $\chi \neq 0$. The ground-state QPT from the non-interacting to the interacting phase happens at the critical interaction strength $\lambda_c = (1+\chi^2)^{-1}$ [129]. An example of the ESQPT structures accompanying a first-order QPT for this Hamiltonian is depicted in Fig. 6. Similar ESQPT patterns (but for $f > 1$ shifted to higher derivatives of the level density) are typical near generic first-order QPTs [10–13]. Many other ESQPT examples disclosed in various Lipkin-like models can be found in Refs. [17, 18, 20, 21, 47, 51, 56, 66, 68, 75] (identification of ESQPTs and description of underlying mechanisms), [84, 85, 87] (thermodynamic consequences) and [85, 89, 92–96, 98, 100, 102, 103] (dynamic effects).

A straightforward extension of the quasispin models results from *coupling* of two or generally $n \geq 2$ quasispin subsystems. Such models work with sets of quasispin operators $\{\hat{\mathbf{J}}_k\}_{k=1}^n$ associated with each subsystem, using Hamiltonians analogous to (12) but with quadratic and eventually higher-order terms combining quasispin operators of various subsystems. The number of DOFs is $f = n$, but in some cases additional integrals of motion reduce the number of effective DOFs in the relevant subspaces. A system of $n = 2$ coupled Lipkin models and its ESQPTs were studied in Ref. [70]. Both subsystems were sent to the classical limit simultaneously by applying the limit $j_1, j_2 \rightarrow \infty$ to both quasispin size quantum numbers. In contrast, in the study of Ref. [64], an integrable two-spin elliptic Gaudin model was analyzed with a strong imbalance between the sizes of both subsystems. This is analogous to the Rabi model discussed in Sec. 2.3. The $f = 1$ ESQPT structures were reported in absence of the ground-state QPT within the selected parametric form of the Hamiltonian.

Another interesting modification of the above approaches was discussed in Ref. [109]. The model considered there is spin model with *variable-range interaction*, which realizes an intermediate case between the Ising and Lipkin regimes of two-level lattice systems. Assuming a $D = 1$ spin chain with spatially regularly arranged sites enumerated consecutively by integer $i = 1, 2, \dots, N$, one can consider the Hamiltonian of the following form

$$\hat{H} = \hat{J}_z - \lambda \sum_{i < i'} \frac{1}{|i-i'|^K} \hat{\sigma}_x^{(i)} \hat{\sigma}_x^{(i')}, \quad (14)$$

where $|i-i'|$ measures the distance between the sites i and i' , and the power $K \geq 0$ is an adjustable parameter which determines the range of the spin-spin interaction. For $K=0$ we have the infinite-range interaction of the Lipkin type, for $K \gg 1$ we get closer to the nearest-neighbor interaction of the Ising type. While the $K=0$ case will exhibit the $f=1$ signatures of ESQPT, the $K>0$ case is characterized by $f=N$. In these studies, the Hamiltonian must be diagonalized in the whole $d = 2^N$ dimensional Hilbert space. When K is infinitesimally increased from zero, huge degeneracy of the $K=0$ energy spectrum is lifted and the $f=1$ ESQPT singularities are gradually washed out. One can then investigate the rate and other features of this process. Note that an alternative for the Hamiltonian (14) in such studies would be the Dicke Hamiltonian (3) with substitution (2), in which the atom-field interaction strength $\lambda^{(i)}$ depends on the atom identifier i . An obvious obstacle of all such studies is the numerical difficulty to diagonalize the non-collective Hamiltonians with large N .

3.2. Interacting boson systems

The SU(2) algebra of quasispin operators can be represented in a bosonic language, either via the Holstein-Primakoff mapping

$$\hat{J}_0 = \hat{b}^\dagger \hat{b} - \frac{1}{2}N, \quad \hat{J}_+ = \hat{b}^\dagger (N - \hat{b}^\dagger \hat{b})^{\frac{1}{2}}, \quad \hat{J}_- = (N - \hat{b}^\dagger \hat{b})^{\frac{1}{2}} \hat{b}, \quad (15)$$

which uses creation and annihilation operators \hat{b}^\dagger and \hat{b} of a single-type scalar bosons, or via the Schwinger mapping

$$\hat{J}_0 = \frac{1}{2} (\hat{t}^\dagger \hat{t} - \hat{s}^\dagger \hat{s}), \quad \hat{J}_+ = \hat{t}^\dagger \hat{s}, \quad \hat{J}_- = \hat{s}^\dagger \hat{t}, \quad (16)$$

written in terms of creation and annihilation opeators \hat{s}^\dagger, \hat{s} and \hat{t}^\dagger, \hat{t} of scalar or pseudoscalar bosons of two types, see Ref. [131]. In both cases, the representation realizes a subspace of \mathcal{H} with a selected quasispin size value $j = \frac{1}{2}N$, where integer N in mapping (15) is associated with a maximal number of b bosons, while N in mapping (16) represents the total number of s and t bosons. Using number operators \hat{N}_\bullet of the respective boson types, we link the states $|j, m\rangle$ with $m = -j, -j+1, \dots, +j$ to the \hat{N}_b eigenstates with $\hat{N}_b = 0, 1, \dots, N$, or to the \hat{N}_s and \hat{N}_t eigenstates with $(N_s, N_t) = (N, 0), (N-1, 1), \dots, (0, N)$.

Switching the size parameter $N = 1, 2, 3, \dots$ into a dynamical quantity is equivalent to moving from the special unitary algebra SU(2) with three generators to the full unitary algebra U(2) with four generators. For the Schwinger mapping (16), the fourth generator is obviously the total boson number operator $\hat{N} = \hat{s}^\dagger \hat{s} + \hat{t}^\dagger \hat{t}$, which commutes with all the other generators and its eigenvalue can be fixed at any N . For the Holstein-Primakoff mapping (15), the additional commuting generator that takes a chosen value N can be associated the number operator $\hat{N}_a = \hat{a}^\dagger \hat{a}$ of a new boson a . The full unitary algebra forms the *dynamical algebra* of the bosonic system in the sense that any observable, including the Hamiltonian, can be written exclusively in terms of the generators of this algebra.

With the aid of the above mappings, any quasispin Hamiltonian (12) can be cast in the form of a Hamiltonian describing an interacting system of bosons. The Hamiltonians resulting from the Holstein-Primakoff mapping with substitution $N \rightarrow \hat{a}^\dagger \hat{a}$ in general change the total number of a and b bosons (conserving \hat{N}_a but changing \hat{N}_b) and contain unlimited k -body terms of boson operators resulting from an expansion of the square-root factors. On the other hand, the Hamiltonians obtained from the Schwinger mapping (16) conserve the total number of s and t bosons and, if we restrict to linear plus quadratic quasispin Hamiltonians, they contain only one- plus two-body terms. The latter approach opens a path to direct generalizations to systems with more than two boson types, or more precisely to systems with the single-boson Hilbert space of a general dimension $n = 2, 3, 4, \dots$, which are associated with unitary dynamical algebras U(n). The general one- plus two-body bosonic Hamiltonian reads

$$\hat{H} = \sum_{k=1}^n \varepsilon_k \hat{b}_k^\dagger \hat{b}_k + \sum_{k,l,k',l'=0}^n \frac{\nu_{klk'l'}}{N} \hat{b}_k^\dagger \hat{b}_{k'}^\dagger \hat{b}_l \hat{b}_{l'} + \dots, \quad (17)$$

where operators \hat{b}_k^\dagger and \hat{b}_k create and annihilate a boson in the k th state (with the label $k = n$, for instance, being reserved for the the scalar boson s) and ε_k and $\nu_{klk'l'}$, respectively, represent single-particle energies and two-body interaction parameters. The N denominator in the interaction term, in analogy to Eqs. (11) and (12), prevents

dominance of this term in large- N cases. Three- and more-body interactions, if needed, can be added in an obvious way.

The nomenclature of these models is as follows: Those with $n = 3$ and 4 correspond to two kinds of *vibron models* used in molecular physics. The $n = 3$ vibron model [132] works with a one-component boson s and a two-component boson (τ_+, τ_-) and is applied in the description of spectra of vibrational states of three-atomic molecules such as H₂O. The $n = 4$ vibron model [133] makes use of the scalar boson s and a vector boson (p_{-1}, p_0, p_{+1}) and simulates vibrations and rotations of two-atomic molecules. A conceivable model with $n = 5$, which in addition to the boson s would use a four-component boson $(\pi_{--}, \pi_-, \pi_+, \pi_{++})$, has presently no application. The case with $n = 6$ is the *interacting boson model* of nuclear physics [134], which is based on the scalar boson s and a quadrupole tensor boson $(d_{-2}, d_{-1}, d_0, d_{+1}, d_{+2})$. The s boson represents a pair of nucleons with angular momentum 0 , while the d boson is interpreted as a pair with angular momentum 2 and simultaneously related to the quadrupole collective DOFs of nuclei. More sophisticated nuclear models are obtained by adding to the $s + d$ system some other types of bosons, namely p , d and/or f with angular momenta 1 , 3 and 4 , respectively, or by separating boson species associated with the proton and neutron DOFs [134]. The latter extension to interacting boson models with two or more “fluids” exploits the standard coupling formalism mentioned above in the context of atom-field and quasispin models. It is also used in the framework of molecular vibron models [135].

A considerable advantage of the the finite- n interacting boson models is the fact that their Hilbert space \mathcal{H} has a finite dimension which grows only polynomially ($\propto N^{n-1}$) with the natural size parameter N . This greatly facilitates the exact numerical solution. Another positive feature is a straightforward construction of the classical limit $N \rightarrow \infty$. The coordinate-momentum representation of the interacting boson Hamiltonians (17) is obtained with the aid of Eq. (5) with $\varkappa = N$, which yields a system with $f = n$ DOFs. Moreover, fixing the conserved total number of bosons on a selected value N allows to perform a canonical transformation which reduces the number of active DOFs to $f = n - 1$. The transformation represents a generalization of the link between Schwinger and Holstein-Primakoff mappings described above for the $n = 2$ case. It is formally equivalent to the transformation (5) performed for all components of all bosons except the boson s (so we obtain operators \hat{q}_i and \hat{p}_i with $i = 1, \dots, n-1$), and to replacing both \hat{s}^\dagger and \hat{s} operators by $[N - \frac{1}{2} \sum_i (\hat{q}_i^2 + \hat{p}_i^2)]^{1/2}$. For details see Refs. [138] and [13].

An important role in the formulation of the interacting boson models is played by *dynamical symmetries* [136]. These generalizations of invariant symmetries are associated with specific decompositions of the dynamical algebra $\mathcal{G}_D \equiv U(n)$ into chains of subalgebras $\mathcal{G}_D \supset \mathcal{G}_1^{(k)} \supset \mathcal{G}_2^{(k)} \supset \dots \supset \mathcal{G}_S$. The highest algebra \mathcal{G}_D as well as the lowest algebra \mathcal{G}_S , which generates the invariant symmetry of the system, are fixed and can be usually connected by several chains, here enumerated by superscript k . The Hamiltonian written solely in terms of Casimir invariants of the algebras involved in one of such chains possesses the corresponding dynamical symmetry and can be proven to be integrable [137]. We note that all invariants within a single chain represent mutually commuting integrals of motion.

It is customary to study transitional Hamiltonians of the general form

$$\hat{H}(\lambda) = (1 - \lambda)\hat{H}(0) + \xi\hat{H}(1), \quad \lambda \in [0, 1], \quad (18)$$

where the single variable λ drives the system along a path in the multiparameter space

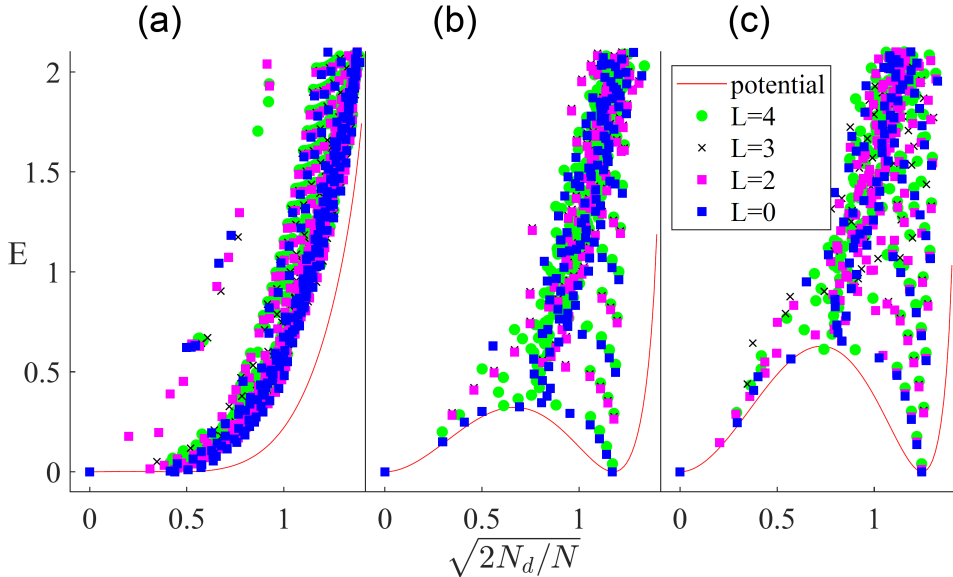


Figure 7. Peres lattices of quantity $(2\hat{N}_d/N)^{1/2}$ in the $n = 6$ interacting boson model at the critical point of the first-order QPT between SU(3) and U(5) ground-state phases. States with angular momenta from $L = 0$ to 4 are included. The total number of bosons $N = 50$. The Hamiltonian and further details are described in Ref. [141]. Three panels correspond to different heights of the phase-separating potential barrier (the respective “potential energy” curves are drawn in each panel). The top of the barrier [invisibly small in panel (a)] is connected with an ESQPT, which affects the distribution of $\langle N_d \rangle_i^{1/2}$. This pattern can be compared to analogous but sharper case of the $n = 2$ Lipkin model in Fig. 11(c) below.

of the model between two distinct dynamical symmetries associated with Hamiltonians $\hat{H}(0)$ and $\hat{H}(0)$. The QPT that eventually appears along the selected path is then linked to phases defined through these limiting dynamical symmetries. For example, the U(6) interacting boson model has three dynamical symmetries denoted according to the highest subgroup in the respective chain as U(5), SO(6) and SU(3). In most studies, the space of all model control parameters is reduced by considering special paths that realize transitions U(5)–SU(3) (with first-order QPT), U(5)–SO(6) (with second-order QPT), and SO(6)–SU(3) (non-critical crossover). The algebraic formulation of collective quantum systems will be further discussed in Sec. 3.3.

The nuclear interacting boson model ($n = 6$) in a certain subset of its parameter space, namely along the second-order QPT path between the U(5) and SO(6) dynamical symmetries, was instrumental in the early studies of ESQPTs [5–8, 43]. Along the whole transitional path, the system conserves the Casimir invariants of the SO(5) and SO(3) subalgebras, the latter one expressing the invariant symmetry under rotations. For states with zero angular momentum, including the ground state of the system, the SO(5) symmetry is spontaneously broken at the QPT from the U(5) to SO(6) phase [7,8]. The ground state is a condensate of s bosons on the U(5) side of the critical point, and condensate in a superposition of s and d boson states on the SO(6) side.

The ESQPT critical borderline starts at the ground-state critical point and propagates towards the SO(6) limit where it reaches the high-energy limit of the spectrum. The dynamical phases separated by the critical borderline have been characterized by the U(5) and SO(6) quasi dynamical symmetries, the word “quasi” emphasizing an approximate character of these symmetries between the limiting points of the path [139–141]. The ESQPTs in other regimes, including first-order QPTs in transitional paths to the SU(3) dynamical symmetry, have been analyzed in Refs. [13, 59, 71]. Peres lattices at the critical point of the first-order QPT along the U(5)–SU(3) path with various heights of the phase-separating energy barrier are illustrated in Fig. 7. Note that both (at the critical point degenerate) minima of the “potential energy” curve (cf. Sec. 4) are associated with one of the competing ground-state phases [141]. The ESQPT at energy coinciding with the top of the barrier is seen here in the merge of two branches of eigenstates localized in both minima into a single branch with the square root of d -boson number average $\langle N_d \rangle_i^{1/2}$ corresponding to the barrier maximum.

The $n = 6$ interacting boson Hamiltonian along its U(5)–SO(6) transition is a special case of a more general class of many-body systems with *pairing interaction*, which are integrable and solvable by algebraic methods [142]. This is related to imperfect breaking of the limiting dynamical symmetries in this transition since the Casimir invariant of the SO(5) algebra, that belongs to both limiting dynamical symmetry chains, remains an integral of motion along the whole path. The full model with fixed N has $f = 5$ DOFs, three of them associated with rotations and two with quadrupole vibrations of nuclei. Conservation of the SO(3) and SO(5) invariants lowers the number of effective DOFs to $f_{\text{eff}} = 1$. Hence, in the spectra with zero values of the SO(3) and SO(5) angular momenta we observe generic ESQPT singularities in the zeroth derivative of the smoothed level density. This is so for all the above-mentioned integrable models of the pairing type.

The phase structure of $n < 6$ boson models is similar to that of the $n = 6$ model in the U(5)–SO(6) pairing regime [143]. These models are also analyzed along transitional paths between dynamical symmetries U($n - 1$) and SO(n). The symmetry preserved along the whole path, which is spontaneously broken for the ground state at the second-order QPT, is connected with the SO($n - 1$) invariant. For the $n = 3$ and $n = 4$ vibron models, the invariant expresses conserved 2D or 3D angular momentum, for the $n = 2$ boson-based Lipkin model the conserved quantity is the parity $(-1)^{N_d}$ associated with the number of d bosons. The spectra of all these models show ESQPTs between quantum phases characterized by U($n - 1$) and SO(n) quasi dynamical symmetries. Since the restriction to states with a given N and zero value of the SO($n - 1$) invariant leads to $f_{\text{eff}} = 1$, the ESQPTs affect the zeroth derivative of smoothed level density in these subsets of states. Besides the $n = 2$ Lipkin model, which was already discussed in Sec. 3.1, the theoretical studies of ESQPTs were focused mostly on the $n = 3$ model [9, 45, 48, 52]. The results for $n = 4$ are similar, an example of the spectrum being shown in Fig. 8. We stress that static signatures of ESQPT in the $n = 3$ model have been verified experimentally in the spectra of various molecules, see Refs. [26, 27, 52].

Note that similar analyses apply to a more general class of bosonic pairing models with the dynamical algebra U($n_1 + n_2$) encompassing two kinds of bosons with numbers of components n_1 and n_2 [9, 46]. The pairing Hamiltonians connecting dynamical symmetries denoted by the algebras SO($n_1 + n_2$) and U(n_1)₁ \oplus U(n_2)₂ that appear at the highest position in the corresponding chains of algebra embeddings (the subscripts 1 and 2 distinguish algebras associated with both kinds of bosons). Here and below

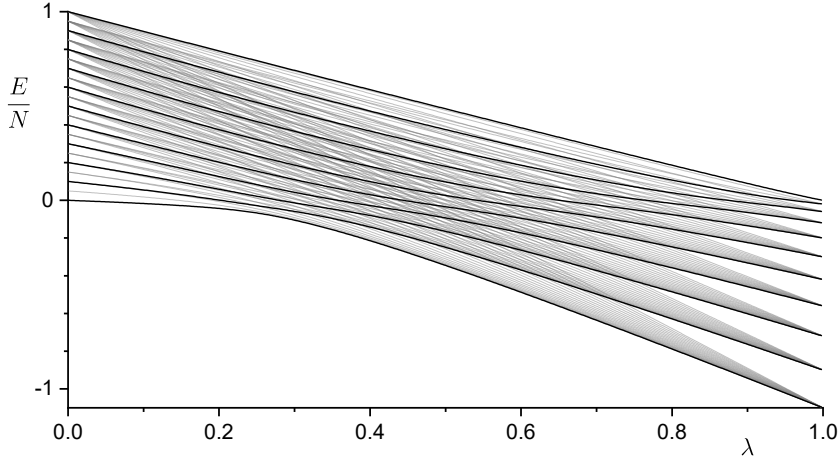


Figure 8. The ESQPT in the spectrum of the $n = 4$ vibron model for $N = 20$. The Hamiltonian has the form (18) with $\hat{H}(0) = \hat{C}_1[U(3)]$ and $\hat{H}(1) = N^{-1}\hat{C}_2[SO(4)]$, where $\hat{C}_1[A]$ and $\hat{C}_2[B]$ are the first- and second-order Casimir invariants of the respective algebras, see Ref. [133]. The spectrum contains states with all values of the $SO(3)$ quantum number $l = 0, 1, \dots, N$ (ordinary 3D angular momentum). Each level is $(2l + 1)$ times degenerate in the angular-momentum projection m . The levels with $l = 0$ are drawn by thicker curves. This subspace corresponds to $f_{\text{eff}} = 1$, while the unconstrained model with all states has $f = 3$. We observe the second-order ground-state QPT at $\lambda_c = \frac{1}{5}$ continued by an ESQPT at $E_c = 0$ (a peak in the level density of $l = 0$ states and an effect in the second derivative of the level density of all states). Spontaneous breaking of the $SO(3)$ symmetry appears in the quantum phase with lower energy. Practically the same spectrum is obtained for an analogous Hamiltonian of the $n = 3$ vibron model with $f = 2$, where the $SO(2)$ angular momentum corresponds to 2D rotations.

we use a direct sum for algebras, implying a direct product for the corresponding groups. The bosonic pairing Hamiltonians conserve the Casimir invariant of the $SO(n_1)_1 \oplus SO(2)_2$ subalgebra and yield the same QPT and ESQPT effects as the above-discussed special cases with $n_1 = 1$, see Refs. [9, 46] and paper 27 in [1].

Another use of the interacting boson models with a limited dimension of the single-particle space is in the physics of Bose-Einstein condensation [144, 145], namely in the framework of the well known *Bose-Hubbard model*. The model in its general form describes a systems of ultracold interacting Bose atoms trapped in a lattice of n sites, see e.g. Ref. [146]. Here we mention explicitly a two-site system of an atomic condensate in a double-well potential, which is applied as a model of the Josephson junction [147]. This and analogous systems are discussed in the literature particularly in connection with their capability to create macroscopic quantum superpositions and their potential use in quantum computation [148]. Experimental realization of such regimes in a two-site system was reported in Ref. [149]. The bosons associated with both sites marked by signs $+$ and $-$ are created and annihilated by operators \hat{b}_{\pm}^{\dagger} and \hat{b}_{\pm} , and the Hamiltonian is assumed to have the following form:

$$\hat{H} = \varepsilon_+ \hat{b}_+^{\dagger} \hat{b}_+ + \varepsilon_- \hat{b}_-^{\dagger} \hat{b}_- - J (\hat{b}_+^{\dagger} \hat{b}_- + \hat{b}_-^{\dagger} \hat{b}_+) + \frac{U}{N} (\hat{b}_+^{\dagger} \hat{b}_+^{\dagger} \hat{b}_+ \hat{b}_+ + \hat{b}_-^{\dagger} \hat{b}_-^{\dagger} \hat{b}_- \hat{b}_-). \quad (19)$$

Here, ε_{\pm} are the site energies, $J > 0$ is a strength of inter-site hopping, and U quantifies

the intra-site interaction (repulsive or attractive for $U > 0$ or < 0 , respectively).

The system with attractive intra-site interactions exhibits a QPT between two distinct ground-state phases: the conductive (superfluid) phase with delocalized atoms (observed for $|U| \ll J$) and the trapped (Mott insulator) phase with atoms localized at individual sites (for $|U| \gg J$). In the symmetric case with $\varepsilon_+ = \varepsilon_-$, the transition is of the second order and corresponds to a spontaneous breaking of the ground-state symmetry expressed by a conserved parity operator exchanging populations N_+ and N_- of both sites. Similar localization and symmetry breaking effects can be observed for excited states of the two-site system with repulsive intra-site interactions [150]. The spectrum of the model (19) with both signs of U contains ESQPTs, which can be described by the same semiclassical techniques as those for the more general Hamiltonians (17). Since the two-site system can be reduced to $f = 1$, the ESQPT singularity appears directly in the zeroth derivative of the smoothed level density [76].

A formally similar two-boson model with the hopping term involving pairs of atoms instead of single ones has been applied to intraband tunneling processes of the Bose-Einstein condensate in periodic $D = 2$ optical lattices [42]. Also this model exhibits clear $f = 1$ ESQPT signatures.

3.3. General algebraic systems

The above considerations can be extended to any algebraically formulated model. The algebraic method [136] anchors the description of any specific system of interest to the definition of a suitable dynamical algebra $\mathcal{G} \equiv \{\hat{G}_l\}_{l=1}^L$. This algebra consists of a set of Hermitian generators \hat{G}_l satisfying the closure relation $[\hat{G}_k, \hat{G}_l] = i \sum_m s_{klm} \hat{G}_m$ with real structure constants s_{klm} . Various combinations of these generators must allow one to express any relevant physical observable of the system. In particular the Hamiltonian can be written as $\hat{H} = H(\{\hat{G}_l\})$, where H on the right-hand side denotes an unspecified function of arguments \hat{G}_l . We assume that the number of generators L is finite. The number $R \leq L$ of mutually commuting generators, called the rank of algebra \mathcal{G} , is related to the number of quantum numbers needed to unambiguously label basis states in the associated Hilbert space. So in typical situations, this number in the classical limit coincides with the number f of DOFs of the system.

We have already seen examples of dynamical algebras for the systems discussed above. It was the $SU(2)$ algebra with generators $(\hat{J}_+, \hat{J}_-, \hat{J}_0)$ for the quasispin systems, and $U(n)$ algebras for the interacting boson systems with n bosonic species. The latter algebras are generated by products of creation and annihilation operators $\hat{b}_k^\dagger \hat{b}_l$ and hence conserve the total boson number $\hat{N} = \sum_{k=1}^n \hat{N}_k$. Coupled systems are described by direct sums of the corresponding algebras. In particular, we mention dynamical groups of the type $SU(2)_1 \oplus SU(2)_2$ describing coupled quasispin systems, or $U(n_1)_1 \oplus U(n_2)_2$ applied to “two-fluid” interacting boson systems with n_1 - and n_2 -component bosons conserving separately both boson numbers \hat{N}_1 and \hat{N}_2 . For coupled atom-field systems from Sec. 2, we use the dynamical algebra $SU(2)_A \boxplus HW(1)_B$, where $SU(2)_A$ stands for the standard quasispin algebra of the atomic subsystem and $HW(1)_B \equiv \{\hat{b}^\dagger, \hat{b}, \hat{I}\}$ (where \hat{I} is unit operator) for the Heisenberg-Weyl algebra of the field subsystem.

With the aid of the algebraic approach, the class of the interacting boson models can be elegantly generalized to describe combined *atom-molecule systems* which enable mutual conversions of bosonic atoms and bosonic molecules built from two or more atoms, or interchanges of bosonic molecules composed of different numbers of atoms.

This kind of boson models can be used in the description of Bose-Einstein condensation involving molecules [151] and similar models are also applied in quantum optics [152]. Such systems do not conserve the number \hat{N} of bosons (atoms and molecules), but rather the number of elementary constituents $\hat{\mathcal{N}} = \sum_{k=1}^n m_k \hat{N}_k$, where \hat{N}_k is the number of bosons of the k th type comprising of m_k atoms. Therefore they can no more be associated with the \hat{N} -conserving dynamical algebras $U(n)$.

As shown in Refs. [90, 153], the simplest case with $n = 2$ bosonic species characterized by atomic numbers $(m_1, m_2) = (1, 2)$ can be associated with the dynamical algebra $SU(1,1)_1 \oplus HW(1)_2$, where the non-compact algebra $SU(1,1)_1 \equiv \{\frac{1}{2}(\hat{b}_1^\dagger \hat{b}_2 + \frac{1}{2}), \frac{1}{2}\hat{b}_1^\dagger \hat{b}_1^\dagger, \frac{1}{2}\hat{b}_1 \hat{b}_1\}$ describes the first boson (atom) and its pairwise creation and annihilation, while the Heisenberg-Weyl algebra $HW(1)_2$ is built of the creation and annihilation operators of the second boson (molecule). Note that the generators of $SU(1,1)$ obey the same commutation relations as the $SU(2)$ ones except the opposite sign of the commutator between the rising and lowering generators. An alternative [57, 152, 154] is to use for the whole system a single polynomially deformed algebra $SU(2)_{pd}$ expressed by generators

$$\hat{K}_0 = \frac{1}{4} (\hat{b}_1^\dagger \hat{b}_1 - 2\hat{b}_2^\dagger \hat{b}_2), \quad \hat{K}_+ = \mathcal{N}^{-\frac{1}{2}} \hat{b}_1^\dagger \hat{b}_1^\dagger \hat{b}_2, \quad \hat{K}_- = \mathcal{N}^{-\frac{1}{2}} \hat{b}_2^\dagger \hat{b}_1 \hat{b}_1 \quad (20)$$

(with \mathcal{N} standing for the selected value of the conserved number operator $\hat{\mathcal{N}}$), whose commutators involving \hat{K}_0 coincide with standard $SU(2)$ ones, but $[\hat{K}_+, \hat{K}_-]$ results in a polynomial expression in \hat{K}_0 and $\hat{\mathcal{N}}$. In the models based on both these approaches, $f = 1$ ESQPT structures were clearly identified in quantum spectra [57, 90]. The latter approach can be generalized to systems with arbitrary values of n and $\{m_i\}$, again with ESQPT effects potentially present [60]. In particular, ESQPTs in the $n = 3$, $(m_1, m_2, m_3) = (1, 1, 2)$ extension of the two-site Bose-Hubbard Hamiltonian of the type (19) were analyzed in Ref. [55].

The algebraic formulation can be naturally extended also to *interacting fermion systems* formulated in terms of algebras of fermionic operators. Let us note that fermionic systems, due to the anticommutation relations of fermion creation and annihilation operators, are generally described by superalgebras rather than algebras, but if relevant dynamical operators involve only the even sector of the fermionic superalgebra, the standard algebraic description can be applied. Giving just the most trivial examples, we point out that the original formulation of the Lipkin model [130] was through the fermionic realization of the $SU(2)$ algebra

$$\hat{J}_0 = \frac{1}{2} \sum_{i=1}^N (\hat{a}_{i+}^\dagger \hat{a}_{i+} - \hat{a}_{i-}^\dagger \hat{a}_{i-}), \quad \hat{J}_+ = \sum_{i=1}^N \hat{a}_{i+}^\dagger \hat{a}_{i-}, \quad \hat{J}_- = \sum_{i=1}^N \hat{a}_{i-}^\dagger \hat{a}_{i+}, \quad (21)$$

where operators $\hat{a}_{i\pm}^\dagger$ and $\hat{a}_{i\pm}$ create and annihilate fermions in states $i = 1, 2, \dots, N$ on two N -fold degenerate levels $+$ and $-$. To obtain the familiar 2^N dimensional Hilbert space known from the qubit realization of the quasispin algebra (2), one needs to set the total conserved number of fermions $\hat{N}_a = \sum_{s=\pm} \sum_{i=1}^N \hat{a}_{is}^\dagger \hat{a}_{is}$ to the value that coincides with the capacity N of a single \pm level, and allow just a single particle to be present in each couple of states $i+$ and $i-$.

Another fermionic incarnation of the $SU(2)$ algebra appears in a schematic pairing model. Here the operators $\hat{a}_{i\pm}^\dagger$ and $\hat{a}_{i\pm}$ describe fermions on a single level, with states $i+$ and $i-$, being conjugate with respect to time reversal (e.g., single-particle states with positive and negative projections of the total angular momentum). Introducing

a fermion-pair creation operator $\hat{A}^\dagger = \sum_{i=1}^N (-1)^{N-i} \hat{a}_{i+}^\dagger \hat{a}_{i-}^\dagger$, and the corresponding Hermitian conjugate annihilation operator \hat{A} , we have

$$\hat{J}_0 = \frac{1}{2} (\hat{N}_a - N), \quad \hat{J}_+ = \hat{A}^\dagger, \quad \hat{J}_- = \hat{A}. \quad (22)$$

These operators do not conserve the particle number and to obtain the Hilbert space \mathcal{H} of dimension 2^N , we assume a basis in which each pair of states $i+$ and $i-$ is either empty or occupied. The quasispin size quantum number is parametrized as $j = j_{\max} - v$, where the quantum number v is called seniority.

The ESQPTs were explicitly studied in a certain generalization of the above SU(2) fermionic pairing system, namely in a two-level pairing model, see Refs. [9, 46] and paper 27 in [1]. The two levels are supposed to have total (orbital plus spin) half-integer angular momenta ℓ_1 and ℓ_2 , and the respective fermion pair creation/annihilation operators are $\hat{A}_1^\dagger, \hat{A}_1$ and $\hat{A}_2^\dagger, \hat{A}_2$. The Hamiltonian is written as

$$\hat{H} = \sum_{k=1,2} \varepsilon_k \hat{N}_k + \sum_{k,l=1,2} \nu_{kl} \hat{A}_k^\dagger \hat{A}_l, \quad (23)$$

where ε_k is the single-particle energy of the k th level, \hat{N}_k the respective occupation number operator, and ν_{kl} expresses pairing interaction strengths. The dynamical algebra of the system is identified with $U(n_1+n_2)$, where $n_k = 2\ell_k + 1$. It is composed of all combinations of fermion creation and annihilation operators conserving the total particle number. Hamiltonians of the form (23) interpolate between dynamical symmetries corresponding to the dynamical algebra decompositions starting with the algebra $U(n_1) \oplus U(n_2)$, on one side of the transition, and with the symplectic algebra $Sp(n_1+n_2)$, on the other side. The situation is similar to the case of bosonic pairing systems discussed in Sec. 3.2. The system exhibits a QPT between both dynamical symmetries (independent-particle and paired forms of the ground state) and an ESQPT on the paired side of the transition. Due to a residual dynamical symmetry, which remains unbroken across the whole transitional path, and the consequent integrability of the system, the effective DOF number for suitable subsets of states is reduced so that the ESQPT spectral singularity is seen in the zeroth derivative of the associated level density. In contrast to the bosonic case, the Pauli exclusion principle enables one to reach the infinite size limit $N = N_1 + N_2 \rightarrow \infty$ only if the angular momentum quantum number ℓ_1 or ℓ_2 becomes infinite. The numerically observed finite-size precursors of both QPT and ESQPT effects are nevertheless very clear [46].

In this overview of ESQPT-related models and systems, we have to mention mixed interacting many-body systems composed of bosons and fermions. In nuclear physics, such *Bose-Fermi systems* naturally appear in the framework of the interacting boson-fermion model applied to nuclei with odd numbers of protons or neutrons [155]. This model separately conserves the numbers of bosons and fermions, and its dynamical algebra can be associated with $U(6)_\pi \oplus U(6)_\nu \oplus U(2k)_F$, where the indices distinguish unitary algebras of proton (π) and neutron (ν) bosons (paired fermions of the respective type), and that of the odd-fermion (F), proton or neutron, on the valence shell with total capacity $2k$. In the analyses of the phase structure, the bosonic subsystem is sent to the asymptotic size regime with the number of bosons $N_\pi + N_\nu \rightarrow \infty$, and the coupling with the single-fermion subsystem (whose quantum character is preserved) results in multiple overlapping semiclassical spectra with modified quantum critical properties [156].

Similar Bose-Fermi systems exist also in condensed matter physics. The most challenging are the systems that allow for mutual conversions between boson-like

particles and pairs of fermions. This happens for instance in the so-called bilayer model [41, 44], which describes a QPT from a fermionic phase of unbound electron-hole pairs to a bosonic phase of electron-hole bound states. Experimental signatures of such transitions were reported in Ref. [157]. Introducing the fermion (particle or hole) creation and annihilation operators for states enumerated by $i = 1, 2, \dots, \frac{1}{2}M$ on two fermionic “layers” denoted as + and −, one can write down a fermion pair creation operator $\hat{A}^\dagger = \sum_{i=1}^{N/2} \hat{a}_i^\dagger - \hat{a}_{i+}^\dagger$. This pair couples to a bosonic exciton quantum created by \hat{b}^\dagger . Employing the constraint on the conserved quantity $\hat{\mathcal{N}} = \hat{N}_a + 2\hat{N}_b$ (where \hat{N}_a and \hat{N}_b are fermion and boson total number operators, respectively) fixed at the overall capacity of the fermion state space M , one can identify the operators

$$\hat{J}_0 = \frac{1}{2}\hat{N}_b - \frac{1}{4}\hat{N}_a, \quad \hat{J}_+ = \hat{N}_b^{-\frac{1}{2}}\hat{b}^\dagger\hat{A}, \quad \hat{J}_- = \hat{A}^\dagger(\hat{N}_b+1)^{-\frac{1}{2}}\hat{b} \quad (24)$$

with generators of the familiar SU(2) algebra. Spectral signatures of the $f = 1$ ESQPT for a Hamiltonian written in terms of these generators were described in Refs. [41, 44].

3.4. Size parameter and classical limit

Having viewed (from bird’s perspective, of course) in the preceding paragraphs a large variety of interacting many-body systems based on the algebraic description, let us finally address the general relation between the infinite-size and classical limits of these systems. We have already highlighted the equivalence of these limits for the specific systems above. The same conclusion holds, in principle, for any quantum system described through a finite-dimensional dynamical Lie algebra (and can be extended to systems with deformed dynamical algebras).

The definition of the *size parameter* of the system is rather obvious in many cases. For instance, it coincides with the number N of **qubit** sites (or the quasispin size j) in **cubit** systems based on the quasispin formalism (Sec. 3.1). It represents the conserved total number N of bosons or fermions for systems based on the particle-number conserving unitary algebras (Secs. 3.2 and 3.3). Or it can be a combination of the type $\mathcal{N} = \sum_k m_k N_k$ in atom-molecule or boson-bifermion systems (Sec. 3.3). On the other hand, some **systems requires** a more careful analysis, like e.g. the asymmetric Rabi regime of the atom-field system (Sec. 2.3).

The choice of a general size parameter \aleph in an arbitrary quantum system with a finite DOF number f follows some common rules. The size parameter depends on a characteristic energy \mathcal{E} that sets the energy scale relevant in the given context. This is clearly not an exactly determined quantity, but its rough knowledge is essential. A trivial example is a harmonic oscillator in which the size parameter, a typical number of phonons, increases with the selected energy scale \mathcal{E} . As argued in Ref. [11], the general size parameter reflects the overall volume $\Omega(\mathcal{E})$ of the domain activated at the selected scale \mathcal{E} in the $2f$ -dimensional phase space. The number \aleph is obtained by expressing this volume in units of elementary quantum cells, namely:

$$\aleph^f \sim \frac{\Omega(\mathcal{E})}{\hbar^f}. \quad (25)$$

This formula is applicable in all the above examples. For instance, in a system of n bosonic species with comparable single-particle energies $\varepsilon_k \approx \bar{\varepsilon}_k$ and interactions $\nu_{klk'l'} \ll \bar{\varepsilon}_k$, see Eq. (17), the volume in the $f = n$ phase space reads $\Omega(\mathcal{E}) \approx (\mathcal{E}/\bar{\varepsilon}_k)^n$, which for $\mathcal{E} = N\bar{\varepsilon}_k$ yields $\aleph \approx N$. In Sec. 4.3, we will return to these considerations in connection with general coupled systems.

We now follow the general algebraic treatment sketched in Sec. 3.3. Once the size parameter \aleph is chosen, the model must be checked (or modified) to satisfy some *scaling properties*. In particular, one can introduce the scaled Hamiltonian $\hat{h} = \hat{H}/\aleph$ and scaled generators $\hat{g}_l = \hat{G}_l/\aleph^{\kappa_l}$, where $\kappa_l > 0$ are suitable powers, and enforce validity of the formula $\hat{h} = H(\{\hat{g}_l\})$. If the original Hamiltonian does not satisfy this relation, its parameters must be redefined so that the transformed Hamiltonian does. Consider as an example the extended Dicke model with $\aleph = N$, where the scaled generators read \hat{J}_α/N and $\hat{b}^\dagger/N^{1/2}$, $\hat{b}/N^{1/2}$, so to satisfy the proper behavior of the scaled Hamiltonian \hat{h} we write the atom-field interaction parameter in Eq. (3) as $\lambda/N^{1/2}$. Similarly, scaled bosonic generators of unitary groups are $\hat{b}_k^\dagger \hat{b}_l/N$, where $N = \aleph$ is the total number of bosons, hence the parameters that measure the overall strength of two-body interactions must have the form $\sim \lambda/N$, see Eq. (17). These requirements ensure that with increasing N , the interaction and non-interaction terms keep roughly the same energy proportions as for small N .

If one considers the scaled quantities instead of the bare ones, the role of the dynamical algebra generators $\{\hat{G}_l\}$ is transmitted to the scaled generators $\{\hat{g}_l\}$. Their commutation relations $[\hat{g}_k, \hat{g}_l] = i \sum_m \aleph^{\kappa_m - \kappa_k - \kappa_l} s_{klm} \hat{g}_m$ usually lead to trivial asymptotic behavior $\lim_{\aleph \rightarrow \infty} [\hat{g}_k, \hat{g}_l] = 0$. This holds for all the models studied above, and in general if $\kappa_k + \kappa_l > \kappa_m$ for all index combinations for which $s_{klm} \neq 0$; also the case of polynomially deformed dynamical algebras can be treated in this way. This means that for large \aleph the scaled quantities become quasiclassical and the infinite-size limit $\aleph \rightarrow \infty$ of the system coincides with the *classical limit*. The identification of QPT and ESQPT phenomena in such systems therefore depends on the analysis of the classical dynamics. Among the vast literature dealing with classical limits of quantum systems we mention Ref. [158], where a general method is described assigning classical canonical variables and the associated phase space to algebraically based systems, and Ref. [131], which shows that the coordinate-momentum resolution of a set of generators can be done via a boson realization of the dynamical algebra.

In conclusion, we have arrived to a somewhat paradoxical result that for algebraic systems with finite DOF numbers all quantum critical effects, which belong to $\aleph \rightarrow \infty$ emergent **phenomena**, must be rooted in purely classical properties. This is true for the determination of the phase structure of the system and for the classification of its phase transitions. However, we emphasize that the classical-like behavior for large values of \aleph applies only to scaled quantities, while the original unscaled quantities keep their quantum properties, in particular near the QPT and ESQPT critical points. Here the quantum finite-size effects are important for any value of \aleph .

4. Classical-limit based singularities in quantum spectra

In this section we develop a general formalism for identification and classification of an ESQPT in the classical limit of the quantum system. At first we overview the effects in the smoothed level density and then show that similar effects appear in the smoothed slope (flow) of the spectrum and energy densities of various quantities. Finally we discuss some ESQPT precursors in the oscillatory component of level density.

4.1. Smoothed level density and classification of excited-state singularities

We assume a quantum system which in the classical limit has f DOFs and is described by a Hamiltonian function $H(\mathbf{q}, \mathbf{p})$, where $\mathbf{q} \equiv (q_1, q_2, \dots, q_f)$ and $\mathbf{p} \equiv (p_1, p_2, \dots, p_f)$

are mutually conjugate sets of canonical coordinates and momenta. For points (\mathbf{q}, \mathbf{p}) in the classical phase space \mathcal{P} we introduce a simplified notation with a single symbol \mathbf{x} , that in individual components means $(q_1, \dots, q_f, p_1, \dots, p_f) = (x_1, x_2, \dots, x_{2f})$.

As we saw above, the most significant signatures of the ESQPTS appear in the smoothed level density of the system. This was introduced in Eq. (7), which however contained a somewhat arbitrary smoothening function $\bar{\delta}(E)$. A unique determination of the smoothed level density is possible through semiclassical methods. The exact level density (6) of a bound quantum system can be expressed via the Fourier transformation of the trace of the evolution operator $\hat{U}(t)$, namely as $\rho(E) = (2\pi\hbar)^{-1} \int_{-\infty}^{+\infty} dt \text{Tr } \hat{U}(t) e^{iEt/\hbar}$. Using a semiclassical approximation based on the path integral in the evaluation of $\hat{U}(t)$, one gets a unique resolution of $\rho(E)$ into the smooth and oscillatory components [160–162]. While the smooth component $\bar{\rho}(E)$ is obtained from the contribution of so-called zero-length orbits, the oscillatory component $\tilde{\rho}(E)$ is approximated by a sum of contributions from classical periodic orbits. The formula for the *smooth component*, also called *Weyl's law* [160], reads

$$\bar{\rho}(E) = \frac{1}{(2\pi\hbar)^f} \int d^{2f}\mathbf{x} \delta(E - H(\mathbf{x})) = \frac{\partial}{\partial E} \left[\underbrace{\frac{1}{(2\pi\hbar)^f} \int d^{2f}\mathbf{x} \theta(E - H(\mathbf{x}))}_{\Omega(E)} \right], \quad (26)$$

where θ is the step function. The quantity in square brackets is the cumulative number of eigenstates for all energies below the given value E , and coincides with the volume $\Omega(E)$ of the classical phase space accessible for systems with energy not exceeding the value E divided by the elementary quantum volume $(2\pi\hbar)^f$.

The dimension of the first integration in Eq. (26) can be reduced by one if we perform a transformation from the original phase-space coordinates \mathbf{x} to new ones $\tilde{\mathbf{x}} \equiv (\tilde{x}_1, \dots, \tilde{x}_{2f-1}, \tilde{x}_{2f}) \equiv (\mathbf{y}, \tilde{x}_{2f})$, for which the component \tilde{x}_{2f} points along the $2f$ -dimensional gradient $\nabla H(\mathbf{x})$ of the Hamiltonian on the hypersurface $H(\mathbf{x}) = E$. This hypersurface coincides with the $(2f-1)$ -dimensional manifold obtained by setting $\tilde{x}_{2f} = 0$ and varying the remaining components of $\tilde{\mathbf{x}}$ denoted by \mathbf{y} . Thus we have

$$\bar{\rho}(E) = \frac{1}{(2\pi\hbar)^f} \int d^{2f-1}\mathbf{y} \left| \det \frac{\partial \mathbf{x}}{\partial \tilde{\mathbf{x}}} \right| |\nabla H(\mathbf{y}, 0)|^{-1}, \quad (27)$$

where $\partial \mathbf{x} / \partial \tilde{\mathbf{x}}$ is the Jacobian matrix of the $\mathbf{x} \mapsto \tilde{\mathbf{x}}$ transformation. The integral in Eq. (27) is not well defined at the classical stationary points, where the gradient vanishes. At these points we can expect non-analyticities of the smoothed level density.

Any classical stationary point $\mathbf{x}^{(i)}$, where the superscript $i = 1, 2, \dots, M$ distinguishes all stationary points of the system, obeys the defining condition $\frac{\partial}{\partial x_k} H(\mathbf{x})|_{\mathbf{x}=\mathbf{x}^{(i)}} \equiv \partial_k H(\mathbf{x})|_{\mathbf{x}=\mathbf{x}^{(i)}} = 0$ for $k = 1, 2, \dots, 2f$, that is $\nabla H(\mathbf{x})|_{\mathbf{x}=\mathbf{x}^{(i)}} = 0$. An important role in the classification of any stationary point $\mathbf{x}^{(i)}$ is played by the eigenvalues of the Hessian matrix $\partial_k \partial_l H(\mathbf{x})|_{\mathbf{x}=\mathbf{x}^{(i)}}$. If all these eigenvalues are non-zero numbers, i.e., if the Hessian matrix has a non-vanishing determinant, we deal with a non-degenerate stationary point. This means that the behavior of the Hamiltonian function $H(\mathbf{x})$ around $\mathbf{x}^{(i)}$ is locally quadratic. If, on the other hand, at least one of the eigenvalues is zero, i.e., if the determinant of the Hessian matrix vanishes, the stationary point is called degenerate. The local dependence of the Hamiltonian function near such a point is flat in the directions determined by eigenvectors associated with the vanishing eigenvalues.

For any *non-degenerate stationary point* $\mathbf{x}^{(i)}$, the singular contribution to integrals (26) and (27) from a close vicinity of $\mathbf{x}^{(i)}$ can be calculated explicitly. Each of such

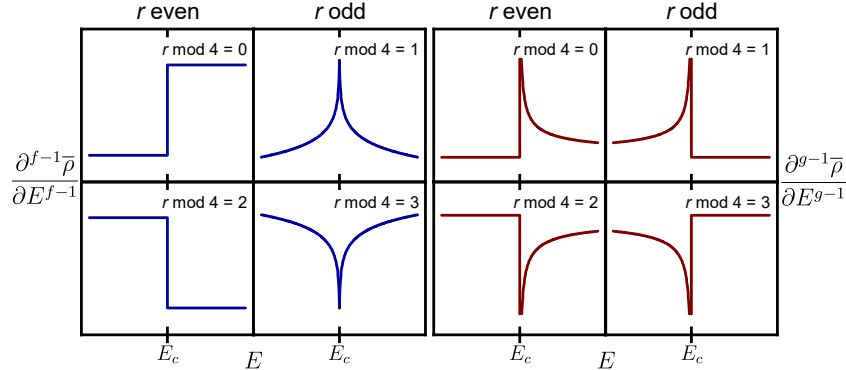


Figure 9. Typology of ESQPT singularities related to non-degenerate stationary points of the classical Hamiltonian in the $(f-1)$ st or $(g-1)$ st derivative of the smoothed level density. The panel on the left corresponds to stationary points in the phase-space of even dimension $2f$, the panel on the right shows effects of stationary points in a space with odd dimension $2g-1$. Adapted from Ref. [159].

points is characterized by an integer $r \in [0, 2f]$ called *index*, which is the number of negative eigenvalues of the Hessian matrix. Hence a non-degenerate stationary point with index r in the phase space of dimension $2f$ represents a local minimum for $r = 0$, local maximum for $r = 2f$, while for intermediate values of r it is a multidimensional saddle point with r and $(2f-r)$ independent directions for which it behaves as a local maximum and minimum, respectively. The effect of index- r non-degenerate stationary point at energy $E_c^{(i)}$ on the smoothed level density was determined in Ref. [14] using the Morse lemma. It is expressed as

$$\frac{\partial^{f-1}}{\partial E^{f-1}} \bar{\rho}(E) \propto h(E) + \begin{cases} (-1)^{r/2} \theta(E - E_c^{(i)}) & \text{for } r \text{ even,} \\ (-1)^{(r+1)/2} \ln |E - E_c^{(i)}| & \text{for } r \text{ odd,} \end{cases} \quad (28)$$

where $h(E)$ is an unspecified smooth function resulting from non-singular contributions to the integrals in Eqs. (26) and (27) from the phase space beyond a vicinity of $\mathbf{x}^{(i)}$. Formula (28) is a more explicit form of Eq. (1), showing how the signs of the step and logarithmic singularities in the $(f-1)$ st derivative depend on the index r . Such singularities are schematically sketched in the left panel of Fig. 9. This enables us to formulate a general classification of the ESQPT effects connected to non-degenerate stationary points in terms of a pair of integers (f, r) . Returning to the $f = 2$ extended Dicke model and its phase diagram in Fig. 2, we can show that ESQPTs between the D–TC and TC–N quantum phases correspond to non-degenerate stationary points of the classical-limit Hamiltonian with indexes $r = 1$ and 2 , respectively. This is consistent with the observed singularities in $\bar{\rho}(E)$. The ESQPT between the N–S phases cannot be classified in this way as the corresponding stationary point lies at the maximal value of j_z and its Hessian matrix is undefined, but as shown in Ref. [73], the singularity of $\bar{\rho}(E)$ is of the same type as for an $r = 2$ stationary point.

The dimension $2f$ of the phase space is always an even number. However, considering integrals (26) formally also in spaces with an odd dimensions $(2g-1)$, where $g = 1, 2, 3\dots$, we find [14] that index- r non-degenerate stationary points lead to

singular dependencies obeying the formula

$$\frac{\partial^{g-1}}{\partial E^{g-1}} \bar{\rho}(E) \propto h(E) + \begin{cases} (-1)^{r/2} \theta(E - E_c^{(i)}) |E - E_c^{(i)}|^{-1/2} & \text{for } r \text{ even,} \\ (-1)^{(r-1)/2} \theta(E_c^{(i)} - E) |E - E_c^{(i)}|^{-1/2} & \text{for } r \text{ odd.} \end{cases} \quad (29)$$

How can these dependencies be relevant for the ESQPT classification? We will see in Sec. 7.1 that the same technique for evaluating the smoothed level density as presented above is used in spatially extended D -dimensional periodic systems, but with the integration of the form (26) performed in the quasi-momentum space instead of phase space. If the quasi-momentum space has an odd dimension, the singularities of the type (29) occur. They are schematically depicted in the right panel of Fig. 9.

The above classification of ESQPT singularities in the level density concerns solely non-degenerate stationary points. We stress that such ESQPTs are the most common ones as the non-degenerate stationary point represents the generic type among all stationary points. Indeed, the vanishing of one or more eigenvalues of the Hessian matrix requires additional constraints which for a typical stationary point are not satisfied or get violated by an infinitesimal perturbation of the Hamiltonian. Nevertheless, in some special cases the *degenerate stationary points*, i.e. those showing a non-quadratic behavior of $H(\mathbf{x})$ near $\mathbf{x}^{(i)}$, appear in the phase space. Effects of such points are remarkable since, in contrast to Eq. (28), they occur in lower than $(f-1)$ st derivatives of $\bar{\rho}(E)$. Because there is no unique classification of degenerate stationary points in arbitrary dimensions, the singularities they generate in the level density must be described case by case.

Consider as an example a degenerate separable local minimum at a point $\mathbf{x}^{(i)}$. The Hamiltonian function in a vicinity of this point can be written as $H(\mathbf{x}) \approx E_c^{(i)} + \sum_{k=1}^{2f} c_k (x_k - x_k^{(i)})^{K_k}$, where c_k are some positive constants and $K_k \geq 2$ powers that quantify the flatness of the minimum. This stationary point produces an extra cumulative phase-space volume $\Omega(E)$ for energies above $E_c^{(i)}$, see Eq. (27). Because the linear size of the additional phase space along the k th axis grows with energy as $(E - E_c^{(i)})^{1/K_k}$, the smoothed level density develops a singularity of the following form,

$$\bar{\rho}(E) \propto g(E) + \theta(E - E_c^{(i)}) (E - E_c^{(i)})^L, \quad L = \sum_{k=1}^{2f} \frac{1}{K_k} - 1, \quad (30)$$

where $g(E)$ is a smooth function. It is clear that if $K_k = 2 \forall k$, we obtain $L = f - 1$, consistently with the case of a non-degenerate minimum, see Eq. (28) with $r = 0$. However, if some of the powers K_k are larger than 2, the ESQPT singularity becomes stronger than in the non-degenerate case. For instance, with $f = 2$ and $K_k = 4$ for all $k = 1, \dots, 4$ (pure quartic minimum of the full Hamiltonian) the step-like dependence at the critical energy appears already in the zeroth derivative of $\bar{\rho}(E)$. Similarly, assuming for $f = 2$ the powers $(K_1, K_2, K_3, K_4) = (4, 4, 2, 2)$ (quartic minimum in coordinates and quadratic in momenta), we obtain a continuous square-root increase of $\bar{\rho}(E)$ with a power-law divergence of $\frac{\partial}{\partial E} \bar{\rho}(E)$ at $E = E_c^{(i)}$.

The most familiar classical Hamiltonian function consists of a quadratic kinetic term with a mass parameter M and a potential energy V :

$$H(\mathbf{q}, \mathbf{p}) = \frac{|\mathbf{p}|^2}{2M} + V(\mathbf{q}). \quad (31)$$

It turns out that a convenient size parameter for systems with this type of classical limit is $\aleph = \sqrt{M/\hbar}$ [11]. Stationary points of Hamiltonians (31) can be disclosed and

classified by analyzing solely the potential function $V(\mathbf{q})$. This reduces the problem from the full $2f$ -dimensional phase space to just an f -dimensional configuration space, implying that the index r of stationary points can take only values between 0 and f . A general analysis of ESQPTs in such systems was presented in Ref. [11].

However, quantum many-body systems usually yield in their classical-limit Hamiltonians $H(\mathbf{q}, \mathbf{p})$ more complicated momentum dependencies than in Eq. (31) (cf. Sec. 3.2). Search for stationary points of such Hamiltonians is more difficult. It is often performed with the aid of a function $\mathcal{V}(\mathbf{q}) \equiv H(\mathbf{q}, \mathbf{p} = 0)$, which looks analogous to the above potential $V(\mathbf{q})$ (cf. Fig. 7). However, the function $\mathcal{V}(\mathbf{q})$ does not, in general, coincide with the potential energy of the system since vanishing of the canonical momentum \mathbf{p} does not generally imply vanishing of the mechanical momentum $\propto \dot{\mathbf{q}}$. Even if the function $H(\mathbf{q}, \mathbf{p})$ depends (perhaps due to its time-reversal symmetry) only on even powers of \mathbf{p} , so that $\mathbf{p} = 0$ implies $\dot{\mathbf{q}} = 0$, one cannot exclude additional $\mathbf{p} \neq 0$ solutions of the $\dot{\mathbf{q}} = 0$ constraint. In this situation, some of the stationary points of $H(\mathbf{q}, \mathbf{p})$ may fail to satisfy the condition $\partial_k \mathcal{V}(\mathbf{q}) = 0$. This leads to a possibility of ESQPT singularities rooted in somewhat counter-intuitive $\mathbf{p} \neq 0$ stationary points. Such ESQPTs were indeed detected in the U(6) interacting boson model on the first-order QPT path between U(5) and SU(3) dynamical symmetries [13].

Stationary points in the classical phase space of the system are not the only classical origin of ESQPTs. Some of these singularities are connected with effects of the *phase-space boundary*. For many-body systems with a finite-dimensional Hilbert space \mathcal{H} the overall volume of the corresponding classical phase space \mathcal{P} must also be finite. For instance, the phase space associated with an interacting boson system at a fixed value N of the total number of bosons (see Sec. 3.2) is a ball (interior of a $2f$ -dimensional sphere with $f = n - 1$) with the radius equal to $\sqrt{2}$ for the usual choice of $\varkappa = N$ in Eq. (5). The finiteness of the phase space \mathcal{P} implies the existence of a boundary $\partial\mathcal{P}$, which can cause additional spectral singularities. In particular, as shown in Ref. [13], stationary points of the Hamiltonian function on the $(2f - 1)$ -dimensional boundary manifold lead to singularities in the smoothed level density calculated from Eq. (26). We stress that stationary points of $H(\mathbf{x})|_{\mathbf{x} \in \partial\mathcal{P}}$ are not true stationary points of the system (excluding exceptional cases) as the derivative of $H(\mathbf{x})$ along the normal direction is not specified. Classification of ESQPTs connected with the phase-space boundary has not yet been given. The studied special cases show that non-degenerate stationary points on $\partial\mathcal{P}$ lead to weaker singularities than non-degenerate stationary points inside \mathcal{P} . However, degenerate stationary points on $\partial\mathcal{P}$ appear more likely than would be guessed because the extremal values of coordinates and momenta on the boundary usually yield somehow restricted behavior of $H(\mathbf{x})|_{\mathbf{x} \in \partial\mathcal{P}}$. Effects of degenerate stationary points on $\partial\mathcal{P}$ may compete with those of non-degenerate stationary points inside \mathcal{P} . Examples of boundary-related ESQPTs were demonstrated in the U(6) interacting boson model along the U(5)–SU(3) transition [13].

4.2. Smoothed level flow and energy densities of various observables

So far the level density has been studied mostly as a function of energy E . Now we fully activate also the variation of the system's control parameter λ . We assume that with running λ individual energy levels $E_i(\lambda)$ just move up or down along the energy axis, i.e., that they do not appear or disappear at any value of λ . This can be expressed by a continuity equation in which the roles of coordinate x and time t are played by

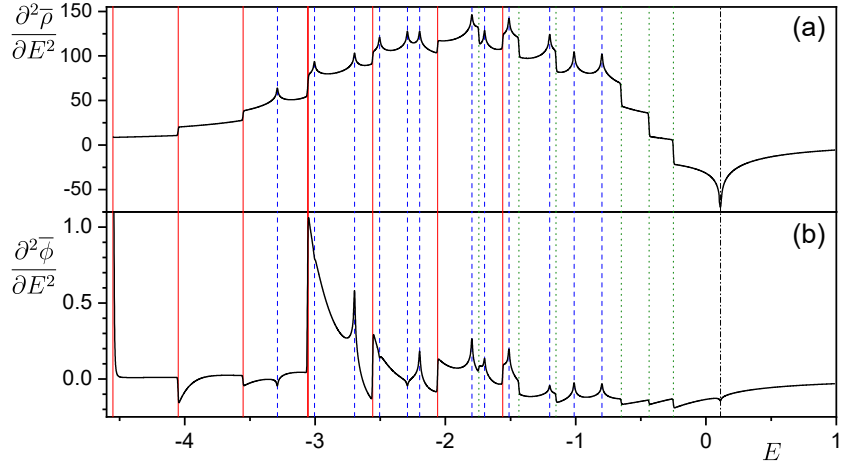


Figure 10. Singularities in the second energy derivatives of (a) the smoothed level density and (b) the smoothed flow rate for a toy $f = 3$ Hamiltonian $\hat{H} = \frac{1}{2}|\hat{\mathbf{p}}|^2 - 2|\hat{\mathbf{q}}|^2 + \frac{1}{4}\hat{q}_1 + \frac{1}{2}\hat{q}_2 + (\frac{3}{4} + \lambda)\hat{q}_3 + \hat{q}_1^4 + \hat{q}_2^4 + \hat{q}_3^4$ at $\lambda = 0$. Energies of stationary points are marked by vertical lines. Adapted from Ref. [14].

E and λ , respectively. For the exact density defined in Eq. (6) the corresponding flow reads $j(\lambda, E) = \sum_i \frac{dE_i}{d\lambda}(\lambda) \delta(E - E_i(\lambda))$. Considering the smoothed density (7) written in terms of the smoothed (differentiable) δ -functions $\bar{\delta}(E - E_i(\lambda))$, we can also define the *smoothed flow*:

$$\bar{j}(\lambda, E) = \sum_i \frac{dE_i(\lambda)}{d\lambda} \bar{\delta}(E - E_i(\lambda)). \quad (32)$$

The continuity equation

$$\frac{\partial}{\partial \lambda} \bar{\rho}(\lambda, E) + \frac{\partial}{\partial E} \bar{j}(\lambda, E) = 0 \quad (33)$$

can then be proven by elementary evaluation of the derivatives involved. Note that the smoothed flow can be also expressed as $\bar{j}(\lambda, E) = \bar{\rho}(\lambda, E) \bar{\phi}(\lambda, E)$ via a smoothed “velocity field” $\bar{\phi}(\lambda, E)$ of levels in the spectrum, called the *flow rate* [11].

The mutual relation of $\bar{\rho}(\lambda, E)$ and $\bar{j}(\lambda, E)$ or $\bar{\phi}(\lambda, E)$ following from the continuity equation (33) leads to the conclusion that in generic situations both quantities share the same type of non-analyticity [14]. Indeed, assuming that both smoothed level density and flow are k times differentiable functions, the continuity equation implies that $\frac{\partial}{\partial \lambda} \frac{\partial^k}{\partial E^k} \bar{\rho} + \frac{\partial^{k+1}}{\partial E^{k+1}} \bar{j} = 0$. Consider now a discontinuity or divergence in the $(k+1)$ st energy derivative of the smoothed level density occurring at an ESQPT critical borderline given by a smooth curve $E = E_c(\lambda)$ in the $\lambda \times E$ plane. If we choose a point (λ, E) at the critical borderline so that $\frac{d}{d\lambda} E_c(\lambda) \neq 0$, the derivative $\frac{\partial}{\partial \lambda} \frac{\partial^k}{\partial E^k} \bar{\rho}(\lambda, E)$ must show the same type of non-analyticity as $\frac{\partial^{k+1}}{\partial E^{k+1}} \bar{\rho}(\lambda, E)$. The differentiated continuity equation implies that this singularity must be compensated by the same type of singularity in the derivative $\frac{\partial^{k+1}}{\partial E^{k+1}} \bar{j}(\lambda, E)$ of the smoothed flow. The same conclusion holds also for the smoothed flow rate $\bar{\phi}(\lambda, E)$ [14]. We stress that the signs and sizes of singular terms in the dependencies $\bar{\rho}(\lambda, E)$, $\bar{j}(\lambda, E)$ and $\bar{\phi}(\lambda, E)$ differ but the type of non-analyticity (discontinuity or divergence) is the same.

The systems with $f = 1$ must be treated separately as their stationary points affect typically the zeroth derivative of the level density. It turns out that in this case a divergence of $\bar{\rho}(\lambda, E)$ causes an indefinite singularity of $\bar{\phi}(\lambda, E)$ [12].

These conclusions are illustrated in Fig. 10. Here we see singularities in $\frac{\partial^2}{\partial E^2}\bar{\rho}(\lambda, E)$ and $\frac{\partial^2}{\partial E^2}\bar{\phi}(\lambda, E)$ at a number non-degenerate stationary points of a toy $f = 3$ Hamiltonian of the form (31). The singularities in the smoothed level density agree with Eq. (28), taking into account the indexes $r = 0, \dots, 3$ assigned to individual stationary points. The corresponding singularities in the smoothed flow rate are of the same types, but are often turned upside down. For details see Ref. [14].

The slopes of individual energy levels $E_i(\lambda)$ can be expressed via the Hellmann-Feynman formula

$$\frac{dE_i(\lambda)}{d\lambda} = \left\langle \psi_i(\lambda) \left| \frac{\partial \hat{H}}{\partial \lambda} \right| \psi_i(\lambda) \right\rangle \equiv \langle H' \rangle_i, \quad (34)$$

where $|\psi_i(\lambda)\rangle$ is the Hamiltonian eigenvector assigned to the i th eigenvalue at the parameter value λ . The smoothed flow in Eq. (32) is then rewritten in the form of Eq. (8) with the general quantity A substituted by the Hamiltonian derivative with respect to λ . Hence we write $\bar{j}(\lambda, E) = \bar{H}'(\lambda, E)$, where H' stands for the quantity associated with operator $\frac{\partial}{\partial \lambda} \hat{H}$. Therefore, returning to Fig. 3 above, we see that the curve depicting the smoothed energy dependence of quantity $\hat{H}'(\delta)$ is also the smoothed flow of the spectrum. This explains why its non-analyticities at the ESQPT critical energies are of the same type as those in the dependence of $\bar{\rho}(\lambda, E)$, see Fig. 2.

We stress that singular dependencies of $\bar{H}'(\lambda, E)$ at the ESQPT critical borderlines must be attributed to singular changes in the structure of eigenstates. For linear Hamiltonians the operator $\frac{\partial}{\partial \lambda} \hat{H}$ is independent of λ and all variations of its expectation values with λ and E are solely due to the variations of $|\psi_i(\lambda)\rangle$. Therefore, the ESQPTs caused by non-degenerate stationary points are likely to affect the $(f-1)$ st derivative of the smoothed energy density from Eq. (8) for almost any generic observable.

An estimate of expectation values revealing the classical origins of their ESQPT singularities can be obtained via the phase-space integration. Indeed, the smoothed energy density $\bar{A}(\lambda, E)$ of a quantity \hat{A} in the energy spectrum for large values of the size parameter N is given by the phase-space average of the corresponding classical observable $A(\mathbf{q}, \mathbf{p}) \equiv A(\mathbf{x})$ over the $H(\lambda, \mathbf{x}) = E$ manifold:

$$\bar{A}(\lambda, E) = \frac{1}{(2\pi\hbar)^f} \int d^{2f}\mathbf{x} A(\mathbf{x}) \delta(E - H(\lambda, \mathbf{x})). \quad (35)$$

This quantity represents the overall density of quantity A at given energy, i.e., its average in a single state times the density of states. The single-state average reads

$$\bar{a}(\lambda, E) = \frac{\bar{A}(\lambda, E)}{\bar{\rho}(\lambda, E)} = \frac{\int d^{2f}\mathbf{x} A(\mathbf{x}) \delta(E - H(\lambda, \mathbf{x}))}{\int d^{2f}\mathbf{x} \delta(E - H(\lambda, \mathbf{x}))}. \quad (36)$$

In particular, using the last formula in $f=1$ systems, we obtain

$$\bar{a}(\lambda, E) = \sum_o \underbrace{\frac{T_o}{\sum_{o'} T_{o'}}}_{w_o} \underbrace{\frac{1}{T_o} \int_0^{T_o} dt A(\mathbf{x}_o(t))}_{\langle A \rangle_o}, \quad (37)$$

where $\langle A \rangle_o$ is the time average of A over a classical orbit $\mathbf{x}_o(t)$ with period T_o (all these quantities depend implicitly on λ and E). We assume that, in general, there **is** more primitive periodic orbits at given energy E , and we sum over them (index o)

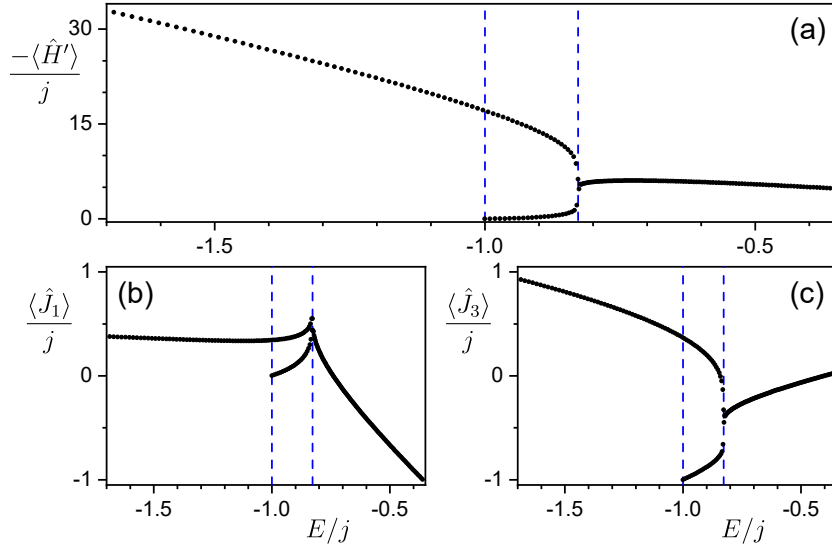


Figure 11. Expectation values of various observables in eigenstates of the same Lipkin Hamiltonian as in Fig. 6. We set $\lambda = 0.8$ (vertical line in Fig. 6) and $N = 2j = 200$. Since $f = 1$, Peres lattices localize along curves. Panel (a) corresponds to observable $-\hat{H}' = N^{-1}(\hat{J}_1 + 4\hat{J}_3 + 2N)^2$, panel (b) to \hat{J}_1 and panel (c) to \hat{J}_3 (note that $\langle \hat{J}_2 \rangle_i = 0 \forall i$). The ESQPT with index $r=0$ at $E_{c1} = -j$ adds a second branch of points to each lattice, so it produces a jump of the smoothed value of the respective observable. The ESQPT with $r=1$ at $E_{c2} > -j$ is seen as a merge of both branches, yielding a singular energy derivative of the smoothed dependence (cf. Fig. 7). Note that the latter singularity differs from that of $\bar{\rho}(\lambda, E)$ as this is the exceptional $f = 1$ case (see the text).

with weight factors w_o . Note that in some calculations equal weights for all orbits are used [56]. The existence of different orbits at the same energy (like the orbits located in different potential wells in the case of a double-well potential) generates distinct branches of the expectation values $\langle A \rangle_i$, which are given by individual time averages $\langle A \rangle_o$ along the corresponding orbits. Energies of the stationary points, at which the orbits undergo non-analytic change (e.g., bifurcate to both wells in the example of a double-well potential), locate non-analyticities of the dependence $\bar{a}(\lambda, E)$ and splittings of the $\langle A \rangle_i$ branches. Such effects are illustrated in Fig. 11 for several choices of the observable \hat{A} in the spectrum of the Lipkin model from Fig. 6. Instead of showing the dependencies of various averages $\langle \hat{A} \rangle_i$ and $\langle \hat{B} \rangle_i$ on energy, the work in Ref. [56] presents mutual dependencies of these observables on each other, which for $f = 1$ systems (there the second-order QPT Lipkin model) form curves with non-analyticities and bifurcations on the ESQPT points.

The above considerations bring us to a more general question about general possibilities to identify quantum phases separated by an ESQPT in an arbitrary system. It is difficult and probably impossible to distinguish these phases by some generally defined ‘‘order parameters’’, i.e., suitable observables whose expectation values $\langle \hat{A} \rangle_i$, or more precisely densities $\bar{A}(\lambda, E)$, are zero in one phase and non-zero in the other. These observables should not be chosen *ad hoc* for a particular system, but are required to follow from some universal principles. Indeed, the ESQPT effects in numerous systems

can be characterized by spontaneous breaking of a particular symmetry of the system for the eigenstates in one of the quantum phases [51, 92]. Considering as an example an ESQPT linked to the local maximum of a symmetric $f = 1$ double-well potential, the symmetry which is spontaneously broken in the quantum phase with lower energy is the parity (parity doublets below the barrier become nearly degenerate). This picture can be generalized to $f > 1$ systems with a second-order ground-state QPT whose critical point is associated with a degenerate minimum of the classical-limit Hamiltonian. In these cases, the order parameter \hat{A} can be derived from the operator generating the broken symmetry, i.e., from the parity in the above examples.

However, the spontaneous symmetry breaking mechanism does not characterize an arbitrary ESQPT in any system. It fails particularly in systems with first-order ground-state QPTs. In such situations, a universal order parameter cannot be identified, but the distinction of quantum phases can still be based on differences in smoothed energy dependencies and ESQPTs can be identified by non-analyticities of these dependencies. Examples of ESQPT singularities in expectation values of various quantities can be found in a number of references, see e.g. Refs. [49–51, 54, 56, 61, 63, 69, 74, 83] for the Dicke and related models, [56, 93, 95, 107] for the Lipkin model, [48, 52] for the vibron model, [59, 141] for the nuclear interacting boson model, and many others.

4.3. Oscillatory level density and finite-size effects in coupled systems

So far we have focused on the smoothed level densities, flows and smoothed energy densities of observables. However, all these quantities have also the oscillatory components, which sometimes play important roles in the description of ESQPTs. The semiclassical approximation of the oscillatory level density $\tilde{\rho}(E) = \rho(E) - \bar{\rho}(E)$ is expressed via so-called *trace formulas*, taking into account periodic orbits generated by the classical-limit Hamiltonian of the system [160]. Returning to the notation in which the dependence on the control parameter λ is implicit, these formulas have the following general form:

$$\tilde{\rho}(E) \approx \frac{1}{\pi\hbar} \sum_o \sum_{\iota=1}^{\infty} \frac{T_o(E)}{C_{o\iota}(E)} \cos \left(\frac{\iota I_o(E)}{\hbar} - \varphi_{o\iota} \right). \quad (38)$$

Here the sums run over all primitive periodic orbits o at energy E with period $T_o(E)$ and their multiple repetitions $\iota = 1, 2, \dots$, the quantity $I_o(E) = \oint_{o(E)} \mathbf{p} \cdot d\mathbf{q}$ represents an action along the primitive orbit, and $\varphi_{o\iota}$ is a phase shift. The form of quantity $C_{o\iota}(E)$ depends on whether the system is chaotic or integrable, the resulting formulas being called after Gutzwiller [161] or Berry and Tabor [162], respectively, for an overview see Ref. [160]. It expresses the degree of “stability” of the given orbit, in the sense of a chaotic or integrable system, and ensures that more stable orbits give larger contributions to $\tilde{\rho}(E)$ than less stable ones.

By its definition, the oscillatory level density $\tilde{\rho}(E)$ has zero mean, expressing only positive and negative deviations of the real density from the average represented by $\bar{\rho}(E)$. The energy scale of these fluctuations for each periodic orbit (o, ι) is determined by the immediate slope of the function inside the cosine term of Eq. (38). The energy period $\Delta E_{o,\iota} \approx 2\pi\hbar/\iota \frac{d}{dE} I_o(E)$ decreases to zero in the classical limit $\hbar \rightarrow 0$, so the classical oscillatory level density is an infinitely fast fluctuating function which gets washed out by smoothening over an infinitesimally narrow energy interval. Hence in the limit $\hbar \rightarrow 0$, equivalent to $N \rightarrow \infty$, only the smooth component $\bar{\rho}(E)$ remains

relevant. However, the oscillatory component $\tilde{\rho}(E)$ is important in finite-size cases, and as discussed below, can produce even stronger finite-size precursors of ESQPTs than visible for the given value of N in the smooth density $\bar{\rho}(E)$. These effects arise in systems composed of two or more subsystems that are fully or partially separable.

Consider a fully *separable system* with the Hilbert space $\mathcal{H} = \mathcal{H}_1 \otimes \mathcal{H}_2$ composed of subspaces \mathcal{H}_k corresponding to the $k = 1$ and 2 subsystems, and with a quantum Hamiltonian $\hat{H} = \hat{H}_1 + \hat{H}_2$ (more precisely $\hat{H} = \hat{H}_1 \otimes \hat{I}_2 + \hat{I}_1 \otimes \hat{H}_2$, where \hat{H}_k and \hat{I}_k are the Hamiltonian and the unit operator, respectively, in \mathcal{H}_k). Also the classical Hamiltonian is a sum of the respective parts $H(\mathbf{x}) = H_1(\mathbf{x}_1) + H_2(\mathbf{x}_2)$ in a $2f$ -dimensional phase space written as the Cartesian product $\mathcal{P} = \mathcal{P}_1 \times \mathcal{P}_2$ of phase spaces of both subsystems, with the overall DOFs being sum of the subsystem's DOFs, $f = f_1 + f_2$. Due to additivity of energies, the total level density $\rho(E)$ of the whole system is a convolution of level densities $\rho_1(E_1)$ and $\rho_2(E_2)$ of the subsystems, namely

$$\rho(E) = \int \int dE_1 dE_2 \rho_1(E_1) \rho_2(E_2) \delta(E_1 + E_2 - E). \quad (39)$$

For the smoothed and oscillatory components of the total level density we obtain [12]:

$$\begin{aligned} \bar{\rho}(E) &= \int dE_1 \bar{\rho}_1(E_1) \bar{\rho}_2(E - E_1), \\ \tilde{\rho}(E) &= \int dE_1 \bar{\rho}_1(E_1) \tilde{\rho}_2(E - E_1) + \int dE_1 \tilde{\rho}_1(E_1) \bar{\rho}_2(E - E_1) + \int dE_1 \tilde{\rho}_1(E_1) \tilde{\rho}_2(E - E_1), \end{aligned} \quad (40)$$

where $\bar{\rho}_k(E)$ and $\tilde{\rho}_k(E)$ are smooth and oscillatory level densities of the k th subsystem. Note that all integrals in Eq. (40) are taken from the minimal energy $E_{1\min}$ of the subsystem 1 up to $(E - E_{2\min})$ given by is the minimal energy $E_{2\min}$ of subsystem 2.

To define size parameters of separable systems, we refine the general treatment described in Sec. 3.4. We chose a characteristic energy scale \mathcal{E} and its “typical” partitioning $\mathcal{E} = \mathcal{E}_1 + \mathcal{E}_2$ to the subsystems. This is of course ambiguous, but we usually choose nearly equal splitting $\mathcal{E}_1 \sim \frac{1}{2}\mathcal{E} \sim \mathcal{E}_2$. Following formula (25) and employing **multiplicability** of volumes $\Omega_k(E_k)$ in the $\mathcal{P}_1 \times \mathcal{P}_2$ phase space, we get:

$$\aleph^f \equiv \frac{\Omega(\mathcal{E})}{\hbar^f} = \frac{\Omega_1(\mathcal{E}_1)}{\hbar^{f_1}} \frac{\Omega_2(\mathcal{E}_2)}{\hbar^{f_2}} \equiv \aleph_1^{f_1} \aleph_2^{f_2}. \quad (41)$$

Here \aleph is the size parameter of the whole system at energy scale \mathcal{E} , and \aleph_1 and \aleph_2 are size parameters of the subsystems at scales \mathcal{E}_1 and \mathcal{E}_2 . To see how it works, let us look for example on the Dicke model (3) with subsystems 1 and 2 identified with the bosonic field and the ensemble of N atoms, respectively. Consider first the balanced regime (Sec. 2.1) with $\omega \sim \omega_0$ represented by a common average $\bar{\omega}$. The characteristic energy can be chosen as twice the saturation energy of the atomic subsystem in absence of interaction, $\mathcal{E} = 2N\omega_0$ (this energy range contains all ESQPTs described in Sec. 2.2), and the equal partitioning $\mathcal{E}_1 = \mathcal{E}_2 = N\omega_0 \approx N\bar{\omega}$ yields equal size parameters $\aleph_1 = \aleph_2 = \aleph = N$. On the other hand, the strongly imbalanced Rabi regime with $R = \omega_0/\omega \gg 1$ (Sec. 2.3) results in different values. The same choice of energy scales \mathcal{E} , \mathcal{E}_1 and \mathcal{E}_2 as above leads now to $\aleph_1 = NR$ (field) and $\aleph_2 = N$ (atoms), while the total size parameter is $\aleph = NR^{1/2}$.

Such imbalanced settings of coupled systems are in our main focus here. Suppose without loss of generality that $\aleph_1 \gg \aleph_2$. This means that subsystem 1 is much closer to classicality, so its energy levels E_{1i} are much denser than energy levels E_{2i} of the subsystem 2 and the oscillatory level density $\tilde{\rho}_1(E_1)$ oscillates much faster than $\tilde{\rho}_2(E_2)$.

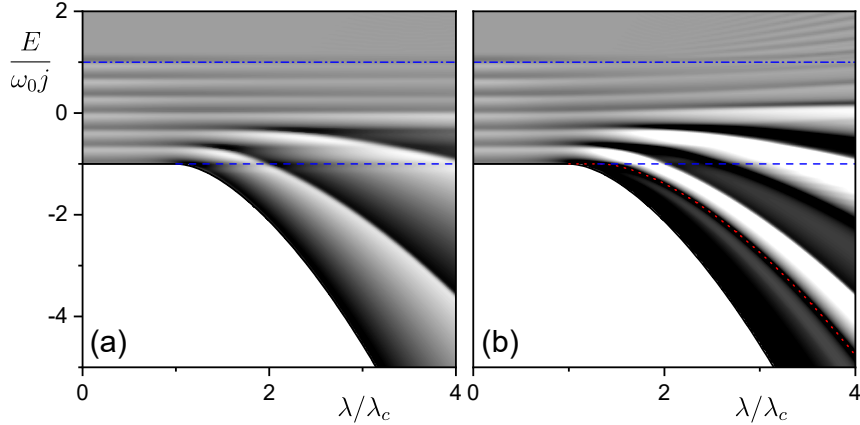


Figure 12. Oscillatory component of the level density of the extended Dicke model (3) in a strongly imbalanced regime with $\omega = 1$, $\omega_0 = 30$ for $N = 2j = 6$. Panel (a) corresponds to $\delta = 1$, panel (b) to $\delta = 0.132$ (cf. Fig. 2). We know from Sec. 2.3 that the full spectrum is approximated by a pile-up of field spectra corresponding to individual quasispin projections. This affects the oscillatory level density, which is calculated as $\tilde{\rho}(E) = \rho_\sigma(E) - \bar{\rho}(E)$, where $\rho_\sigma(E)$ is the exact density folded with a Gaussian of width $\sigma = 0.04$ and $\bar{\rho}(E)$ is the semiclassical density (26). Dashed and dotted lines, respectively, mark ESQPT borderlines associated with jumps and peaks of $\frac{\partial}{\partial E}\bar{\rho}(E)$. Similar structures appear repeatedly in $\tilde{\rho}(E)$, whose positive (negative) values correspond to dark (light) shades.

Under these conditions, the second and third integrals in the second line of Eq. (40) can be neglected.

For the sake of concreteness we assume that: (i) a non-degenerate stationary point with index r_1 in the phase space of subsystem 1 induces the corresponding ESQPT non-analyticity in $\frac{\partial^{f_1-1}}{\partial E_1^{f_1-1}}\bar{\rho}_1(E_1)$ at energy $E_{1c} > E_{1\min}$, and (ii) the only stationary point of subsystem 2 is a non-degenerate global minimum (index $r_2 = 0$) at $E_{2\min}$, so $\bar{\rho}_2(E_2)$ has no ESQPT. Then the whole system exhibits at the total energy $E = E_c = E_{1c} + E_{2\min}$ the same type of non-analyticity as subsystem 1 but in the derivative $\frac{\partial^{f-1}}{\partial E^{f-1}}\bar{\rho}(E)$. This conclusion follows from the analysis of the first line in Eq. (40) as well as from the properties of the corresponding stationary point with index $r = r_1 + r_2 = r_1$ in the coupled phase space $\mathcal{P}_1 \times \mathcal{P}_2$. The singularity in $\bar{\rho}(E)$ is shifted up to the $(f_1 + f_2 - 1)$ st derivative, consistently with the larger DOF number of the whole system, so it is weaker than that in $\bar{\rho}_1(E_1)$. However, summing both the smooth and oscillatory components of the level density in Eq. (40) yields (neglecting the integrals involving quickly oscillating functions)

$$\rho(E) \approx \sum_i \bar{\rho}_1(E - E_{2i}), \quad (42)$$

where we see a cumulative repetition of the level density of subsystem 1 above each discrete level E_{2i} of subsystem 2. The density in Eq. (42) shows a multiple occurrence of the singularity in the $(f_1 - 1)$ st derivative at energies $E = E_{1c} + E_{2i}$ for $i = 1, 2, \dots$

Similar analyses as presented above would apply also in other situations, e.g., in cases with multiple and/or degenerate stationary points in \mathcal{P}_1 , or with additional stationary points in \mathcal{P}_2 . The general result is an enhancement of ESQPT signatures

in strongly imbalanced separable systems. These effects represent only finite-size precursors (subsystem 2 is small) and would disappear in the full semiclassical limit. It is worth noting that the effect is contained in the first term of the second-line formula in Eq. (40), which is on the contrary neglected for balanced systems. As shown in Ref. [12], this term is not included in the quasiclassical formula (38) as the corresponding periodic orbits are scarce.

Exact separability implies full integrability of the system. However, it has been shown [12] that even an approximate separability can produce effects very close to those described above, although in less perfect forms. Islands of separable classical orbits, i.e., orbits composed of independent components corresponding to different DOFs, can coexist with the others in the phase space of partially (even strongly) chaotic systems. If one of the DOFs has an ESQPT, the presence of such islands—including maybe infinitesimally small ones—leads to appearance of the above-described ESQPT precursors. Interestingly, if subsystem 1 shows more stationary points above the global minimum, the orbits located in the phase-space domains near these points generate selectively only the precursors of the corresponding ESQPT [12].

There exist numerous examples of separable or partially separable many-body systems with the above type of ESQPT related finite-size effects. We have already described the Rabi regime of the atom-field system [63, 65] (Sec. 2.3). Oscillatory structures in the spectrum of this system caused by imbalance of elementary excitation energies of the atomic and field subsystems are shown in Fig. 12. We have also mentioned the two-spin Gaudin model [64] (Sec. 3.1) and the interacting boson-fermion models (Sec. 3.2). Recently, a neat example of separability-induced ESQPT effects was presented in the U(6) interacting boson model along the first-order QPT path between U(5) and SU(3) dynamical symmetries [13].

5. Thermodynamic consequences

Critical effects in excited states must show up in thermodynamic properties of the system. At the first sight, there seems to be a direct link between the ESQPTs and the TPTs, i.e., standard phase transitions induced by thermal excitations. However, it turns out that although these two types of criticality are related, they represent distinct phenomena which can be applied only in mutually incompatible contexts. In this section, we overview the presently known thermodynamic aspects of ESQPTs, noting that research in this field still needs to be continued. In all derivations below we set the Boltzmann constant k_B to unity.

5.1. Thermodynamics of finite quantum systems

In spite of the early application of quantum mechanics in thermodynamics through Einstein's 1905 solution of the specific heat problem, fundamental reconsideration of the laws of thermodynamics in the quantum framework became a subject of systematic research only relatively recently, see e.g. Ref. [163]. This is related to the fact that the present experimental quantum simulation techniques make quantum effects in thermodynamics accessible to experimentation and potentially applicable in quantum technologies [146]. Quantum effects, including QPTs and ESQPTs, can serve as resources for some particular functionalities of the corresponding nanostructures, but they can also generate obstacles. Let us mention, for example, a recent analysis [87] of a

quantum heat engine based on the quasispin system, in which quantum criticality (both QPT and ESQPT) played a negative role for the engine function.

We start our discussion with some general relations between thermodynamic quantities and properties of quantum energy spectra $E_i(\lambda)$. The Hamiltonian control parameter λ appears explicitly in all expressions. In *canonical thermodynamics*, we assume that the quantum system exchanges its energy with an external heat bath, which leads to the familiar form of the occupation probabilities of individual levels,

$$p_i(\lambda, T) = \frac{e^{-E_i(\lambda)/T}}{Z(\lambda, T)}, \quad Z(\lambda, T) = \sum_i e^{-E_i(\lambda)/T} = \int dE \rho(\lambda, E) e^{-E/T}, \quad (43)$$

where $Z(\lambda, T)$ is the canonical partition function. The thermal distribution of energy of the system $w_T(\lambda, E) = \sum_i \delta(E - E_i(\lambda)) p_i(\lambda, T)$ then in a smoothed form reads

$$\bar{w}_T(\lambda, E) = \bar{\rho}(\lambda, E) \frac{e^{-E/T}}{Z(\lambda, T)}. \quad (44)$$

Consider a quantity with values $A_i(\lambda)$ assigned to individual energy levels, yielding a smoothed energy dependence

$$\bar{A}(\lambda, E) = \sum_i A_i(\lambda) \bar{\delta}(E - E_i(\lambda)) \equiv \bar{a}(\lambda, E) \bar{\rho}(\lambda, E). \quad (45)$$

Here we do not aim at standard quantum mechanical observables \hat{A} , but rather associate $A_i(\lambda)$ with some definite characteristics of individual energy levels, e.g. with their slopes $\frac{d}{d\lambda} E_i(\lambda) \equiv E'_i(\lambda)$ or curvatures $\frac{d^2}{d\lambda^2} E_i(\lambda) \equiv E''_i(\lambda)$. We use notation with $\langle A(\lambda) \rangle_T = \sum_i p_i(\lambda, T) A_i(\lambda)$ standing for the thermal average at temperature T , and with $\langle\langle A(\lambda)^2 \rangle\rangle_T = \langle A(\lambda)^2 \rangle_T - \langle A(\lambda) \rangle_T^2$ denoting the corresponding variance. Besides the density $\bar{A}(\lambda, E)$ we introduce in Eq. (45) also a smoothed single-level contribution $\bar{a}(\lambda, E)$, which represents a local average of values $A_i(\lambda)$ assigned to individual levels near energy E [cf. Eq. (36)]. For the slopes $E'_i(\lambda)$, e.g., the overall dependence is the smoothed flow $\bar{j}(\lambda, E)$ from Sec. 4.2, while the single-level contribution is what we called the smoothed flow rate $\bar{\phi}(\lambda, E)$. The single-level contribution yields the following approximation of the thermal average: $\langle A(\lambda) \rangle_T \approx \int dE \bar{a}(\lambda, E) \bar{w}_T(E)$.

The description of TPTs in standard thermodynamics is based on the behavior of the free energy $F = \langle E \rangle_T - TS$, where $S = -\sum_i p_i \ln p_i$ is the entropy associated with an arbitrary occupation probabilities p_i of energy levels. Minimization of the free energy (i.e., maximization of the entropy with $\langle E \rangle_T$ fixed) over all sets $\{p_i\}$ leads to the canonical occupation probabilities (43). The equilibrium value of the free energy reads $F = -T \ln Z$. Its temperature derivatives are given by

$$\frac{\partial}{\partial T} F(\lambda, T) = -S(\lambda, T), \quad \frac{\partial^2}{\partial T^2} F(\lambda, T) = -\frac{\langle\langle E(\lambda)^2 \rangle\rangle_T}{T^3} = -\frac{C(\lambda, T)}{T}, \quad (46)$$

where we used the canonical entropy $S = \langle E \rangle_T / T + \ln Z$, the energy variance $\langle\langle E^2 \rangle\rangle_T$ associated with the spectrum at given λ , and the specific heat C . For derivatives of the free energy with respect to λ we obtain relations

$$\frac{\partial}{\partial \lambda} F(\lambda, T) = \langle E'(\lambda) \rangle_T, \quad \frac{\partial^2}{\partial \lambda^2} F(\lambda, T) = \langle E''(\lambda) \rangle_T - \frac{\langle\langle E'(\lambda)^2 \rangle\rangle_T}{T}, \quad (47)$$

and a similar one for $\frac{\partial^2}{\partial \lambda \partial T} F(\lambda, T)$ [10].

Formulas (46) and (47) interconnect standard thermodynamic functions describing the thermally equilibrated system and the thermal averages of quantities

of the type (45) characterizing the spectrum of energy levels. This forms a bridge between thermodynamic and quantum phases of the system. The strongest link can be expected near the thermodynamic limit, when the canonical distribution of energy (44) is supposed to form a peak centered at energy $E \approx \langle E(\lambda) \rangle_T$ whose width $\Delta E \approx \langle\langle E(\lambda)^2 \rangle\rangle_T^{1/2}$ satisfies the condition $\Delta E \ll E$. This activates the microcanonical approximation, in which the partition function is given by $Z(\lambda, T) \approx \bar{\rho}(\lambda, E) \Delta E e^{-E/T}$ and the canonical entropy by the original Boltzmann definition $S(\lambda, T) \approx \ln [\bar{\rho}(\lambda, E) \Delta E]$.

Using Eqs. (46) and (47) in the microcanonical approximation, one can evaluate all thermal averages and variances via the formula $\langle A(\lambda) \rangle_T \approx \bar{a}(\lambda, \langle E(\lambda) \rangle_T)$, where the right-hand side is the smoothed single-level contribution from Eq. (45) taken at energy $E = \langle E(\lambda) \rangle_T$. Now, consider a TPT at a critical temperature $T = T_c(\lambda)$ forming a phase separating curve in the $\lambda \times T$ plane and suppose that this curve is not parallel with either of the λ and T directions. If the TPT is of the first order, it shows up as a discontinuity in the first derivatives of the free energy. This is equivalent to a jump in $\ln \bar{\rho}(\lambda, E)$ if the phase separatrix is crossed in the T direction, see the first formula in Eq. (46), and to a jump in the flow rate $\langle E'(\lambda) \rangle_T$ if the separatrix is crossed in the λ direction, see the first formula in Eq. (47). These look like signatures of a generic ESQPT in a $f = 1$ system (see Secs. 4.1 and 4.2). On the other hand, a second-order TPT generates a discontinuity in the second derivatives of the free energy, that is in the first derivative of $\ln \bar{\rho}(\lambda, E)$ and $\langle E'(\lambda) \rangle_T$, resembling a generic ESQPT for $f = 2$. The second formulas in Eqs. (46) and (47) moreover imply singular evolutions of quantities $\langle\langle E(\lambda)^2 \rangle\rangle_T$, $\langle E''(\lambda) \rangle_T$, and $\langle\langle E'(\lambda)^2 \rangle\rangle_T$.

We have to quickly declare that part of the suggestions in the previous paragraph is misleading. It is true that Eqs. (46) and (47) connect thermodynamic and spectral properties, and this is indeed interesting for systems that show TPTs rooted in canonical thermodynamics. However, the opposite implication—that each ESQPT in a moderate- f system leads to a TPT in its canonical description—would be incorrect. This is because canonical thermodynamics *does not* converge to the microcanonical one in the infinite-size limit $N \rightarrow \infty$ of systems with finite DOF numbers, i.e., in the systems for which the ESQPTs are relevant. Therefore, the canonical averages in the above relations cannot be replaced by the microcanonical ones and the suggested equivalence of canonical TPTs and ESQPTs breaks down.

Finite- f systems violate standard thermodynamic rules in many ways. We immediately see that if the Hamiltonian is scaled so that the total energy is extensive in the size parameter N , the average thermal energy per DOF diverges with $N \rightarrow \infty$. This is in conflict with the equipartition theorem. The discrepancies between canonical and microcanonical pictures in the infinite-size limit of finite- f systems can be linked to anomalous forms of the canonical thermal energy distribution (44). Indeed, searching for points satisfying $\frac{\partial}{\partial E} \bar{w}_T(\lambda, E) = 0$, we obtain the equation

$$\frac{\partial}{\partial E} \ln \bar{\rho}(\lambda, E) = \frac{1}{T}. \quad (48)$$

This implies that for the distribution $\bar{w}_T(\lambda, E)$ having a single maximum at energy increasing with T we need that the microcanonical entropy $\ln \bar{\rho}(\lambda, E)$ is a monotonously increasing concave function of energy. For the energy distribution satisfying $\Delta E/E \ll 1$ we moreover need that $C(\lambda, T) \ll \langle E(\lambda) \rangle^2/T^2$. All these conditions can be broken in finite- f systems, and the most flagrant violation is observed in systems with ESQPTs.

Non-standard thermal properties of collective quantum systems, such as quasispin systems with infinite-range interactions constrained to a single- j subspace of states, become a subject of recent study. For example, anomalously wide (“non-concentrating”) thermal distributions of various quantities and insufficiency of thermal averages to capture relevant thermal properties were discussed in Ref. [84]. Anomalous thermalization properties, involving some memory effects connected with apparently thermalized states prepared by different non-equilibrium procedures, were reported in Ref. [85]. Although the role of ESQPTs in many of these phenomena is not decisive, they are present in the models used and participate in the results obtained. Examples of anomalous relaxation of systems dynamically excited to the ESQPT energy region will be further discussed in Sec. 6.1.

5.2. Microcanonical singularities

Microcanonical thermodynamics, already mentioned above, represents a natural ground for studying thermal critical properties of finite quantum systems [29–31, 164–166]. It assumes that the system is isolated, having a fixed energy (uniformly distributed within a narrow interval), and that its thermalization proceeds only via internal interactions. The microcanonical description is based on the microcanonical entropy $\mathcal{S}(\lambda, E) = \ln \bar{\rho}(\lambda, E)$ (neglecting an arbitrary additive constant). The definition of the microcanonical temperature, $\mathcal{T}^{-1}(\lambda, E) = \frac{\partial}{\partial E} \mathcal{S}(\lambda, E)$, parallels the basic relation for canonical temperature, $T^{-1} = \frac{\partial}{\partial U} S$, where S is the canonical entropy and U the internal energy. If the canonical thermal energy distribution $\bar{w}_T(\lambda, E)$ forms a single peak, we see from Eq. (48) that the microcanonical temperature \mathcal{T} assigned to energy E is the canonical temperature T for which E is the maximum probable energy. Under such circumstances, the microcanonical and canonical pictures shall converge to each other with increasing size \aleph .

However, as indicated above, for systems with small DOF numbers, and specifically for systems with ESQPTs, the microcanonical and canonical pictures remain inconsistent even in the $\aleph \rightarrow \infty$ limit. In such systems, the setting of the microcanonical thermodynamics via Eq. (48) is even problematic as this equation may be completely undefined, or may yield for a fixed temperature T either multiple energy solutions, or no solution at all. The microcanonical picture is undefined if $\ln \bar{\rho}(\lambda, E)$ shows jumps or divergences, like in typical ESQPTs systems with $f = 1$. Then the right-hand side of microcanonical equation (48) does not exist. The cases with multiple or no solutions of Eq. (48) in wide energy intervals apply if $\frac{\partial}{\partial E} \ln \bar{\rho}(\lambda, E)$ is nonanalytic, as typically happens in $f = 2$ ESQPTs systems. This leads to nonanalytic distributions $\bar{w}_T(\lambda, E)$ which sometimes takes bimodal, multimodal or other exotic forms [11]. As discussed in Ref. [82], multiple branches of the microcanonical temperature in narrow energy intervals can arise even from non-analyticities in $\frac{\partial^2}{\partial E^2} \ln \bar{\rho}(\lambda, E)$, so in typical ESQPT systems with $f = 3$.

The above-discussed effects can be visualized via so-called *caloric curves* in the $E \times T$ plane. The canonical caloric curve displays the dependence of the canonical average energy $\langle E(\lambda) \rangle_T$ on temperature T . The microcanonical caloric curve is the dependence of $[E(\lambda)]_T$ on T , where we introduce the symbol $[E]_T$ for the most probable energy at temperature T , i.e., the maximum of the thermal energy distribution. The derivative $C(\lambda, T) = \frac{\partial}{\partial T} \langle E(\lambda) \rangle_T$ or $C(\lambda, T) = \frac{\partial}{\partial T} [E(\lambda)]_T$ is the canonical or microcanonical *heat capacity*, respectively (in the microcanonical case, we expect that temperature T will be replaced by the energy $[E]_T$). Figure 13 shows

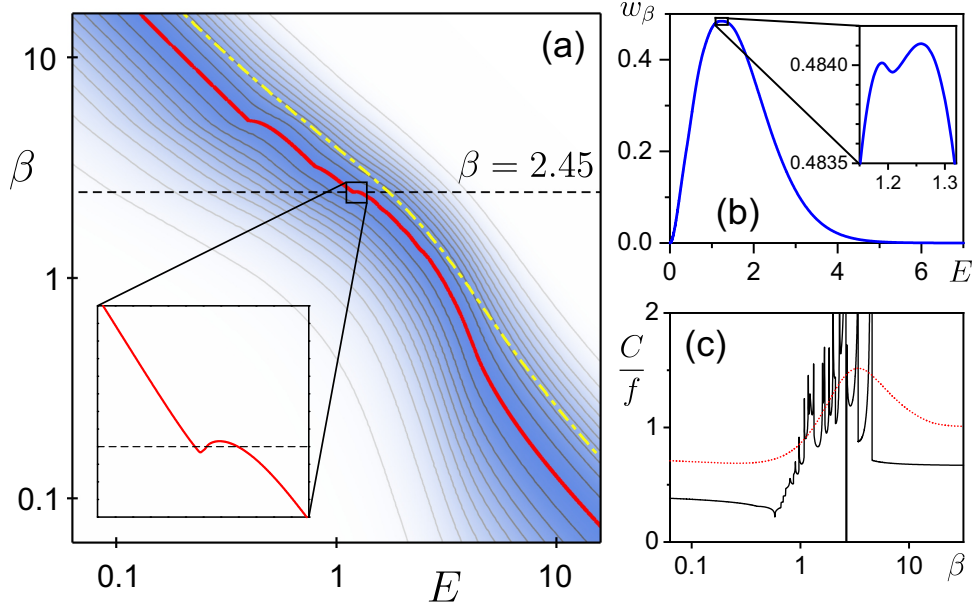


Figure 13. Thermal properties of an $f = 3$ system with a toy Hamiltonian $\hat{H} = \frac{1}{2}|\hat{p}|^2 - 2|\hat{q}|^2 + \frac{1}{5}\hat{q}_1 + \frac{2}{5}\hat{q}_2 + \frac{3}{5}\hat{q}_3 + \hat{q}_1^4 + \hat{q}_2^4 + \hat{q}_3^4$. The system has ESQPTs connected with 27 non-degenerate stationary points of the potential (cf. Fig. 10). Panel (a): The thermal energy distributions $\bar{w}_T(E)$ as a function of $E \times T^{-1}$ is visualized by the colored contour diagram; the darker band is the region with large values (the maximum normalized to unity). The microcanonical and canonical caloric curves, respectively, are drawn by the thicker full line (red online) and the dotdashed line (yellow online). Panel (b): Thermal energy distribution at $T^{-1} = 2.45$ with the region of bimodality (expanded in the inset) corresponding to the kink of the caloric curve expanded in the inset of panel (a). Panel (c): The microcanonical and canonical heat capacity (full and dotdashed line, respectively). Adapted from Ref. [82].

examples of both canonical and microcanonical caloric curves and heat capacities, and the corresponding thermal energy distributions for an artificial $f = 3$ system that shows ESQPTs associated with $3^f = 27$ non-degenerate stationary points. We observe in panel (c) that the microcanonical heat capacity shows a dense chain of anomalous structures, associated with each ESQPT, and is even negative and/or multivalued (undefined) in some narrow temperature intervals. These structures result from the shape of the microcanonical caloric curve in panel (a) (transformed to the form with E on the horizontal axis and $\beta = T^{-1}$ on the vertical axis) and reflect the complex forms of the thermal energy distributions exemplified in panel (b).

The ESQPTs in higher than second energy derivatives of $\ln \bar{\rho}(\lambda, E)$, which typically appear in systems with $f > 3$, do not affect the existence and uniqueness of solutions of the microcanonical equation (this is however not guaranteed anyway). The resulting non-analyticities of the microcanonical entropy and related thermodynamic functions at the microcanonical temperatures corresponding to the critical ESQPT energies represent a special type of critical effects rooted exclusively in microcanonical thermodynamics. They can have important consequences in the processes involving internal thermalization mechanisms in isolated systems with not too high values of f ,

but with increasing f their significance fades away.

Stationary points of the classical dynamics were nevertheless considered as a possible source of thermal critical behavior even for standard thermodynamic systems with $f \sim N \rightarrow \infty$. This link was proposed in Ref. [29] and further investigated in Refs. [30–32, 167–169]. What makes these analyses relevant, in spite of expected weakening of effects of stationary points with increasing DOF number, is the fact that the total number of stationary points of the system grows exponentially with f . This can be readily proven for a separable system with classical Hamiltonian $H(\mathbf{q}, \mathbf{p}) = \sum_{k=1}^f H_k(q_k, p_k)$. If m_k is the number of stationary points of each one-dimensional component H_k , the total number of stationary points is $M = \prod_{k=1}^f m_k = \bar{m}^f$ (where $\ln \bar{m}$ is the arithmetic average of $\ln m_k$), and qualitatively the same conclusion holds also for non-separable systems. Hence some infinitesimal intervals of scaled energy E/N for a large value of f may exhibit very large accumulation of stationary points. Moreover, among the quickly diverging total number of stationary points there may be a sufficiently large subset of points that become asymptotically flat (degenerate) in the $N \rightarrow \infty$ limit.

The Hamiltonian in these studies was assumed to have the form (31) with a quadratic kinetic term and the potential energy function $V(\mathbf{q})$ depending on an f -dimensional coordinate vector \mathbf{q} . The collection of values \mathbf{q} accessible for the system at a given energy, i.e., the coordinates for which $V(\mathbf{q}) \leq E$, forms the available configuration space. In Ref. [29], the occurrence of a TPT at some temperature T_c is related to the change of topology of the available configuration space at the corresponding scaled microcanonical energy E_c/N . Such changes are indeed connected with stationary points of $V(\mathbf{q})$. However, in presently discussed systems with non-moderate values of $f \sim N$, we have to expect an exponential abundance of microcanonical non-analyticities that appear in very high derivatives of the thermodynamic functions.

The way how stationary points in the configuration space of an $f \sim N$ system may give rise to a real TPT, affecting low derivatives of thermodynamics functions in the infinite-size limit, was explained in Refs. [32, 167, 168]. Roughly speaking, the proposed mechanism relies on a high enough density of degenerate stationary points in an infinitesimal interval of scaled energy near E_c/N , which is the microcanonical energy corresponding to the critical temperature T_c . Necessary (but not sufficient) conditions for a TPT to occur at this temperature read approximately as follows: (i) faster than exponential growth of the overall number of stationary points in the interval with increasing $f \sim N$, and (ii) vanishing infinite-size limit of the quantity $|\bar{\mathcal{H}}(E_c)|^{1/N}$, where $\bar{\mathcal{H}}(E_c)$ is a local average of $\text{Det } \partial_k \partial_l H(\mathbf{q}^{(i)}, \mathbf{p}=0)$ (determinant of the Hessian matrix of the Hamiltonian) over all stationary points $\mathbf{q}^{(i)}$ in an infinitesimal vicinity of E_c . For the exact formulation of these conditions and for illustrative examples of systems where they can be applied see the quoted references.

5.3. ESQPT-related effects in canonical thermodynamics

Let us return back to ESQPT systems with moderate numbers of collective DOFs. In such systems, in contrast to the microcanonical case, the canonical thermodynamic functions must be fully analytic even in the $N \rightarrow \infty$ limit. We have already seen that the canonical heat capacity of an ESQPT system in Fig. 13 shows no singularities, in a sharp contrast to its microcanonical counterpart. As follows from numerical examples of Ref. [82], the canonical heat capacity of systems with ESQPTs is likely to become

a non-monotonous function of temperature, with maxima and minima located in the temperature regions that yield the average thermal energy near the ESQPT borderlines. However, such structures may appear also for Hamiltonians which are close to but not really in the ESQPT control parameter domains. The link of ESQPTs to canonical thermodynamics seems therefore rather ambiguous.

Detailed comparative studies of canonical and microcanonical thermodynamic treatments, searching for mutual relations between TPTs and ESQPTs, were performed in the *extended Dicke model* from Sec. 2 [81, 83]. Canonical thermodynamics of the superradiance models disclosing their TPT was presented already in Refs. [119, 120], but at that time the ESQPTs were not known. A crucial assumption of all these analyses is that they consider the *full* 2^N -dimensional Hilbert space \mathcal{H} including all subspaces $\mathcal{H}_j^{(s)}$ with the quasispin quantum number j taking integer or half-integer values between $j_{\min} = 0$ of $\frac{1}{2}$ and $j_{\max} = \frac{1}{2}N$ and $s = 1, \dots, \nu_j$ counting all replicas of the given- j subspace within \mathcal{H} (see Sec. 3.1). The number of relevant DOFs is then $f = N + 1$ and the model shows standard behavior in the true thermodynamic limit $N \rightarrow \infty$ (with converging canonical and microcanonical results).

To describe thermodynamic properties of the extended Dicke model with Hamiltonian $\hat{H}(\lambda, \delta)$ from Eq. (3), we use a method in which the partition function is evaluated by tracing the exponential of the Hamiltonian over the atomic subsystem only (instead of over the whole system) while the field subsystem is kept in the Glauber coherent state $|\alpha\rangle \propto \exp(\alpha\hat{b}^\dagger)|0\rangle$ characterized by a single complex parameter α , see Ref. [122]. The thermal average of the number of photons in the cavity $\langle \hat{N}_b \rangle_T = |\alpha|^2$ is expected to be of the same order as N in the superradiant phase, i.e., above a critical temperature $T_c(\lambda, \delta)$ for $\lambda > \lambda_c(\delta)$, and zero in the normal phase below $T_c(\lambda, \delta)$. Thus we have $Z(T, \alpha; \lambda, \delta) = \text{Tr}_A \langle \alpha | \exp(-\hat{H}(\lambda, \delta)/T) | \alpha \rangle$ and the corresponding “trial” equilibrium value of the free energy $F(T, \alpha; \lambda, \delta) = -T \ln Z(T, \alpha; \lambda, \delta)$. The true equilibrium is obtained by minimization of $F(T, \alpha; \lambda, \delta)$ in parameter $\alpha \in \mathbb{C}$, which therefore becomes an order parameter of the superradiant phase transition in the sense of the Landau theory.

This procedure leads the following results [73]. The critical temperature of the superradiant phase transition above the critical coupling $\lambda_c(\delta) = \sqrt{\omega\omega_0}/(1+\delta)$ is given by $T_c(\lambda, \delta) = \frac{1}{2}\omega_0(\text{arctanh}(\lambda_c(\delta)^2/\lambda^2))^{-1}$. Moreover, for $\delta \in (0, 1)$ in between the Tavis-Cummings and Dicke limits, and for $\lambda > \lambda_0(\delta) = \sqrt{\omega\omega_0}/(1-\delta) \geq \lambda_c(\delta)$, there exists yet another “critical” temperature $T_0(\lambda, \delta) = \frac{1}{2}\omega_0 \text{arctanh}^{-1}(\lambda_0(\delta)^2\lambda^{-2})$. This is not a real critical temperature of an equilibrium TPT, but a temperature where the free energy $F(T, \alpha; \lambda, \delta)$ as a function of order parameter α changes its form in the regions away from the global minimum. It is interesting that the above control parameter value $\lambda_0(\delta)$ coincides with the coupling at which the TC phase appears in the quantum phase diagram associated with the $j = j_{\max}$ subspace of \mathcal{H} . In particular, we observe in Fig. 2 that at this parameter value the ESQPT critical borderline linked to a saddle point of the classical Hamiltonian function (peak in the level density derivative) starts descending in energy while $E = -\frac{1}{2}N\omega_0$ becomes the energy of a local maximum (jump of the level density derivative).

The analysis in the full Hilbert space of the extended Dicke model must take into account results from all subspaces $\mathcal{H}_j^{(s)}$ with $j = j_{\min}, \dots, j_{\max}$, including typically (for $0 \ll j \ll j_{\max}$) huge numbers ν_j of the subspace replicas. Introducing a parameter $\gamma = j/j_{\max} = 2j/N$, which in the infinite-size limit becomes a continuous variable $\gamma \in [0, 1]$, we define a scaled coupling strength $\lambda^{(\gamma)} = \lambda^{(1)}/\sqrt{\gamma}$ and a scaled energy

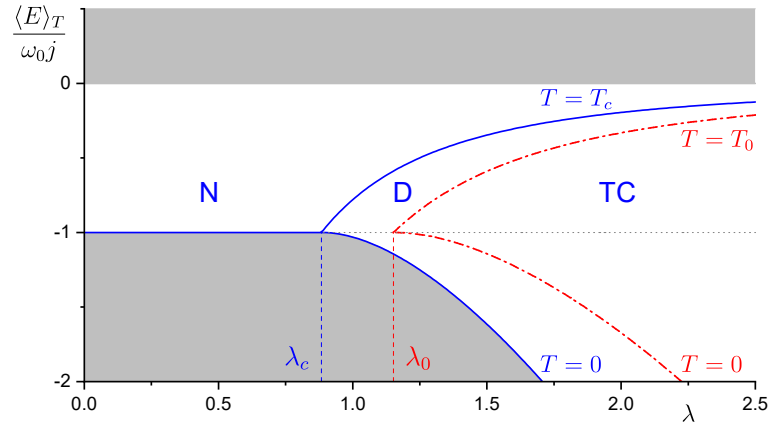


Figure 14. Canonical thermal phase diagram of the extended Dicke Hamiltonian (3) with $\omega = \omega_0 = 1$ and $\delta = 0.132$ (cf. Fig. 2). The vertical axis shows the thermal average of energy $\langle E(\lambda) \rangle_T$. Acronym N denotes the normal phase, and acronyms D and TC, respectively, mark the superradiant phases without and with the “false equilibria” connected with saddle points of the free energy. The full (dashdotted) curves labeled by $T = 0, T_c$ ($T = 0, T_0$) correspond to the global minima (saddle points) of the free energy at the respective temperatures. The gray areas represent unreachable domains of $\langle E(\lambda) \rangle_T$. Based on Ref. [81].

$E^{(\gamma)} = \gamma E^{(1)}$. It turns out (see, e.g., Ref. [74]) that from the perspective of the semiclassical analysis the point $(\lambda^{(1)}, E^{(1)})$ in the $\lambda \times E$ plane for the $j = j_{\max}$ subspace is equivalent to the point $(\lambda^{(\gamma)}, E^{(\gamma)})$ for a $j < j_{\max}$ subspace. The pairs $(\lambda^{(\gamma)}, E^{(\gamma)})$ with $\gamma \in [0, 1]$ demarcate a smooth curve in the $\lambda \times E$ plane uniquely specified by the point $(\lambda^{(1)}, E^{(1)})$ crossed in the $\gamma = 1$ limit. These curves connect points with the same semiclassical properties in subspaces with various j . Note that among the subspaces contributing to the given energy domain those with the largest multiplicity ν_j (which for $N \rightarrow \infty$ means those with the lowest j) are most significant.

It was shown in Ref. [81] that a curve $(\lambda^{(\gamma)}, E^{(\gamma)})$ passing the ground-state QPT point $(\lambda^{(1)}, E^{(1)}) = (\lambda_c(\delta), -j_{\max}\omega_0)$ is identical with the $\lambda > \lambda_c(\delta)$ dependence of the thermal average of energy evaluated right at the TPT critical temperature, $\langle E(\lambda, \delta) \rangle_{T=T_c(\delta)}$. This suggests that the TPT in the Dicke model results from adding up effects of ground-state QPTs occurring in multiple subspaces $\mathcal{H}_j^{(s)}$. A similar interpretation was developed also for the second “critical” temperature $T_0(\delta)$ [81]. In this case, the “false equilibria” associated with the saddles of the free energy landscape $F(T, \alpha; \lambda, \delta)$ are used. If the field subsystem is assumed to be in the coherent state with α corresponding to these saddles, the average energy at temperature $T = T_0(\delta)$ coincides with the curve $(\lambda^{(\gamma)}, E^{(\gamma)})$ passing the point $(\lambda^{(1)}, E^{(1)}) = (\lambda_0(\delta), -j_{\max}\omega_0)$, i.e., the splitting point of ESQPTs in Fig. 2. Moreover, assuming the field subsystem in the states corresponding to the saddle points and setting the temperature to zero, $T = 0$, the energy average coincides with the lowest ESQPT critical energy separating the D and TC quantum phases. The resulting canonical thermodynamic phase diagram of the extended Dicke model is shown in Fig. 14.

Though these findings do not certainly imply any kind of direct ESQPT-TPT correspondence, they disclose interesting relations of ESQPTs to canonical

thermodynamic properties. Note, however, that the other ESQPTs of the extended Dicke model seem to have no implications on canonical thermal averages. It turns out [81, 83] that the average energy of the canonical ensemble with arbitrary temperature $T \in [0, \infty)$ satisfies the relation $\langle E(\lambda, \delta) \rangle_T \leq 0$, which means that the ESQPT at $E_c = +j\omega_0$ lies in an inaccessible energy region if the system is heated via interaction with a thermal bath. Possible effects of ESQPTs in thermal fluctuations were not studied. As we see, the question of thermodynamic consequences of ESQPTs is open to further investigations.

6. Dynamic signatures

In this section, we discuss consequences of ESQPTs in the dynamics induced by non-thermal excitations of the system, namely by excitations due to *external driving* of the control parameter in the Hamiltonian. This potentially invokes a rather broad area of non-equilibrium effects [170], which we however outline only selectively. First we describe the limit of very fast (instantaneous) parameter changes (so called quantum quenches). Then we investigate slow changes and conditions for excitation-free (adiabatic) driving. At last, we look at driven dynamics in presence of dissipation.

6.1. Quantum quench dynamics

Quantum quench is a diabatic limit of driving in a quantum system [171, 172]. It is a sudden jump of parameter λ of the Hamiltonian $\hat{H}(\lambda)$ from a value λ_{in} to λ_{fi} . The system is prepared in an initial state $|\psi_{\text{in}}\rangle$, which is supposed to coincide with an eigenstate of $\hat{H}(\lambda_{\text{in}})$. The usual (but not the only) choice is the ground state, $|\psi_{\text{in}}\rangle = |\psi_{\text{gs}}(\lambda_{\text{in}})\rangle$. Assuming a generic case with $[\hat{H}(\lambda_{\text{in}}), \hat{H}(\lambda_{\text{fi}})] \neq 0$, we see that $|\psi_{\text{in}}\rangle$ is not an eigenstate of $\hat{H}(\lambda_{\text{fi}})$ and hence evolves with elapsing time $t \in [0, \infty)$ (with $t = 0$ setting the time of quench). In the following, the Hamiltonian is supposed to be linear in parameter λ , so having the form $\hat{H}(\lambda) = \hat{H}(0) + \lambda \hat{H}'$. Thus we can write $\hat{H}(\lambda_{\text{fi}}) = \hat{H}(\lambda_{\text{in}}) + \Delta\lambda \hat{H}'$, where $\Delta\lambda = \lambda_{\text{fi}} - \lambda_{\text{in}}$.

The time evolution of the system after the quench depends on the overlaps of the initial state $|\psi_{\text{in}}\rangle$ with individual eigenvectors $|\psi_i(\lambda_{\text{fi}})\rangle$ of the final Hamiltonian. To characterize properties of these overlaps, we introduce the strength function $W(E)$ (also called the local density of states) and the autocorrelation function $R(\varepsilon)$:

$$W(E) = \sum_i \overbrace{|\langle \psi_i(\lambda_{\text{fi}}) | \psi_{\text{in}} \rangle|^2}^{w_i} \delta(E - E_i(\lambda_{\text{fi}})), \quad (49)$$

$$R(\varepsilon) = \sum_i \sum_{i'} w_i w_{i'} \delta(\varepsilon - E_i(\lambda_{\text{fi}}) + E_{i'}(\lambda_{\text{fi}})). \quad (50)$$

While the strength function $W(E)$ represents the energy distribution of the initial state in the final Hamiltonian spectrum, the autocorrelation function $R(\varepsilon)$ characterizes mutual correlation of overlaps of the initial state with the final eigenstates with energy difference ε . To simplify the notation, the specifications of $|\psi_{\text{in}}\rangle$ and λ_{fi} are skipped in $W(E)$ and $R(\varepsilon)$.

The survival probability of the initial state in the evolving final state can be expressed via Fourier images of the strength and autocorrelation functions:

$$P(t) = \left| \langle \psi_{\text{in}} | e^{-i\hat{H}(\lambda_{\text{fi}})t/\hbar} | \psi_{\text{in}} \rangle \right|^2 = \left| \int dE W(E) e^{-iEt/\hbar} \right|^2 = \int d\varepsilon R(\varepsilon) e^{i\varepsilon t/\hbar}. \quad (51)$$

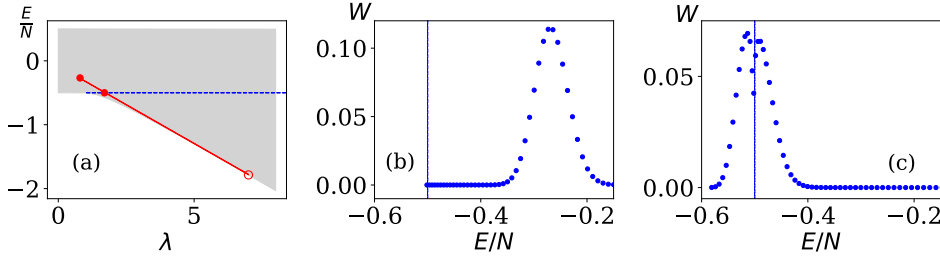


Figure 15. Strength functions of two backward quenches in the Lipkin model. The second-order QPT Hamiltonian (13) with $\chi = 0$ is used with $N = 2j = 200$. Panel (a) depicts the $\lambda \times E$ diagram, where the gray area represents the region where individual levels are located and the horizontal (blue) line marks an ESQPT of type $(f, r) = (1, 1)$. The initial ground state at $\lambda_{in} = 7$ (open circle) is “quenched” along the tilted (red) line to the excited domain at $\lambda_{fi} = 0.8$ and $\lambda_{fi} \approx 1.75$; the full dots mark the respective final average energies. The corresponding strength functions are shown in panels (b) and (c). The strength function of the critical quench in panel (c) exhibits a singularity at the ESQPT energy (the vertical line). Evolutions of the survival probability and Wigner functions are shown in Fig. 16.

As shown in numerous studies (see, e.g., Refs. [101, 171–175], paper 19 in Ref. [163], and the references therein), the survival probability (51) in most situations undergoes a rather nontrivial evolution. After an initial decay and passage through a minimal overlap stage, it usually grows again and shows an infinite aperiodic sequence of partial revivals and breakdowns of the initial state. The evolution of $P(t)$ on a given time scale reflects the energy distribution (49) with resolution $\Delta E \propto t^{-1}$ determined by the energy-time uncertainty relation. Thus on the initial stage of evolution, at very short times, the dependence $P(t)$ reveals only a rough outline of the distribution $W(E)$, while finer and finer details, including tiny correlations captured by Eq. (50), become relevant on later stages. For t exceeding a value corresponding to the smallest energy spacing between the populated levels, the perpetually oscillating function $P(t)$ reaches a stabilized regime, showing no further qualitative modifications.

The average value $\langle E \rangle$ and width $\langle\langle E^2 \rangle\rangle^{1/2}$ of the energy distribution (49) are determined from

$$\underbrace{\langle E \rangle}_{\langle \hat{H}(\lambda_{fi}) \rangle_{in}} - \underbrace{\langle \hat{H}(\lambda_{in}) \rangle_{in}} = \Delta\lambda \underbrace{\frac{d}{d\lambda} E_{gs}(\lambda_{in})}_{\langle \hat{H}' \rangle_{in}}, \quad \underbrace{\langle\langle E^2 \rangle\rangle}_{\langle\langle \hat{H}(\lambda_{fi})^2 \rangle\rangle_{in}} = \Delta\lambda^2 \langle\langle \hat{H}'^2 \rangle\rangle_{in}, \quad (52)$$

where $\langle \hat{A} \rangle_{in} = \langle \psi_{in} | \hat{A} | \psi_{in} \rangle$ and $\langle\langle \hat{A}^2 \rangle\rangle_{in} = \langle \hat{A}^2 \rangle_{in} - \langle \hat{A} \rangle_{in}^2$ is the expectation value and variance of quantity \hat{A} in the state $|\psi_{in}\rangle$. The first formula shows that the energy average after the quench is determined by the initial energy $E_{gs}(\lambda_{in})$ and its tangent $\frac{d}{d\lambda} E_{gs}(\lambda_{in})$. This permits a simple geometrical prediction of the centroid of the final energy distribution, allowing us to design a quench focused to the middle of the selected final energy domain. The second formula implies that the width of the energy distribution is proportional to the width of distribution of \hat{H}' in the initial state and grows linearly with $\Delta\lambda$. This sets limits on the energy resolution with which the selected final energy can be tuned. The geometrical visualization and strength functions of two quenches in the Lipkin model are shown in Fig. 15.

The decay of the survival probability at very short times is approximated by

$P(t) \approx 1 - \langle\langle E^2 \rangle\rangle t^2/\hbar^2$ and hence depends only on the energy width from the second formula of Eq. (52). On the other hand, elementary statistical measures of the survival probability fluctuations in infinite time, namely the average $\langle P(t) \rangle_{t \in [0, \infty)} \equiv \lim_{\tau \rightarrow \infty} \tau^{-1} \int_0^\tau dt P(t)$ and variance $\langle\langle P(t)^2 \rangle\rangle_{t \in [0, \infty)}$, follow from the fragmentation of the strength function among individual eigenstates of $\hat{H}(\lambda_{\text{fi}})$. It is quantified by the so-called participation ratio $\mathcal{P} = (\sum_i w_i^2)^{-1}$, which takes values between $\mathcal{P} = 1$ for states fully localized in one of the selected basis states and $\mathcal{P} = d$ for states uniformly distributed among all d basis states. The following relations hold,

$$\langle P(t) \rangle_{t \in [0, \infty)} = \mathcal{P}^{-1}, \quad \langle\langle P(t)^2 \rangle\rangle_{t \in [0, \infty)} = \mathcal{P}^{-2} - \sum_i w_i^4, \quad (53)$$

where the second term on the right-hand side of the second formula is of order \mathcal{P}^{-3} for strongly delocalized states and can often be neglected.

Quantum quench dynamics has been subject of extensive research. Particularly the implications of quantum criticality [171] and quantum chaos (see, e.g., paper 19 in Ref. [163]) were studied in the evolution of the survival probability on the medium time scale (between the initial decay and the stabilized regime). Influence of ESQPTs on quantum quench dynamics was discussed in several works. An initial study of Ref. [90] reported an ESQPT-induced suppression of the survival probability at medium times for quenches within the interacting phase in the Dicke model and a related atom-molecule boson model (see Sec. 3.3). An opposite effect, namely an ESQPT-induced stabilization of the initial state for quenches from the non-interacting to the interacting phase in the Lipkin model, was described in Refs. [94–97]. In Ref. [101], both these complementary results were treated on a unified ground and qualitatively explained for the extended Dicke model.

It turns out that essential insight into the consequences of ESQPTs in quantum quench dynamics follows from the semiclassical description based on the Wigner quasiprobability distribution in the phase space [176]. At time $t = 0$, when the initial state is still intact, its Wigner distribution reads

$$\mathcal{W}(\mathbf{q}, \mathbf{p}, t=0) = \frac{1}{\pi\hbar} \int d\boldsymbol{\delta} \langle \mathbf{q} + \boldsymbol{\delta} | \psi_{\text{in}} \rangle \langle \psi_{\text{in}} | \mathbf{q} - \boldsymbol{\delta} \rangle e^{-2i\boldsymbol{\delta} \cdot \mathbf{p}/\hbar}, \quad (54)$$

where $|\mathbf{q} \pm \boldsymbol{\delta}\rangle$ are generalized coordinate eigenstates of the system. As the time increases, for $t > 0$, the Wigner distribution evolves to $\mathcal{W}(\mathbf{q}, \mathbf{p}, t)$, which is given by the same formula as Eq. (54) but with $|\psi_{\text{in}}\rangle$ replaced by $|\psi(t)\rangle = e^{-i\hat{H}(\lambda_{\text{fi}})t/\hbar}|\psi_{\text{in}}\rangle$. The survival probability (51) is expressed as

$$P(t) = 2\pi\hbar \int d\mathbf{q} d\mathbf{p} \mathcal{W}(\mathbf{q}, \mathbf{p}, t) \mathcal{W}(\mathbf{q}, \mathbf{p}, 0). \quad (55)$$

The evolution of $\mathcal{W}(\mathbf{q}, \mathbf{p}, t)$ is considerably influenced by the existence of stationary points of the classical-limit Hamiltonian corresponding to $\hat{H}(\lambda_{\text{fi}})$ at energies close to average $\langle E \rangle \equiv \langle \hat{H}(\lambda_{\text{fi}}) \rangle_{\text{in}}$ of the distribution (49). This is what makes quantum quench dynamics near ESQPT critical energies different from the same dynamics in noncritical energy domains. If the stationary point $(\mathbf{q}^{(i)}, \mathbf{p}^{(i)})$ is located inside the support of the initial Wigner distribution $\mathcal{W}(\mathbf{q}, \mathbf{p}, t=0)$, the semiclassical overlap (55) decays much slower and may keep increased even on long time scales. Of course, an unstable stationary point cannot completely stop the decay as the Wigner distribution is never perfectly localized at this point and therefore must gradually deviate from the initial form. Nevertheless, the effect of stabilization can be very strong, as shown in the above-mentioned ESQPT studies of Refs. [94–97, 101]. This scenario applies particularly

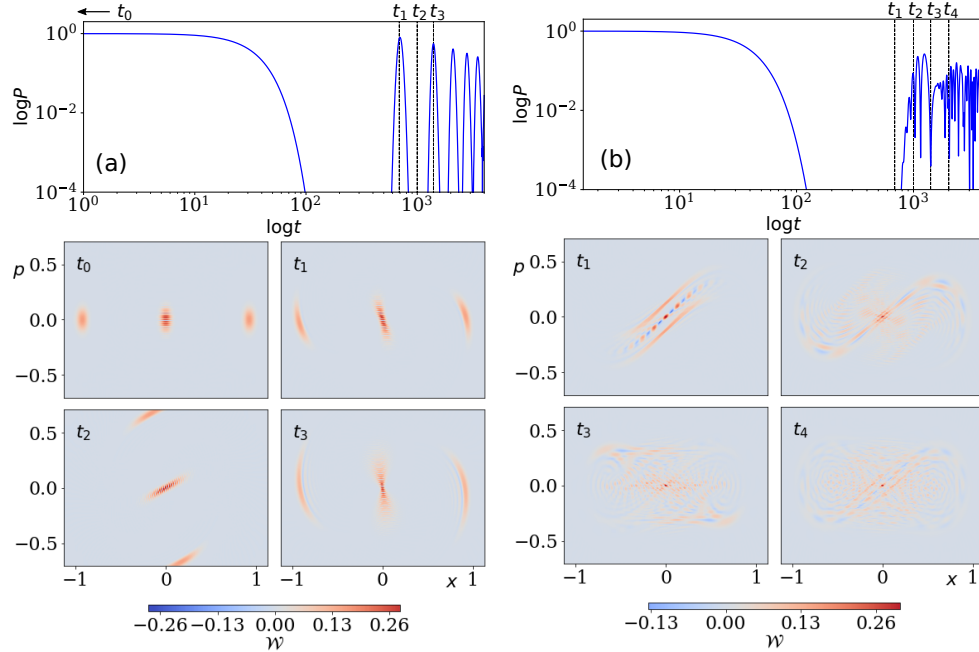


Figure 16. Evolutions of the survival probability (upper panels) and snapshots of the Wigner function (lower panels) for the two quenches from Fig. 15. The noncritical quench from Fig. 15(b) is shown on the left [panel (a)], the critical quench from Fig. 15(c) is on the right [panel (b)]. The noncritical quench shows repeated partial revivals of the initial state (with a power-law decrease of fidelity), which result from approximate returns of the Wigner distribution to the initial form. The critical quench shows no revivals as the Wigner function gets captured at the stationary point $(q, p) = (0, 0)$ associated with the ESQPT of the final Hamiltonian. The Wigner functions are taken at dimensionless times $(t_0, t_1, t_2, t_3, t_4) = (0, 690, 1000, 1400, 2000)$, see vertical lines in the upper panels.

to “forward” quenches of the ground state from the non-interacting ($\lambda_{\text{in}} < \lambda_c$) to interacting phase ($\lambda_{\text{fi}} > \lambda_c$), across the second-order QPT, in which the global minimum of the classical-limit Hamiltonian becomes a local maximum or a saddle point with the same energy. Note that the existence of two different types of suppressed decay regimes associated with ESQPTs of the types $(f, r) = (2, 2)$ and $(2, 1)$ was distinguished in the extended Dicke model [73, 101].

On the other hand, if the stationary point $(\mathbf{q}^{(i)}, \mathbf{p}^{(i)})$ of the final Hamiltonian $\hat{H}(\lambda_{\text{fi}})$ near the average energy $\langle \hat{H}(\lambda_{\text{fi}}) \rangle_{\text{in}}$ is located away from the support of the initial Wigner distribution $\mathcal{W}(\mathbf{q}, \mathbf{p}, t=0)$, it does not affect the early stage of the evolution. It nevertheless shows up in later stages. Quasiclassical dynamics in absence of stationary points usually leads to a sequence of repeated but algebraically weakening partial revivals, which are caused by classical orbits that again and again drive the Wigner distribution through the phase space domains close to the initial ones. These revivals are suppressed or completely avoided if a stationary point at any place in the energetically available phase space effectively captures a considerable part of the distribution. This mechanism is responsible for the observed weakening of the

power-law revivals in $P(t)$ dependencies after “backward” quenches of the ground state from the strongly interacting to less interacting regime of the Dicke and other models [97, 101]. Usually, the suppression of revivals is observed for quenches fine tuned right to the ESQPT region, while for the neighboring shorter or longer quenches the revivals are present. This is illustrated for the Lipkin model (for both critical and noncritical quenches from Fig. 15) in Fig. 16.

Quantum quench represents a general technique for exciting an isolated system to a selected domain of energy and control parameters. The dynamical response to the quench can be examined not only by the survival probability, as outlined above, but also by time dependencies of expectation values of various suitably selected observables, or even through some more complex techniques. A lot of attention in recent years has been attracted by the concept of a so-called *out-of-time-order correlator*, see Refs. [177, 178] and the references therein. This quantity is defined as

$$C_{\hat{A}, \hat{B}, \hat{\varrho}}(t) = \langle \hat{B}(t)^\dagger \hat{A}(0)^\dagger \hat{B}(t) \hat{A}(0) \rangle_{\hat{\varrho}}, \quad (56)$$

where $\hat{A}(0)$ and $\hat{B}(t) = \hat{U}(-t)\hat{B}(0)\hat{U}(t)$ are Heisenberg pictures of two chosen “probe” operators (usually unitary or Hermitian) at times 0 and t , and $\langle \bullet \rangle_{\hat{\varrho}}$ denotes an expectation value in a general state, which in the Heisenberg picture is described by a time-independent density operator $\hat{\varrho}$. If evaluated in a pure state $\hat{\varrho} = |\psi\rangle\langle\psi|$, the expression (56) is a scalar product $\langle \hat{A}(0) \hat{B}(t) \psi | \hat{B}(t) \hat{A}(0) \psi \rangle$. Even if both operators at $t=0$ commute, we assume that $[\hat{A}(0), \hat{B}(t)] \neq 0$ for $t > 0$, which reflects the scrambling of initially separated information over the system. The quantity (56) is an efficient measure of this process. It was shown that the out-of-time-order correlator can also serve as a quantum counterpart of the classical Lyapunov exponent [179–181] and has close links to the Renyi entropy [182], giving therefore opportunity to measure properties related to quantum chaos and quantum entanglement. A recent proposal [183] describes an experimental setup capable of measuring a particular out-of-time-order correlator in the Dicke model.

We assume that $\hat{\varrho} = |\psi_i(\lambda_{\text{in}})\rangle\langle\psi_i(\lambda_{\text{in}})|$ is an eigenstate of the Hamiltonian with parameter λ_{in} , while the evolution $\hat{U}(t) = e^{-i\hat{H}(\lambda_{\text{fi}})t/\hbar}$ of operator $\hat{B}(t)$ is realized by the Hamiltonian with parameter λ_{fi} . This enables us to interpret Eq. (56) in the language developed for the description of quantum quench dynamics. In particular, associating the $t = 0$ operators $\hat{A}(0)$ and $\hat{B}(0)$ with the respective Schrödinger pictures \hat{A} and \hat{B} , we identify the out-of-time-order correlator with the expectation value of time-dependent operator $\hat{C}(t) = \hat{B}^\dagger \hat{U}(t) \hat{A}^\dagger \hat{U}(-t) \hat{B} \hat{U}(t) \hat{A} \hat{U}(-t)$ in the state $|\psi(t)\rangle = \hat{U}(t)|\psi_i(\lambda_{\text{in}})\rangle$ evolving by the post-quench Hamiltonian. If the initial state expressed in the final Hamiltonian eigenbasis is localized in the ESQPT critical region, or on its either side, the time dependence (56) may exhibit some specific features. The theoretical analysis of the Lipkin model with the second-order QPT and the corresponding $(f, r) = (1, 1)$ ESQPT in Ref. [103] confirms this anticipation. It shows that using operators $\hat{A} = \hat{B} \propto \hat{J}_x$, one can distinguish quenches to the normal and parity breaking quantum phases by the long-time averages of the corresponding $C_{\hat{A}, \hat{B}, \hat{\varrho}}(t)$ dependence. Another theoretical study [104] of a similar system with ESQPT disclosed a tendency for long-time periodicity of a particular out-of-time-order correlator for quenches to the critical region, with the period determined by the local increase of the level density at the critical borderline. The work in Ref. [105] uses the out-of-time-order correlator to detect an ESQPT based instability of semiclassical dynamics in the integrable version of the Dicke model.

6.2. Adiabatic and counterdiabatic driving

Let us now briefly outline effects of finite-speed driving with a general, externally prescribed time dependence of the Hamiltonian control parameters. Such protocols are usually applied with the aim to prepare a desired final state, taken in general as the i th eigenstate (mostly the ground state) of the Hamiltonian at the final value of the control parameter. The final Hamiltonian keeps the required state intact but it is implicitly assumed to be so complex that a direct preparation of its eigenstate is too difficult. The most popular protocols make use of the adiabatic theorem. They achieve the task by initiating the system in the i th Hamiltonian eigenstate at another parameter value (where it is easier, for some reasons) and by driving it very slowly to the final parameter value. To assure that this procedure is transitionless (i.e., that the system all the time remains in the i th instantaneous eigenstate), one needs to satisfy conditions for adiabaticity, which depend on the chosen trajectory in the parameter space [184, 185]. For the purposes of the present section we consider a multidimensional parameter space $\boldsymbol{\lambda} \equiv (\lambda_1, \lambda_2, \dots) \equiv \{\lambda_\alpha\}$ with a general trajectory $\boldsymbol{\lambda}(t)$ implying a time-dependent driving speed $\frac{d}{dt}\boldsymbol{\lambda}(t) \equiv \dot{\boldsymbol{\lambda}}(t) \equiv \{\dot{\lambda}_\alpha(t)\}$. We introduce the gradient operator in the parameter space, $\nabla \equiv \{\nabla_\alpha \equiv \frac{\partial}{\partial \lambda_\alpha}\}$, which is applied to the Hamiltonian $\hat{H}(\boldsymbol{\lambda})$ as well as to its individual eigenvectors $|\psi_i(\boldsymbol{\lambda})\rangle$.

The exact evolution of the system obeys time dependent Schrödinger equation $i\hbar \frac{d}{dt}|\psi(t)\rangle = \hat{H}(\boldsymbol{\lambda}(t))|\psi(t)\rangle$ with the initial state $|\psi(0)\rangle = |\psi_i(\boldsymbol{\lambda}_{in})\rangle$ coinciding with an eigenstate of $\hat{H}(\boldsymbol{\lambda}_{in})$. Expanding the solution in the eigenbasis of the instantaneous Hamiltonian $H(\boldsymbol{\lambda}(t))$, that is $|\psi(t)\rangle = \sum_j a_j(t)|\psi_j(\boldsymbol{\lambda}(t))\rangle$, one derives the following set of differential equations for complex amplitudes $a_j(t)$,

$$\begin{aligned} \frac{da_j(t)}{dt} = & \left[-\frac{i}{\hbar} E_j(\boldsymbol{\lambda}) + \dot{\boldsymbol{\lambda}}(t) \cdot \underbrace{\langle \psi_j(\boldsymbol{\lambda}) | \nabla \psi_j(\boldsymbol{\lambda}) \rangle}_{-\frac{i}{\hbar} \langle \psi_j(\boldsymbol{\lambda}) | \hat{\mathbf{A}}(\boldsymbol{\lambda}) | \psi_j(\boldsymbol{\lambda}) \rangle} \right] a_j(t) \\ & + \sum_{j'(\neq j)} \dot{\boldsymbol{\lambda}}(t) \cdot \underbrace{\frac{\langle \psi_{j'}(\boldsymbol{\lambda}) | \nabla \hat{H}(\boldsymbol{\lambda}) | \psi_j(\boldsymbol{\lambda}) \rangle}{E_j(\boldsymbol{\lambda}) - E_{j'}(\boldsymbol{\lambda})}}_{\langle \psi_{j'}(\boldsymbol{\lambda}) | \nabla \psi_j(\boldsymbol{\lambda}) \rangle = -\frac{i}{\hbar} \langle \psi_{j'}(\boldsymbol{\lambda}) | \hat{\mathbf{A}}(\boldsymbol{\lambda}) | \psi_j(\boldsymbol{\lambda}) \rangle} a_{j'}(t), \end{aligned} \quad (57)$$

where the dot product standardly means the sum of component products and the argument $\boldsymbol{\lambda}$ is always meant as a shorthand for $\boldsymbol{\lambda}(t)$. Both terms in the square brackets in Eq. (57) describe just phase changes of the amplitude $a_j(t)$ and do not modify its absolute value. The first term corresponds to the ordinary dynamical phase, while the second term (which is pure imaginary) generates the geometrical (Berry) phase [186]. The term on the second line is responsible for transitions to other states $|\psi_{j'}(\boldsymbol{\lambda}(t))\rangle$, with $j' \neq j$, hence it enforces changes of the absolute value $|a_j(t)|$. To keep the driving adiabatic, these effects must be suppressed by reducing the speed $\dot{\boldsymbol{\lambda}}$ at the places where the last term is large.

The form of Eq. (57) refers to deep mathematical background for the description of parameter dependent systems, the so-called *adiabatic gauge theory* [185]. It follows from a local gauge transformation $\hat{U}(\boldsymbol{\lambda}) = \sum_j |\phi_j\rangle\langle\psi_j(\boldsymbol{\lambda})|$ of the system with variable $\boldsymbol{\lambda}$ to the “moving frame” with a fixed basis $\{|\phi_j\rangle\}$. As a result of this transformation, the second and third terms on the right-hand side of Eq. (57) appear as diagonal and off-diagonal matrix elements of a gauge potential $\hat{\mathbf{A}}(\boldsymbol{\lambda})$. The geometry behind the

adiabatic gauge theory is deduced from the geometric tensor [186, 187]

$$\begin{aligned}\chi_{i\alpha\beta}(\boldsymbol{\lambda}) &= \frac{1}{\hbar^2} \left[\langle \hat{A}_\alpha(\boldsymbol{\lambda}) \hat{A}_\beta(\boldsymbol{\lambda}) \rangle_{|\psi_i(\boldsymbol{\lambda})\rangle} - \langle \hat{A}_\alpha(\boldsymbol{\lambda}) \rangle_{|\psi_i(\boldsymbol{\lambda})\rangle} \langle \hat{A}_\beta(\boldsymbol{\lambda}) \rangle_{|\psi_i(\boldsymbol{\lambda})\rangle} \right] \\ &= \sum_{i'(\neq i)} \frac{\langle \psi_{i'}(\boldsymbol{\lambda}) | \nabla_\alpha \hat{H}(\boldsymbol{\lambda}) | \psi_i(\boldsymbol{\lambda}) \rangle \langle \psi_{i'}(\boldsymbol{\lambda}) | \nabla_\beta \hat{H}(\boldsymbol{\lambda}) | \psi_i(\boldsymbol{\lambda}) \rangle^*}{(E_{i'}(\boldsymbol{\lambda}) - E_i(\boldsymbol{\lambda}))^2},\end{aligned}\quad (58)$$

defined for an arbitrary (i th) eigenstate through the expectation values of the gauge potential in the instantaneous vector $|\psi_i(\boldsymbol{\lambda})\rangle$. The symmetric (real) part of the geometric tensor forms the metric tensor, $g_{i\alpha\beta}(\boldsymbol{\lambda}) = \frac{1}{2}[\chi_{i\alpha\beta}(\boldsymbol{\lambda}) + \chi_{i\beta\alpha}(\boldsymbol{\lambda})] = \text{Re}\chi_{i\alpha\beta}(\boldsymbol{\lambda})$, and the antisymmetric (imaginary) part determines the Berry curvature tensor, $F_{i\alpha\beta}(\boldsymbol{\lambda}) = i[\chi_{i\alpha\beta}(\boldsymbol{\lambda}) - \chi_{i\beta\alpha}(\boldsymbol{\lambda})] = -2\text{Im}\chi_{i\alpha\beta}(\boldsymbol{\lambda})$. We stress that all these definitions are apparently invariant under a local phase transformation $|\psi_j(\boldsymbol{\lambda})\rangle \rightarrow e^{i\varphi(\boldsymbol{\lambda})}|\psi_j(\boldsymbol{\lambda})\rangle$ of all eigenvectors.

Both metric and curvature tensors describe the response of the system to nearly adiabatic driving. It is well known that the integral of the Berry curvature tensor over an area inside a closed curve in the parameter space determines the geometric phase acquired by the adiabatically evolving system during a single loop along the curve [186]. The variation of the phase of the i th eigenstate by adiabatic driving can be understood as a parallel transport of a vector on a curved manifold. The metric tensor defines an infinitesimal distance on this manifold. In particular, we have

$$ds_i^2(\boldsymbol{\lambda}) = \sum_{\alpha,\beta} g_{i\alpha\beta}(\boldsymbol{\lambda}) d\lambda_\alpha d\lambda_\beta = 1 - |\langle \psi_i(\boldsymbol{\lambda}+d\boldsymbol{\lambda}) | \psi_i(\boldsymbol{\lambda}) \rangle|^2, \quad (59)$$

where the second expression shows that the squared distance $ds_i^2(\boldsymbol{\lambda})$ represents a probability of finding the system in other than i th eigenstate after an infinitesimal quench from $\boldsymbol{\lambda}$ to $\boldsymbol{\lambda}+d\boldsymbol{\lambda}$. Moreover, the quantity $\hbar^2 s_i(\boldsymbol{\lambda})^2$, proportional to squared metric velocity, can be shown to coincide with the local energy variance $\langle\langle E_i(\boldsymbol{\lambda})^2 \rangle\rangle_{\text{ad}} = \langle\langle \hat{H}(\boldsymbol{\lambda})^2 \rangle\rangle_{|\psi(t)\rangle}$ of the state $|\psi(t)\rangle$ evolving from $|\psi_i(\boldsymbol{\lambda})\rangle$ in the leading order of the adiabatic perturbation theory [185, 188]. While $E_i(\boldsymbol{\lambda})$ is analogous to a potential energy that measures the reversible energy costs of adiabatic driving of the i th eigenstate, $\Delta E_i^2(\boldsymbol{\lambda})$ determines sort of friction induced by this driving. Maximizing the fidelity of the system delivery into the i th eigenstate of the final Hamiltonian is equivalent to minimizing the friction induced by driving.

Consider a set of trajectories $\boldsymbol{\lambda}(t)$ in the parameter space leading from point $\boldsymbol{\lambda}_{\text{in}}$ at time $t = 0$ to point $\boldsymbol{\lambda}_{\text{fi}}$ at time $t = \tau$. The final time must be sufficiently large for the first-order adiabatic perturbation formulas be valid. Minimization of the energy variance averaged along the whole trajectory,

$$\frac{1}{\tau} \int_0^\tau dt \langle\langle E_i(\boldsymbol{\lambda})^2 \rangle\rangle_{\text{ad}} = \frac{\hbar^2}{\tau} \int_0^\tau dt \underbrace{\sum_{\alpha,\beta} g_{i\alpha\beta}(\boldsymbol{\lambda}) \dot{\lambda}_\alpha(t) \dot{\lambda}_\beta(t)}_{s_i(\boldsymbol{\lambda})^2}, \quad (60)$$

selects the geodesic path minimizing the distance between both points, with the time dependence such that the squared metric velocity remains constant at each point of the path [185, 188]. This means that near points where the metric tensor is small, the speed $\dot{\boldsymbol{\lambda}}(t)$ is large, and vice versa, near points where the metric tensor is large, the speed must become small. As seen from Eq.(58), the latter situation applies when gaps between energy levels are reduced and/or when the corresponding matrix elements of the Hamiltonian gradient are large. Note that these conclusions hold also

Figure 17. Evolution of eigenstate populations (encoded in the color of the curve corresponding to the respective energy level with running λ) for a system described by the first- and second-order QPT Lipkin Hamiltonian (upper and lower rows, respectively) during a slow change of the control parameter λ across QPT and ESQPTs spectral structures. In panels from left to right in each row, the drive to the strongly interacting phase behind the QPT is shown for the system initially prepared in the ground state, and in the first and second excited state of the non-interacting Hamiltonian. Panels (a)–(c) corresponds to the passage through the first-order QPT region [Hamiltonian (13) with $\chi = 4$ and $N = 4$] at speed $\dot{\lambda} = 10^{-4.5}$, panels (d)–(f) to the passage through the second-order QPT region [Hamiltonian (13) with $\chi = 0$ and $N = 100$] at speed $\dot{\lambda} = 0.2$. We observe that non-adiabatic transitions to other states occur during the passage through avoided crossings of energy levels. Adapted from Ref. [189] by J. Dolejší.

in systems with a single parameter λ , for which the shape of the geodesic curve is of course trivial.

The reduction of speed $\dot{\lambda}(t)$ must be performed particularly near quantum critical points. This applies if the ground state of the system is driven through a QPT. If an excited state is involved, the slow down is needed during the passage through ESQPTs characterized by a local increase of the level density or by a higher occurrence of sharp avoided crossing of levels. These conclusions are schematically illustrated in Fig. 17 using the familiar Lipkin model. The ESQPTs are relevant also for driving of thermal states, so they influence the ground-state results in realistic situations with low but nonzero temperatures. The increased duration of quasiadiabatic driving in presence of QPTs and ESQPTs may represent a serious obstacle to the related quantum

information protocols. This was discussed in connection with adiabatic quantum computation in Ref. [190], showing that for the first-order QPT the time requirements grow exponentially with the system's size which kills any potential advantage of quantum computing. In a more general context, excitations generated by a passage of an isolated quantum system through a second-order QPT were presented in parallel to creation of topological defects in the early Universe [191]. Extensive literature devoted to this subject can be traced in Ref. [184].

An elegant way to bypass time problems of adiabatic driving is a so-called *counterdiabatic driving* (also known as adiabatic shortcut) [192, 193]. The idea [194, 195] is simply to add to the Hamiltonian $\hat{H}(\boldsymbol{\lambda})$ a new component $\hat{H}'(\boldsymbol{\lambda}, \dot{\boldsymbol{\lambda}})$ which precisely compensates the action of the last term in Eq. (57) during the drive. The additional Hamiltonian has vanishing diagonal matrix elements in the instantaneous eigenbasis of $\hat{H}(\boldsymbol{\lambda})$, the off-diagonal elements being written via the gauge potential: $\langle \psi_{j'}(\boldsymbol{\lambda}) | \hat{H}'(\boldsymbol{\lambda}, \dot{\boldsymbol{\lambda}}) | \psi_j(\boldsymbol{\lambda}) \rangle = \dot{\boldsymbol{\lambda}} \cdot \langle \psi_{j'}(\boldsymbol{\lambda}) | \hat{\mathbf{A}}(\boldsymbol{\lambda}) | \psi_j(\boldsymbol{\lambda}) \rangle$.

The counterdiabatic driving allows one, at least in theory, to shorten the time needed for a transitionless drive between $\boldsymbol{\lambda}_{\text{in}}$ and $\boldsymbol{\lambda}_{\text{fi}}$ to an arbitrarily small value. The price to pay includes the costs of creating the counterbalancing field in the Hamiltonian. With only limited resources there will exist a lower bound of the drive time, which brings us to the hot field of *quantum speed limits*. The works in Refs. [185, 188, 196] present very close links of quantum speed limits to geodesic paths and the theory outlined above. As follows from these analyses, the minimal time τ_i needed to complete the counterdiabatic drive of the i th eigenstate between points $\boldsymbol{\lambda}_{\text{in}}$ and $\boldsymbol{\lambda}_{\text{fi}}$ is given by a simple relation:

$$\tau_{i \min}(\boldsymbol{\lambda}_{\text{in}}, \boldsymbol{\lambda}_{\text{fi}}) \geq \frac{\hbar}{\Delta E_{\text{CD}}} s_{i \min}(\boldsymbol{\lambda}_{\text{in}}, \boldsymbol{\lambda}_{\text{fi}}). \quad (61)$$

Here, $\Delta E_{\text{CD}} = [\tau^{-1} \int_0^\tau dt \langle \hat{H}_{\text{CD}}^2 \rangle_{|\psi(t)\rangle}]^{1/2}$ is the square root of the variance of the counterdiabatic driving Hamiltonian $\hat{H}_{\text{CD}}(\boldsymbol{\lambda}, \dot{\boldsymbol{\lambda}}) = \hat{H}(\boldsymbol{\lambda}) + \hat{H}'(\boldsymbol{\lambda}, \dot{\boldsymbol{\lambda}})$ averaged along the path (note that $\langle \hat{H}_{\text{CD}} \rangle_{|\psi(t)\rangle} = 0$). This quantity estimates the energy cost of the driving protocol. On the other hand, $s_{i \min}(\boldsymbol{\lambda}_{\text{in}}, \boldsymbol{\lambda}_{\text{fi}})$ is the length of the geodesic path connecting the initial and final parameter points. It has a crucial impact on the feasibility of the protocol. In some cases, it can be just a factor of an order of unity, but for paths crossing QPT or ESQPT singularities, where the size of the metric tensor quickly increases with the size of the system, the diverging geodesic length puts unrealistic energy requirements on the driving Hamiltonian. In these cases, the **counterdiabatic** driving protocol cannot be run in a short enough time.

We stress that the above-outlined field is currently a subject of intense research and many of its important questions remain open. One of the open problems is a systematic application of the adiabatic gauge theory in systems with ESQPTs. Nevertheless, several studies of adiabatic and quasiadiabatic driving in such systems have already been presented. They are all based on the Lipkin model with second-order ground-state QPT and a subsequent ESQPT of the $(f, r) = (1, 1)$ type, but focus on diverse aspects of dynamics. We proceed in items:

- The work in Ref. [91] examines the behavior of the Berry phase for the Lipkin Hamiltonian subject the full rotation of the \hat{J}_x quasispin operator around the z direction. The Berry phase of the ground state has a non-analyticity at the QPT critical point, while the phases of excited states are shown to exhibit even stronger singularities at the points corresponding to the passage of the given level through the ESQPT critical borderline.

- The work in Ref. [92] explores another ESQPT-related effect in nearly adiabatic dynamics of the Lipkin model, namely a mixing of neighboring eigenstates with different parity quantum numbers observed in a cyclic adiabatic evolution connecting normal and parity breaking quantum phases. The observed phenomenon represents an example of irreversibility arising within completely non-dissipative dynamics.
- The work in Ref. [98] studies various quantities characterizing the departure from adiabatic dynamics for individual excited states of the Lipkin Hamiltonian driven at different rates through the ESQPT region. That the ESQPT represents an obstacle to adiabaticity is demonstrated also by visualization of the evolving states on the semiclassical Bloch sphere.
- The work in Ref. [102] investigates the quantum-speed limit for a single qubit interacting with a spin environment via the Lipkin Hamiltonian. The framework of this study is different from the above-outlined problem of counterdiabatic driving, but the physics is similar. The authors observe an increase of the quantum speed limit if the spin environment gets located in the ESQPT region. This is closely related to the increase of the qubit decoherence rate reported for the same model in Refs. [88,89], both phenomena being rooted in the logarithmic divergence of the level density at the ESQPT.

6.3. Dissipative systems and feedback control

An interesting question concerns the fate of ESQPT effects in presence of dissipation. So far, this question was addressed only in a rather limited number of studies. The state of a quantum system interacting with a Markovian environment is commonly modeled by a time-dependent density operator $\hat{\rho}(t)$ obeying a master equation in the Lindblad form [146,163,197]. For instance, for a Lipkin-type system, expressed solely in terms of collective quasispin operators (2), the Lindblad master equation can read as follows [93,198],

$$\frac{d\hat{\rho}(t)}{dt} = -\frac{i}{\hbar} \left[\hat{H}_{\text{NH}}(\lambda, \kappa) \hat{\rho}(t) - \hat{\rho}(t) \hat{H}_{\text{NH}}^\dagger(\lambda, \kappa) \right] + \frac{\kappa}{N} \hat{J}_+ \hat{\rho}(t) \hat{J}_-, \quad (62)$$

$$\hat{H}_{\text{NH}}(\lambda, \kappa) = \hat{H}(\lambda) - i \frac{\kappa}{2N} \hat{J}_- \hat{J}_+, \quad (63)$$

where $\hat{H}_{\text{NH}}(\lambda, \kappa)$ is an effective non-Hermitian Hamiltonian composed of a Hermitian term $\hat{H}(\lambda)$ describing the original conservative system depending on parameter λ , and an anti-Hermitian term weighted by coefficient κ describing the coupling to the environment. The last terms in Eqs. (62) and (63) express the action of the environment on the system. It needs to be stressed, however, that it is implicit in form of these equations that the system and environment remain decoupled for all times. More complex dynamics obtained if this assumption is lifted leads to non-Markovian master equations [146,163], which are generally difficult to solve and have not been considered yet in connection with ESQPTs.

If the original Hamiltonian $\hat{H}(\lambda)$ shows an ESQPT, one can look whether the complex-valued spectrum of the effective Hamiltonian $\hat{H}_{\text{NH}}(\lambda, \kappa)$ carries some signatures of the original singularity. The answer found in Ref. [93] is positive. An example for another Hamiltonian (the same as in Fig. 6) can be seen in Fig. 18, where we show, for several values of κ , individual complex energies $\mathcal{E}_j(\lambda, \kappa) = E_j(\lambda, \kappa) - i\Gamma_j(\lambda, \kappa)/2$ (with $E_j \in \mathbb{R}$ and $\Gamma_j \in \mathbb{R}$, respectively, standing for the real energy

Figure 18.

and decay width of the level) in the domain containing the ESQPTs accompanying the first-order QPT of the original Hamiltonian $\hat{H}(\lambda)$. The complex spectra in Fig. 18 can be characterized by a “non-Hermitian” level density defined as

$$\rho_{\text{NH}}(\lambda, \kappa, E) = -\frac{1}{\pi} \text{Im} \text{Tr} \frac{1}{E - \hat{H}_{\text{NH}}(\lambda, \kappa)} = \sum_j \frac{1}{\pi} \frac{\frac{1}{2}\Gamma_j(\lambda, \kappa)}{(E - E_j(\lambda, \kappa))^2 + \frac{1}{4}\Gamma_j(\lambda, \kappa)^2}. \quad (64)$$

Note that in the limit $\kappa \rightarrow 0$ (no dissipation) we get $\Gamma_j \rightarrow 0$, so the level density (64) becomes a chain of δ -functions defining the ordinary level density (6) of a closed system. In Fig. 18 we use some κ -dependent smoothing of $\rho_{\text{NH}}(\lambda, \kappa, E)$, hence the density showed there represents an extension of the smoothed level density (7) to an open system. It is clear from this figure that the singularities present in the smoothed level density at $\kappa=0$ survive in the density (64) up to relatively large values of κ .

However, a different conclusion concerning the ESQPT effects in presence of dissipation is drawn from the behavior of expectation values of various observables. Using the classical Hamiltonian dynamics for a closed system with $\kappa = 0$, one can determine relations between time averages $\langle J_\alpha \rangle$ of individual quasispin operators along individual trajectories [56]. These relations capture mutual dependencies of the corresponding quantum expectation values $\langle \hat{J}_\alpha \rangle_i$ in individual eigenstates for large values of the size parameter N , and reveal singularities related to the ESQPTs (cf. Sec. 4.2). A similar problem can be solved also for a dissipative system. The time-dependent expectation value of quantity \hat{A} in density matrix $\hat{\varrho}(t)$ following the master equation (62) is calculated as $A(t) = \text{Tr}[\hat{A}\hat{\varrho}(t)]$. Using the mean-field approach, in which one assumes $\text{Tr}[\hat{A}\hat{B}\hat{\varrho}(t)] \approx A(t)B(t)$, it is possible to derive from Eq. (62) a set of coupled first-order differential equations for quasispin components $J_\alpha(t)$ [93]. Since these equations conserve $J^2(t) = \sum_{\alpha=x,y,z} J_\alpha^2(t)$, the dynamics can be visualized on the Bloch sphere, which allows us to analyze various dynamical phases of the dissipative Lipkin model. We can also calculate time averages $\langle J_\alpha \rangle$ and compare them with the situation at $\kappa=0$. The outcome of this analysis is that in presence of

dissipation, the ESQPT singularities of the $\kappa=0$ case get smoothed [93].

A specific way to restore the “ESQPT signal” in dissipative quantum systems was studied in Ref. [93]. The method was based on so-called *feedback control* of the system. This type of control is achieved by variations of the Hamiltonian parameter λ with respect to the values of some dynamical quantities characterizing the system’s actual evolution. For example, consider the Lipkin Hamiltonian (13) with $\chi = 0$, which shows the second-order QPT from the non-interacting to interacting phase at $\lambda = \lambda_c$. In this case, the interaction strength can be controlled via the formula $\lambda(t) = \lambda_0 + \gamma[J_z^2(t) - J_z^2(t-\tau)]/N^2$, where $\lambda_0 > \lambda_c$ and $\gamma > 0$ are constants and $J_z(t') = \text{Tr}[\hat{J}_z \hat{\rho}(t')]$ is the average of \hat{J}_z at time t' [93]. The value $\lambda(t)$ reflects the difference between $J_z^2(t')$ at the current time $t' = t$ and a past time $t' = t - \tau$, where τ is a selected time delay. This means that an increase (decrease) of $|J_z(t)|$ over the period τ induces an increase (decrease) of the interaction strength. The full description of the controlled system is a nontrivial task involving stability analysis of the resulting dynamic equations in various regimes and the determination of dynamic phases. Here we focus only on a single output of Ref. [93], namely the fact that the $\kappa > 0$ system controlled according to the above formula with a suitable choice of parameters restores the non-analytic dependencies of observables characterizing the $\lambda > \lambda_c$ ESQPT in the $\kappa=0$ system. This seemingly surprising result may be understood from the anomalous localization of the Hamiltonian eigenstates close to the ESQPT in the $m=-j$ component of the $|jm\rangle$ basis, which is associated with the $J_z = -j$ saddle point of the $\lambda > \lambda_c$ classical-limit Hamiltonian. This unstable stationary point is a remnant of the global minimum of the $\lambda < \lambda_c$ classical Hamiltonian and its stability decreases with λ increasing above the critical point. Hence the above feedback control works so that any departure of the system from the stationary point induces decrease of λ , which enforces stabilization of the system at the stationary point. An analogous technique can be used also in the Tavis-Cummings regime of the Dicke model with similar types of QPT and ESQPT [199]. Stabilization of another type of ESQPT would probably require a different type of feedback control. Note also that an alternative control scheme for the same Lipkin Hamiltonian was studied in Ref. [100].

An entirely different perspective on quantum dissipative dynamics was presented in Ref. [99], where the Lindblad formalism was used for a specific task to efficiently determine properties of the Hamiltonian eigenstates of non-dissipative systems. The method was applied in the determination of the ESQPT scaling behavior in the Tavis-Cummings version of the Dicke model.

7. Extensions

7.1. Extended periodic systems

Level density from dispersion relations

Van Hove singularities

Bose-Hubbard model

Two-dimensional crystals

7.2. Periodically kicked systems

Kicked systems, Floquet theory, Tobias’ work

see also [200]

7.3. Unbound systems

ESQPTs in the continuum, resonances

8. Conclusions

- [1] Carr LD (editor) 2010 *Understanding Quantum Phase Transitions* (Boca Raton, Taylor & Francis)
- [2] Vojta M 2003 *Rep. Prog. Phys.* **66**, 2069
- [3] Sachdev S 1999 *Quantum Phase Transitions* (Cambridge University Press)
- [4] Gilmore R 1981 *Catastrophe Theory for Scientists and Engineers* (New York, Wiley)
- [5] Cejnar P, Macek M, Heinze S, Jolie J and Dobeš J 2006 *J. Phys. A* **39** L515
- [6] Cejnar P, Heinze S and Macek M 2007 *Phys. Rev. Lett.* **99**, 100601
- [7] Heinze S, Cejnar P, Jolie J and Macek M 2006 *Phys. Rev. C* **73** 014306
- [8] Macek M, Cejnar P, Jolie J and Heinze S 2006 *Phys. Rev. C* **73** 014307
- [9] Caprio M A, Cejnar P and Iachello F 2008 *Ann. Phys.* **323** 1106
- [10] Cejnar P and Stránský P 2008, *Phys. Rev. E* **78**, 031130
- [11] Stránský P, Macek M and Cejnar P 2014 *Ann. Phys. (N.Y.)* **345** 73
- [12] Stránský P, Macek M, Leviatan A and Cejnar P 2015 *Ann. Phys. (N.Y.)* **356** 57
- [13] Macek M, Stránský P, Leviatan A and Cejnar P 2019 *Phys. Rev. C* **99** 064323
- [14] Stránský P and Cejnar P 2016 *Phys. Lett. A* **380** 2637
- [15] Cary JR and Rusu P 1992 *Phys. Rev. A* **45** 8501
- [16] Cary JR and Rusu P 1993 *Phys. Rev. A* **47** 2496
- [17] Leyvraz F and Heiss WD 2005 *Phys. Rev. Lett.* **95** 050402
- [18] Reis M, Terra Cunha M O, Oliveira A C and Nemes M C 2005 *Phys. Lett. A* **344** 164
- [19] Zhang W, Zhou D L, Chang M-S, Chapman M S and You L 2005 *Phys. Rev. A* **72** 013602
- [20] Ribeiro P, Vidal J and Mosseri R 2007 *Phys. Rev. Lett.* **99** 050402
- [21] Ribeiro P and Paul T 2009 *Phys. Rev. A* **79** 032107
- [22] Zhao L, Jiang J, Tang T, Webb M and Liu Y 2014 *Phys. Rev. A* **89** 023608
- [23] Duistermaat JJ 1980 *Comm. Pure Appl. Math.* **33** 687
- [24] Cushman R H and Duistermaat JJ 1988 *Bull. Am. Math. Soc.* **19** 475
- [25] Vũ Ngoc S 1999 *Comm. Math. Phys.* **203** 465
- [26] Winnewisser B P, Winnewisser M, Medvedev I R, Behnke M, De Lucia F C, Ross S C and Koput J 2005 *Phys. Rev. Lett.* **95** 243002
- [27] Zobov N F, Shirin S V, Polyansky O L, Tennyson J, Coheur P-F, Bernath P F, Carleer M and Colin R 2005 *Chem. Phys. Lett.* **414** 193
- [28] Larese D, Pérez-Bernal and Iachello F 2013 *J. Mol. Struct.* **1051** 310
- [29] Franzosi F and Pettini M 2004 *Phys. Rev. Lett.* **92** 060601
- [30] Kastner M, Schreiber S and Schnetz O 2007 *Phys. Rev. Lett.* **99** 050601
- [31] Kastner M, *Rev. Mod. Phys.* 2008 **80** 167
- [32] Kastner M and Schnetz O 2008 *Phys. Rev. Lett.* **100** 160601
- [33] Kanamoto R, Carr LD and Ueda M 2009 *Phys. Rev. A* **79** 063616
- [34] Kanamoto R, Carr LD and Ueda M 2010 *Phys. Rev. A* **81** 023625
- [35] Pal A and Huse D A 2010 *Phys. Rev. B* **82** 174411
- [36] Huse D A, Nandkishore R, Oganesyan V, Pal P and Sondhi S L 2013 *Phys. Rev. B* **88** 014206
- [37] Van Hove L 1953 *Phys. Rev.* **89** 1189
- [38] Dietz B, Iachello F, Miski-Oglu M, Pietralla N, Richter A, von Smekal L and Wambach J 2013 *Phys. Rev. B* **88** 104101
- [39] Iachello F, Dietz B, Miski-Oglu M and Richter A *et al.* 2015 *Phys. Rev. B* **91** 214307
- [40] Dietz B, Iachello F and Macek M 2017 *Crystals* **7** 246
- [41] Moreira T, Pellegrino G Q, Peixoto de Faria J G, Nemes M C, Camargo F and de Toledo Piza A F R 2008 *Phys. Rev. E* **77** 051102
- [42] Schchesnovich V S and Konotop V V 2009 *Phys. Rev. Lett.* **102** 055702
- [43] Cejnar P and Jolie J 2009 *Prog. Part. Nucl. Phys.* **62** 210
- [44] Figueiredo M C, Cotta T M and Pellegrino G Q 2010 *Phys. Rev. E* **81** 012104
- [45] Pérez-Bernal F and Álvarez-Bajo O 2010 *Phys. Rev. A* **81** 050101(R)
- [46] Caprio M A, Skrabacz J H and Iachello F 2011 *J. Phys. A: Math. Theor.* **44** 075303
- [47] López-Moreno E, Grether M and Velázquez V 2011 *J. Phys. A: Math. Theor.* **44** 475301
- [48] Larese D and Iachello F 2011 *J. Mol. Struct.* **1006** 611

- [49] Pérez-Fernández P, Relaño A, Arias J, Cejnar P, Dukelsky J and García-Ramos JE 2011 *Phys. Rev. E* **83** 046208
- [50] Brandes T 2013 *Phys. Rev. E* **88** 032133
- [51] Puebla R and Relaño A 2013 *EPL* **104** 50007
- [52] Larese D, Pérez-Bernal F and Iachello F 2013 *J. Mol. Struct.* **1051** 310
- [53] Bastarrachea-Magnani M A, Lerma-Hernández S and Hirsch J G 2014 *Phys. Rev. A* **89** 032101
- [54] Bastarrachea-Magnani M A, Lerma-Hernández S and Hirsch J G 2014 *Phys. Rev. A* **89** 032102
- [55] Relaño A, Dukelsky J, Pérez-Fernández P and Arias JM 2014 *Phys. Rev. E* **90** 042139
- [56] Engelhardt G, Bastidas V M, Kopylov W and Brandes T 2015 *Phys. Rev. A* **91** 013631
- [57] Graefe E-M, Graney M and Rush A 2015 *Phys. Rev. A* **92** 012121
- [58] Chumakov S M and Klimov A B 2015 *Phys. Scr.* **90** 074044
- [59] Zhang Y, Zuo Y, Pan F and Draayer J P 2016 *Phys. Rev. C* **93** 044302
- [60] Graefe E-M, Korsch H J and Rush A 2016 *Phys. Rev. A* **93** 042102
- [61] López C M and Relaño A 2016 *Phys. Rev. E* **94** 012140
- [62] Chávez-Carlos J, Bastarrachea-Magnani M A, Lerma-Hernández and Hirsch J G 2016 *Phys. Rev. E* **94** 022209
- [63] Puebla R, Hwang M-J and Plenio M B 2016 *Phys. Rev. A* **94** 023835
- [64] Relaño A, Esebbag C and Dukelsky J 2016 *Phys. Rev. E* **94** 052110
- [65] Relaño A, Bastarrachea-Magnani M A and Lerma-Hernández S 2016 *EPL* **116** 50005
- [66] Šindelka M, Santos L F and Moiseyev N 2017 *Phys. Rev. A* **95** 010103(R)
- [67] Eckle H P and Johannesson H 2017 *J. Phys. A: Math. Theor.* **50** 294004
- [68] Romera E, Castaños O, Calixto M and Pérez-Bernal F 2017 *J. Stat. Mech.* **2017** 013101
- [69] Bastarrachea-Magnani M A, Relaño A, Lerma-Hernández S, López-del-Carpio B, Chávez-Carlos J and Hirsch J G 2017 *J. Phys. A: Math. Theor.* **50** 144002
- [70] García-Ramos JE, Pérez-Fernández P and Arias JM *Phys. Rev. C* **95** 054326
- [71] Zhang Y and Iachello F 2017 *Phys. Rev. C* **95** 061304(R)
- [72] Karampagia S, Renzaglia A and Zelevinsky V 2017 *Nucl. Phys. A* **962** 46
- [73] Kloc M, Stránský P and Cejnar P 2017 *Ann. Phys.* **382** 85
- [74] Kloc M, Stránský P and Cejnar P 2017 *J. Phys. A: Math. Theor.* **50** 315205
- [75] Opatrný T, Richterek L and Opatrný M 2018 *Sci. Rep.* **8** 1984
- [76] Bychek A A, Maksimov D N and Kolovsky A R 2018 *Phys. Rev. A* **97** 063624
- [77] Rodriguez J P J, Chilingaryan S A and Rodríguez-Lara B M 2018 *Phys. Rev. A* **98** 043805
- [78] Nyawo P T and Touchette H 2018 *Phys. Rev. E* **98** 052103
- [79] Zhu G-L, Lü X-Y, Bin S-W, You C and Wu Y 2019 *Front. Phys.* **14** 52602
- [80] Khalouf-Rivera J, Carvajal M, Santos L F and Pérez-Bernal F 2019 *J. Phys. Chem. A* **123** 9544
- [81] Bastarrachea-Magnani M A, Lerma-Hernández S and Hirsch J G 2016 *J. Stat. Mech.* **2016** 093105
- [82] Cejnar P and Stránský P 2017 *Phys. Lett. A* **381** 984
- [83] Pérez-Fernández P and Relaño A 2017 *Phys. Rev. E* **96** 012121
- [84] Webster J R and Kastner M 2018 *J. Stat. Phys.* **171** 449
- [85] Relaño A 2018 *Phys. Rev. Lett.* **121** 030602
- [86] Garcia-March M A, van Frank S, Bonneau M, Schmiedmayer J, Lewenstein M and Santos L F 2018 *New J. Phys.* **20** 113039
- [87] Kloc M, Cejnar P and Schaller G 2019 *Phys. Rev. E* **100** 042126
- [88] Relaño A, Arias J M, Dukelsky J, García-Ramos JE and Pérez-Fernández P 2008 *Phys. Rev. A* **78** 060102(R)
- [89] Pérez-Fernández P, Relaño A, Arias J M, Dukelsky J and García-Ramos JE 2009 *Phys. Rev. A* **80** 032111
- [90] Pérez-Fernández P, Cejnar P, Arias J M, Dukelsky J, García-Ramos JE and Relaño A 2011 *Phys. Rev. A* **83** 033802
- [91] Yuan Z-G, Zhang P, Li S-S, Jing J and Kong L-B 2012 *Phys. Rev. A* **85** 044102
- [92] Puebla R and Relaño A 2015 *Phys. Rev. E* **92** 012101
- [93] Kopylov W and Brandes T 2015 *New J. Phys.* **17** 103031
- [94] Santos L F and Pérez-Bernal F 2015 *Phys. Rev. A* **92** 050101(R)
- [95] Santos L F, Távora M and Pérez-Bernal F 2016 *Phys. Rev. A* **94** 012113
- [96] Wang Q and Quan H T 2017 *Phys. Rev. E* **96** 032142
- [97] Pérez-Bernal and F Santos L F 2017 *Fortschr. Phys.* **65** 1600035
- [98] Kopylov W, Schaller G and Brandes T 2017 *Phys. Rev. E* **96** 012153
- [99] Furtmaier O and Mendoza M 2017 *Phys. Rev. A* **96** 022134
- [100] Zimmermann S, Kopylov E and Schaller G 2018 *J. Phys. A: Math. Theor.* **51** 385301
- [101] Kloc M, Stránský and Cejnar P 2018 *Phys. Rev. A* **98** 013836

- [102] Wang Q and Pérez-Bernal F 2019 *Phys. Rev. A* **100** 022118
- [103] Wang Q and Pérez-Bernal F 2019 *Phys. Rev. A* **100** 062113
- [104] Hummel Q, Geiger B, Urbina JD and Richter K 2019 *Phys. Rev. Lett.* **123** 160401
- [105] Pilatowsky-Cameo S, Chávez-Carlos J, Bastarrachea-Magnani M A, Stránský P, Lerma-Hernández S, Santos L F and Hirsch J G 2019 *Phys. Rev. E* **101** 010202(R)
- [106] Bastidas V M, Pérez-Fernández P, Vogl M and Brandes T 2014 *Phys. Rev. Lett.* **112** 140408
- [107] Bastidas V M, Engelhardt G, Pérez-Fernández P, Vogl M and Brandes T 2014 *Phys. Rev. A* **90** 063628
- [108] Bandyopadhyay J N and Sarkar T G 2015 *Phys. Rev. E* **91** 032923
- [109] Gessner M, Bastidas V M, Brandes T and Buchleitner A 2016 *Phys. Rev. B* **93** 155153
- [110] Stránský P, Šindelka M, Kloc M and Cejnar P 2020 *Phys. Rev. Lett.* **125** 020401
- [111] Dicke R H 1954 *Phys. Rev.* **93** 99
- [112] Jaynes E T and Cummings F W 1963 *Proc. IEEE* **51** 89
- [113] Tavis M and Cummings F W 1968 *Phys. Rev.* **170** 379
- [114] Baumann K, Guerlin C, Brennecke F and Esslinger T 2010 *Nature* **464** 1301
- [115] Baumann K, Mottl R, Brennecke F and Esslinger T 2011 *Phys. Rev. Lett.* **107** 140402
- [116] Baden M P, Kyle J A, Grimsom A L, Parkins S and Barrett M D 2014 *Phys. Rev. Lett.* **113** 020408
- [117] Klinder J, Keßler H, Wolke M, Mathey L and Hemmerich A 2015 *Proc. Nat. Acad. Sci.* **112** 3290
- [118] Hayn M and Brandes T 2017 *Phys. Rev. E* **95** 012153
- [119] Wang Y K and Hioe F T 1973 *Phys. Rev. A* **7** 831
- [120] Hepp K and Lieb E H 1973 *Phys. Rev. A* **8** 2517
- [121] Rzażewski K, Wódkiewicz K and Żakowicz W 1975 *Phys. Rev. Lett.* **35** 432
- [122] Keeling J 2014 *Light–Matter Interactions and Quantum Optics* (CreateSpace Independent Publishing Platform)
- [123] Emary C and Brandes T 2003 *Phys. Rev. Lett.* **90** 044101
- [124] Lambert N, Emary C and Brandes T 2004 *Phys. Rev. Lett.* **92** 073602
- [125] Cejnar P, Stránský P, Kloc M and Macek M 2019 *AIP Conference Proceedings* **2150** 020017
- [126] Babelon O, Cantini L and Douçot B 2009 *J. Stat. Mech.* **2009** P07011
- [127] Hwang M-J, Puebla R and Plenio M B 2015 *Phys. Rev. Lett.* **115** 180404
- [128] Ma S 1976 *Modern Theory of Critical Phenomena* (Reading, Benjamin)
- [129] Cejnar P and Stránský P 2016 *Phys. Scr.* **91** 083006
- [130] Lipkin H J, Meshkov N and Glick A J 1965 *Nucl. Phys.* **62** 188; Meshkov N, Glick N and Lipkin H J 1965 *Nucl. Phys. A* **62** 199; Glick N, Lipkin H J and Meshkov N 1965 *Nucl. Phys. A* **62** 211
- [131] Klein A and Marshalek E R 1991 *Rev. Mod. Phys.* **63** 375
- [132] Iachello F and Oss S 1996 *J. Chem. Phys.* **104** 6956
- [133] Iachello F and Levine R D 1995 *Algebraic Theory of Molecules* (Oxford, Oxford Univ. Press)
- [134] Iachello F and Arima A 1987 *The Interacting Boson Model* (Cambridge, Cambridge Univ. Press)
- [135] Iachello F and Pérez-Bernal F 2008 *Mol. Phys.* **106** 223
- [136] Iachello F 2014 *Lie Algebras and Applications*, Lecture Notes in Physics 891 (Heidelberg, Springer)
- [137] Zhang W-M and Feng D H 1995 *Phys. Rep.* **252** 1
- [138] Blaizot J P and E.R. Marshalek E R 1978 *Nucl. Phys. A* **309** 422 and 453
- [139] Rowe D J 2004 *Nucl. Phys. A* **745** 47
- [140] Macek M, Dobeš, Stránský P and Cejnar P 2010 *Phys. Rev. Lett.* **105** 072503
- [141] Macek M and Leviatan A 2014 *Ann. Phys. (N.Y.)* **351** 302
- [142] Dukelsky J, Pittel S and Sierra G 2004 *Rev. Mod. Phys.* **76** 643
- [143] Cejnar P and Iachello F 2007 *J. Phys. A: Math. Theor.* **40** 581
- [144] Pitaevskii L and Stringari S 2003 *Bose-Einstein Condensation* (Oxford, Oxford Univ. Press)
- [145] Anglin J R and Ketterle W 2002 *Nature* **416** 211
- [146] Gardiner C and Zoller P 2014, 2015, 2016 *The Quantum World of Ultra-Cold Atoms and Light*, Book I, II, III (London Imperial College Press)
- [147] Milburn G J, Corney J, Wright E M and Walls D F 1997 *Phys. Rev. A* **55** 4318
- [148] Cirac J I, Lewenstein M, Mølmer K and Zoller P 1998 *Phys. Rev. A* **57** 1208
- [149] Albiez M, Gati R, Fölling J, Hunsmann S, Cristiani M and Oberthaler M K 2005 *Phys. Rev. Lett.* **95** 010402
- [150] Juliá-Díaz B, Dagnino D, Lewenstein M, Martorell J and Polls A 2019 *Phys. Rev. A* **81** 023615
- [151] Zoller P 2002 *Nature* **417** 493

- [152] Karassiov VP and Klimov A 1994 *Phys. Lett. A* **191** 117
- [153] Dukelsky J, Dussel G G, Esebbag C and Pittel S 2004 *Phys. Rev. Lett.* **93** 050403
- [154] Lee Y-H, Yang W-L and Zhang Y-Z 2010 *J. Phys. A: Math. Theor.* **43** 185204 and 375211
- [155] Iachello F and Van Isacker P 1991 *The Interacting Boson-Fermion Model* (Cambridge, Cambridge Univ. Press)
- [156] Petrellis D, Leviatan A and Iachello F 2011 *Ann. Phys.* **326** 926
- [157] Eisenstein J P and MacDonald A H 2004 *Nature* **432** 691
- [158] Bulgac A and Kusnezov D 1990 *Ann. Phys. (N.Y.)* **199** 187
- [159] Stránský P, Kloc M and Cejnar P 2017 *AIP Conference Proceedings* **1912** 020018
- [160] Haake F 2010 *Quantum Signatures of Chaos* (Berlin: Springer)
- [161] Gutzwiller M C 1971 *J. Math. Phys.* **12** 343
- [162] Berry M V and Tabor M 1976 *Proc. R. Soc. Lond. Ser. A* **349** 101
- [163] Binder F, Correa L A, Gogolin C, Anders J and Adesso G (editors) 2019 *Thermodynamics in the Quantum Regime* (Berlin: Springer)
- [164] Gross D H E 2001 *Microcanonical Thermodynamics* (Singapore: World Scientific)
- [165] Dunkel J and Hilbert S 2006 *Physica A* **370** 390
- [166] Brody D C, Hook D W and Hughston L P 2007 *Proc. R. Soc. A* **463** 2021
- [167] Kastner M, Schnetz O and Schreiber S 2008 *J. Stat. Mech.* **2008** P04025
- [168] Kastner M 2009 *J. Stat. Mech.* **2009** P02016
- [169] Casetti L, Kastner M and Nerattini R 2009 *J. Stat. Mech.* **2009** P07036
- [170] Eisert J, Friesdorf M and Gogolin C 2015 *Nature Phys.* **11** 124
- [171] Sengupta K, Powell S and Sachdev S 2004 *Phys. Rev. A* **69** 053616
- [172] Calabrese P and Cardy J 2006 *Phys. Rev. Lett.* **96** 136801
- [173] Távora M, Torres-Herrera E J and Santos L F 2017 *Phys. Rev. A* **95** 013604
- [174] Torres-Herrera E J, García-García A M and Santos L F 2018 *Phys. Rev. B* **97** 060303(R)
- [175] Lerma-Hernández S, Chávez-Carlos J, Bastarrachea-Magnani M A, Santos L F and Hirsch J G 2018 *J. Phys. A: Math. Theor.* **51** 475302
- [176] Hillery M, O'Connell R F, Scully M O and Wigner EP 1984 *Phys. Rep.* **106** 121
- [177] Hashimoto K, Murata K and Yoshii R 2017 *J. High Energy Phys.* **10** 138
- [178] Swingle B 2018 *Nature Phys.* **14** 988
- [179] Maldacena J, Shenker S H and Stanford D 2016 *J. High Energ. Phys.* **2016** 106
- [180] Rozenbaum E B, Ganeshan S and Galitski V 2017 *Phys. Rev. Lett.* **118** 086801
- [181] Chávez-Carlos J, López-Del-Carpio B, Bastarrachea-Magnani M A, Stránský P, Lerma-Hernández S, Santos L F and Hirsch J G 2019 *Phys. Rev. Lett.* **122** 024101
- [182] Fan R, Zhang P, Shen H and Zhai H 2017 *Science Bulletin* **62** 707
- [183] Lewis-Swan R J, Safavi-Naini A, Bollinger J J and Rey A M 2019 *Nature Commun.* **10** 1581
- [184] Polkovnikov A, Sengupta K, Silva A and Vengalattore M 2011 *Rev. Mod. Phys.* **83** 863
- [185] Kolodrubetz M, Sels D, Mehta P and Polkovnikov A 2017 *Phys. Rep.* **697** 1
- [186] Wilczek F and Shapere A (editors) 1989 *Geometric Phases in Physics* (Singapore: World Scientific)
- [187] Provost J P and Vallee G 1980 *Cummun. Math. Phys.* **76** 289
- [188] Bukov M, Sels D and Polkovnikov A 2019 *Phys. Rev. X* **9** 011034
- [189] Dolejší J 2020 *Diploma Thesis* (Prague: Charles University) unpublished
- [190] Schützhold R and Schaller G 2006 *Phys. Rev. A* **74** 060304(R)
- [191] Zurek W H 1985 *Nature* **317** 505
- [192] del Campo A 2013 *Phys. Rev. Lett.* **111** 100502
- [193] Sels D and Polkovnikov A 2017 *Proc. Nat. Acad. Sci.* **114** E3909
- [194] Demirplak M and Rice S A 2003 *J. Phys. Chem. A* **107** 9937
- [195] Berry M V 2009 *J. Phys. A: Math. Theor.* **42** 365303
- [196] Funo K, Zhang J-N, Chatou C, Kim K, Ueda M and del Campo A 2017 *Phys. Rev. Lett.* **118** 100602
- [197] Manzano D 2020 *AIP Advances* **10** 025106
- [198] Lee T E, Chan C K and Yelin S F 2014 *Phys. Rev. A* **90** 052109
- [199] Kopylov W, Emary C, Schöll E and Brandes T 2015 *New J. Phys.* **17** 013040
- [200] Engelhardt G, Bastidas V M, Emary C and Brandes T 2013 *Phys. Rev. E* **87** 052110